

For Reference

NOT TO BE TAKEN FROM THIS ROOM

Ex libris
UNIVERSITATIS
ALBERTAENSIS



THE UNIVERSITY OF ALBERTA

Release Form

NAME OF AUTHOR . GORDON RICHARD WINKEL
TITLE OF THESIS WIND TUNNEL MODELING OF PLUME RISE AND .
DISPERSION
.
DEGREE FOR WHICH THESIS WAS PRESENTED MASTER OF SCIENCE .
YEAR THIS DEGREE GRANTED . 1979

Permission is hereby granted to THE UNIVERSITY OF ALBERTA LIBRARY to reproduce single copies of this thesis and to lend or sell such copies for private, scholarly or scientific research purposes only.

The author reserves other publication rights, and neither the thesis nor extensive extracts from it may be printed or otherwise reproduced without the author's written permission.

THE UNIVERSITY OF ALBERTA

WIND TUNNEL MODELING OF PLUME RISE
AND DISPERSION

by



GORDON RICHARD WINKEL

A THESIS

SUBMITTED TO THE FACULTY OF GRADUATE STUDIES AND RESEARCH
IN PARTIAL FULFILLMENT OF THE REQUIREMENTS FOR THE DEGREE
OF MASTER OF SCIENCE

DEPARTMENT OF MECHANICAL ENGINEERING

EDMONTON, ALBERTA

FALL, 1979

UNIVERSITY OF ALBERTA

FACULTY OF GRADUATE STUDIES AND RESEARCH

The undersigned certify that they have read, and recommend to the Faculty of Graduate Studies and Research for acceptance, a thesis entitled "Wind Tunnel Modeling of Plume Rise and Dispersion," submitted by Gordon Richard Winkel in partial fulfillment of the requirements for the degree of Master of Science.

DEDICATION

TO ALL THOSE WHO PERSONALLY CONTRIBUTED TO
AND SUPPORTED MY EDUCATION

ABSTRACT

Experiments were conducted in a wind tunnel to investigate plume rise and plume growth in neutral atmospheric conditions. The modeling of fullscale plumes in the wind tunnel was studied.

The use of plume momentum and the flux of buoyancy as scaling criteria proved successful in modeling plume behaviour. If this criteria is used the stack gas density can be varied between model and fullscale to achieve higher wind tunnel speeds with no effect on plume rise or dispersion. The study shows that careful attention must be given in modeling source conditions such as the stack efflux velocity profile due to its strong influence on plume rise and plume spread.

The effects of both initial upward stack gas momentum and buoyant forces on plume rise were combined in a single expression that correlated with plume rise data in the wind tunnel. Plume rise was found to terminate at a downwind distance of $2200 L_B$, where L_B is a buoyancy length scale for a plume, for the simulated atmospheric boundary layer shear flow tested. The effect of wind shear in the approach flow reduced plume rise by about 20% as compared to a uniform flow. The theory of Djurfors and Netterville (1978) closely predicted the reduction in plume rise due to wind shear.

The Gaussian dispersion model for an elevated point source correctly characterized plume dispersion in the wind tunnel. Freestream velocity at stack height was chosen as a representative plume convection velocity for the Gaussian model.

The plume spread due to buoyancy induced turbulence was measured in the wind tunnel and an expression was found to fit the data. Subsequent measurements showed that the interaction of buoyancy induced turbulence and atmospheric turbulence was nonlinear. An appropriate nonlinear correction was developed and successfully corrected for the initial growth due to buoyancy induced turbulence so that the spread due to atmospheric turbulence was recovered.

ACKNOWLEDGEMENTS

I wish to express my sincere gratitude to Dr. D. J. Wilson for his supervision of the experiments and preparation of this thesis. I have enjoyed working with him on numerous projects which proved both rewarding and educational.

I wish to also thank my wife Jan for her patience and support during my studies.

The financial support received in the form of a Graduate Teaching Assistantship from the University of Alberta is gratefully acknowledged.

Special thanks are extended to Owen Neiman for his friendship during my course of study. Fellow graduate students are also thanked for their companionship and providing a stimulating atmosphere in which to work.

I gratefully acknowledge the work done by the Mechanical Engineering Machine Shop and the Technicians in support of the experiments. Special thanks are extended to Don Fuhr for his precision work in constructing inserts for model stacks.

I also wish to express my appreciation to Marilyn Wahl whose excellent typing skills were an asset in the preparation of this thesis.

TABLE OF CONTENTS

CHAPTER		PAGE
I	INTRODUCTION	1
II	EXPERIMENTAL PROCEDURE	7
	2.1 Wind Tunnel Facility	7
	2.2 Velocity Measurements	7
	2.3 Concentration Measurements	9
	2.4 Volume Flow Measurements	10
	2.5 Simulation of the Atmospheric Boundary Layer	11
	2.6 Wind Tunnel Experiments Behind Grids	14
	2.7 Velocity Measurements Across Stack Exit	18
III	MODELING BUOYANT PLUMES	30
	3.1 Similarity Parameters for Buoyancy	30
	3.2 Similarity Parameters for Momentum and Mass	32
	3.3 Comparison of Modeling Techniques	34
	3.4 Correction for Non-Uniform Flow at Stack Exit	36
	3.5 Modeling Techniques in the Present Study	40
	3.6 The Influence of Stack Exit Conditions on Modeling Buoyant Plumes	41
	3.7 The Effects of Stack Gas Density Ratio	46
IV	PLUME RISE	53
	4.1 Introduction to Plume Rise	53
	4.2 The Combination of Momentum Rise and Buoyancy Rise	54
	4.3 Final Rise of a Buoyant Plume	58

CHAPTER		PAGE
	4.4 Entrainment Constants for Momentum Rise of a Plume	61
	4.5 The Effect of Turbulence and Velocity Shear on Plume Rise	64
	4.6 Entrainment Constants for Buoyant Plume Rise	69
V	PLUME DISPERSION	78
	5.1 The Gaussian Plume Model	78
	5.2 Calculation of Plume Spread From Concentration Data	83
	5.3 Accuracy and Validity of the Gaussian Plume Model	85
	5.4 Choosing an Average Plume Convection Speed	90
	5.5 Corrections for the Effect of Buoyancy on Plume Spread	92
	5.6 Comparing Measured Spread to Full Scale σ_y and σ_z	100
VI	CONCLUSIONS AND RECOMMENDATIONS	124
	6.1 Modeling Plume Buoyancy	124
	6.2 Modeling Plume Momentum	125
	6.3 Effect of Stack Gas Density	126
	6.4 Plume Rise	126
	6.5 Plume Dispersion	128
	6.6 Recommendations	130
	REFERENCES	132

LIST OF TABLES

TABLE		PAGE
2-1	Comparison of Wind Tunnel Boundary Layer with Full Scale Atmospheric Data of Counihan (1975). From Wilson (unpublished)	15
3-1	Similarity Parameters Modelled in Different Studies	42
3-2	Comparison of Vertical Dispersion, σ_z , for Plumes with Laminar and Turbulent Velocity Profiles at Stack Exit	45
4-1	Comparison of Formulas for Finding Downwind Position of Final Rise	61
4-2	Comparison of Calculated and Fitted Values of β_1 for Different Plumes	64
4-3	Comparison of β_2 for Plumes with Different Source Conditions in a Uniform Crossflow	71
5-1	Equivalent Velocity Variation for Fig. 5-7	91
5-2	Magnitudes of Characteristic Velocities From Experiments	92
5-3	Determination of Plume Radius	96
5-4	Comparison of Measured and Calculated Values of σ_{self}	98
5-5	Investigations on the Effect of Sample Time on Concentration Measurements	103

LIST OF FIGURES

FIGURE		Page
2-1	Wind Tunnel Facility and Elements Used to Generate a Simulated Atmospheric Boundary Layer	21
2-2	Apparatus for Measurement of Mean and Turbulent Velocities	22
2-3	Apparatus for Generating Model Plumes and Measuring Their Concentration	23
2-4	Probe Traverser and Instrumentation	24
2-5	Spikes, Barrier and Roughness Used in the Simulation of an Atmospheric Boundary Layer	24
2-6	Mean Velocity and Turbulence Structure of Simulated Atmospheric Boundary Layer	25
2-7	Adjustment of Concentration Sample Probe for Experiments in Grid Wake Turbulence. The Kurtz Hot Film Probe is shown to the Right of the Stack	26
2-8	Plugs used in Modifying the Velocity Profiles of the Stack Gas	26
2-9	Decay of Grid Wake Turbulence	27
2-10	Mean Velocity Profiles in Boundary Layer Shear Flow and Grid Wake Turbulence	28
2-11	Turbulence Intensity Profiles in Boundary Layer Shear Flow and Grid Wake	29
3-1	Comparison of Measured and Theoretical Velocity Profiles at Stack Exit	48
3-2	Comparison of Plume Rise for Different Momentum Effects	49
3-3	Comparison of Concentration Profiles for a Laminar and Turbulent Stack Gas	50
3-4	Comparison of Plume Rise for Different Stack Gas Densities	51

FIGURE		Page
3-5	Comparison of Vertical Plume Spread for Different Stack Gas Densities	52
4-1	Combination of Momentum Rise and Buoyant Rise	73
4-2	Final Rise of Plumes	74
4-3	Fitting the Combined Rise Expression for Calculated Values of β_1	75
4-4	Effects of Shear and Turbulence on Plume Rise	76
4-5	Comparison of Different Shear Corrections	77
5-1	Gaussian Plume Model for a Continuous Point Source. From Stern (1976)	106
5-2	The Application of an Image Source to Correct for Ground Level Reflection. From Stern (1976)	107
5-3	Vertical and Ground Level Concentration Profiles Along Plume Centerline. From Stern (1976)	107
5-4	Area Under a Concentration Profile with Ground Reflection	108
5-5	Fitted Concentration Profiles at $x = 10$ cm Downwind	109
5-6	Fitted Concentration Profiles at $x = 50$ cm Downwind	110
5-7	Comparison of Different Diffusion Models to Centerline Concentration Data	111
5-8	Comparison of Vertical Spread for Different Approach Flows	112
5-9	Correcting Crosswind Plume Spread for Buoyancy Induced Spreading	113
5-10	Correcting Crosswind Plume Spread for Buoyancy Induced Spreading	114
5-11	Correcting Vertical Plume Spread for Buoyancy Induced Spreading	115
5-12	Correcting Vertical Plume Spread for Buoyancy Induced Spreading	116

FIGURE		Page
5-13	Computed Vertical Plume Spreads From a Single Power Law Relation for Nonbuoyant Plume Spread	117
5-14	Computed Crosswind Plume Spreads From a Single Power Law Relation for Nonbuoyant Plume Spread	118
5-15	Prediction of Ground Level Concentrations for $U_s = 0.9$ M/S	119
5-16	Prediction of Ground Level Concentrations for $U_s = 0.45$ M/S	120
5-17	Comparison of Vertical Plume Spread From Model and Fullscale Studies	121
5-18	Comparison of Crosswind Plume Spread From Model and Fullscale Studies	122
5-19	Effect of Sample Time on Measurement of Concentration Profiles	123

LIST OF SYMBOLS

C	Volume concentration (ppth)
C_{cr}	Volume concentration at source height for plume with ground reflection (ppth), see Eq. 5-14
C_{cnr}	Volume concentration at source height for plume with no ground reflection (ppth), see Eq. 5-15
C_f	Skin friction coefficient (dimensionless), see Table 2-1
d	Stack diameter (m)
F_B	Buoyancy flux (m^4/s^3), see Eq. 3-3
F_M	Momentum flux (m^4/s^2), see Eq. 3-13
F_r	Froude number (dimensionless), see Eq. 3-2
F_v	Uniform flow momentum flux (m^4/s^2), see Eq. 3-7
g	Acceleration due to gravity (m/s^2)
$h=h_e$	Effective stack height (m)
h_s	Stack height (m)
Δh	Total plume rise (m)
Δh_B	Plume rise due to buoyancy (m)
Δh_{Bf}	Final rise of a purely buoyant plume (m)
Δh_M	Plume rise due to momentum (m)
K	Eddy diffusivity (m^2/s)

L_B	Buoyancy length (m), see Eq. 3-4
L_I	Length scale accounting for momentum and buoyant effects in a plume (m), see Eq. 4-28
L_M	Momentum length (m), see Eq. 3-14
L_V	Uniform flow momentum length (m), see Eq. 3-8
m	Mass flow rate (kg/s)
n	Exponent for power law velocity profile (dimensionless)
Q	Volume flow rate (m^3/s)
r	Plume radius (m)
R_i	Bulk Richardson number. Note this is <u>not</u> the gradient Richardson number referred to in meteorological studies. (Dimensionless) see Eq. 3-2
R_s	Stack or initial plume radius (m)
t	Travel time for plume rise or sample time for concentration measurements (s)
u	Downwind turbulent velocity (m/s)
u_*	Friction velocity (m/s)
U	Mean freestream velocity (m/s)
U_s	Mean freestream velocity at stack height (m/s)
v	Lateral turbulence velocity (m/s)
w	Vertical turbulence velocity (m/s)
W_s	Mean efflux velocity of stack gas (m/s)
x	Downwind position coordinate with source location as origin (m)
x_f	Downwind location for final rise of a plume (m)

y	Lateral position coordinate (m)
z	Vertical position coordinate (m)
α	Kinetic energy correction factor (dimensionless), see Eq. 3-11
β	Entrainment constant (dimensionless)
β_1	Entrainment constant for momentum rise (dimensionless)
β_2	Entrainment constant for buoyant rise (dimensionless)
β_*	Effective entrainment constant in wind shear (dimensionless), see Eq. 4-24
λ	Ratio of freestream velocity at stack height to local velocity at height h (dimensionless), see Eq. 4-19
λ_x	Taylor microscale. This is used to characterize the eddy sizes in a turbulent flow. (m) See Fig. 2-6
μ_p	Mean of a Gaussian distribution (m)
ν	Kinetic viscosity (m^2/s)
ξ	Plume radius normalized with plume spread (dimensionless), see Eq. 5-30
ρ_s	Stack gas density (kg/m^3)
ρ_a	Ambient density (kg/m^3)
$\Delta\rho$	Difference between stack gas and ambient density (kg/m^3)
σ_b	Total plume spread (m), see Eq. 5-22
σ_{nb}	Plume spread due to atmospheric turbulence (m)

σ_p	Standard deviation of Gaussian distribution (m)
σ_{self}	Plume spread due to buoyancy induced turbulence (m)
σ_y	Crosswind plume spread (m)
σ_z	Vertical plume spread (m)
ϕ	Mass flux parameter (dimensionless), see Eq. 3-10
ϕ_B	Buoyancy flux parameter (dimensionless), see Eq. 3-1
ϕ_M	Momentum flux parameter (dimensionless), see Eq. 3-12
ϕ_v	Uniform flow momentum flux parameter (dimensionless), see Eq. 3-6
χ	Mass concentration (kg/m ³)

CHAPTER I

INTRODUCTION

The tall stack is employed by industrial operations as an economically viable technique for disposal of pollutants. Stacks are designed to be high enough so that pollutants are sufficiently diluted by the atmosphere when they reach the ground. The adverse or favourable aspects of plume behaviour in influencing the design height of stacks was investigated in this study.

At present three general approaches are available for investigating plume behaviour. They are:

1. To measure full scale plumes in the atmosphere.
2. To numerically simulate plumes.
3. To measure model plumes simulated in the laboratory.

Studies into the behaviour of full scale plumes have the advantage that physical processes are being measured without any modelling approximations. However, the observation and measurement of plumes in the field is very difficult because of the uncontrolled variability of atmospheric conditions during a test. Measurements that require specific conditions or long time averages are difficult to obtain. The physical size of a plume in the atmosphere also requires expensive equipment for measurements at substantial heights, typically

100 m above ground.

Numerical simulations allow the testing of different formulations for flow behaviour but still require comparison to data. At present the flow around the complex geometries in the fullscale cannot be practically modelled by numerical methods.

The motivation for modeling plumes in the laboratory stems from the ability to control and reproduce environmental conditions. Scale models, by virtue of their size, are also easily modified so that different geometries or source conditions may be tested. A wind tunnel simulation also allows local effects under complex boundary conditions to be studied.

In the present study a neutrally stable atmosphere was modelled in the wind tunnel. Neutral conditions occur about 40% of the time in the fullscale atmosphere. For large wind-speeds, in a neutral atmosphere, concentration levels at ground can be as high as those encountered under other undesirable atmospheric conditions.

Study Objectives

In the present study, experiments for the investigation of plume rise and plume dispersion were conducted in a wind tunnel. The results are applicable to a neutrally stable atmospheric condition. Six different areas were investigated.

1. Wind Tunnel Modelling

The greatest concern in wind tunnel experiments was ensuring that a model plume exhibits the same behaviour as the

full scale system. The simulation of mean and turbulent quantities in the atmosphere and the consideration of similarity parameters such as Reynolds number is required. Modeling of buoyant plumes also requires consideration of momentum and buoyancy effects in the plume.

Different approaches to plume modeling are available in the literature. The investigations of Melbourne (1968) and Isyumov et.al. (1979) reflect the modeling of buoyant forces in a unit volume. Ludwig and Skinner (1976) require the modeling of buoyant forces emitted per unit time. Hewett et.al. (1971) and Hoult et. al. (1977) model both the buoyant force and the buoyant forces per unit time but neglect any effects of plume momentum.

In the present study, source conditions such as stack gas density and efflux velocity were adjusted following systematic scaling expressions to determine the accuracy of scaling.

2. Plume Rise in the Atmosphere

The rise of a buoyant plume in the atmosphere has a strong effect on ground level concentrations. To accurately model this effect required the consideration of plume rise due to the initial upward momentum of stack gas and that due to buoyant forces. An expression that combines these effects was suggested by Briggs (1975). Briggs found the expression correlated well with laboratory data of Fan (1967). To

determine the nature of plume rise in a neutral atmosphere, experiments with different plumes were conducted in a simulated atmospheric boundary layer.

The rise of a plume in a turbulent environment is limited. The termination of plume rise is important due to the strong dependence of ground level concentrations on rise. To account for this effect expressions have been proposed by the A.S.M.E. Task Group (1973) and Briggs (1975) which predict the downwind position where plume rise terminates. In the present study, experiments were done to determine the downwind position of this final rise in an atmospheric boundary layer and to correlate this distance with stack conditions.

3. Buoyancy Induced Plume Spread

The plume spread is due to the entrainment of ambient air into a plume. Entrainment also has a strong influence on both plume rise and ground level concentration.

One component of this spread is due to buoyant forces generating turbulence which enhances the initial growth of the plume. Pasquill (1976) suggests a correlation based on plume rise to account for added plume spread due to buoyancy. To measure the buoyancy induced spreading of a plume, experiments were carried out in a laminar crossflow so that there was no spread due to background turbulence. These spreading rates will be compared to those in an atmospheric boundary layer to determine the interaction of atmospheric turbulence with buoyancy induced turbulence.

4. Effects of Wind Shear

The higher velocities that a plume encounters as it rises in a boundary layer shear flow causes the plume to bend over more than a plume in a flow with uniform velocity.

Djurfors and Netterville (1978) proposed an expression for the decrease in plume rise due to the wind shear present in an atmospheric boundary layer. In the present study the local wind velocity at the local plume height was also used in an attempt to predict the drop in plume rise due to wind shear. To test these theories a plume was released in uniform velocity grid wake turbulence and the rise compared to that in a turbulent boundary layer.

5. Effects of Turbulence in the Approach Flow

The background turbulence in an approach flow eventually causes a plume to break up into smaller components. This affects the rise and dispersion, which in turn determines ground level concentrations. The effect of background turbulence was studied here by conducting plume experiments in grid wake turbulence and a laminar crossflow.

6. Effect of Turbulence in the Stack Gas

Intuitively one would not expect turbulence in the stack gas to strongly affect plume spread because atmospheric and buoyancy induced turbulence are likely to dominate plume behaviour. No information on the effect of stack gas

turbulence is available in the literature. To study this parameter, plumes with both laminar and turbulent stack gas were released in the same approach flow.

CHAPTER II

EXPERIMENTAL PROCEDURE

2.1 Wind Tunnel Facility

The measurements were made in a closed circuit wind tunnel with a fixed blade pitch fan powered by a 200 horsepower direct current electric motor. The wind tunnel is located in the Mechanical Engineering Building at the University of Alberta. The test section was 11 meters long and had a fixed cross-section 1.2 meters high by 2.4 meters wide. The ability of this wind tunnel to operate at low speeds made it suitable for plume rise studies. The absence of temperature control equipment restrict studies to modeling a neutral atmosphere in this facility. Fig. 2-1 illustrates the wind tunnel facility and indicates the elements necessary to develop a simulated atmospheric boundary layer in the test section.

2.2 Velocity Measurements

The required velocity measurements were:

1. To evaluate the mean velocity and turbulent structure in a simulated atmospheric boundary layer.
2. To determine the mean velocity and turbulence intensity in grid wakes.
3. To measure the mean velocity and turbulence intensity of vented stack gas across the outlet of model stacks.

4. To continuously monitor mean velocity in the wind tunnel for all experiments.

In the present study hot wire and hot film sensors were used to measure velocity. The probes were calibrated in a nozzle tipped chamber that was calibrated over various velocity ranges. Air was passed through a stilling chamber and entered a pipe of large cross-section after which it passed through a small nozzle. Good accuracy was obtained by relating the large velocities in the nozzle to the very low velocities in the pipe where the sensors were located. For velocities between 0.3 and 2.0 m/sec, sensors could be calibrated to give accurate readings within $\pm 2\%$ of the measured velocity.

Initial measurements of turbulence were made using a Disa Type 55D01 constant temperature anemometer with single and x-type hot wires. Later a Thermo-Systems Inc. (TSI) model 1050 constant temperature anemometer was available and made possible the use of hot film probes. Fig. 2-2 shows a schematic of the apparatus used to obtain mean and turbulent velocity measurements.

For measurement of mean velocity in the wind tunnel a Kurtz model 435 hot film anemometer was employed. An analog voltage output allowed velocity to be read within a constant factor. This factor was adjusted for daily variations in temperature and atmospheric pressure. The sensitivity of buoyant plumes to freestream velocity required continuous

monitoring of mean velocity by the Kurtz probe in all experiments. Typical mean velocities ranged between 0.3 and 1.0 m/sec and could be measured within an accuracy of $\pm 2\%$.

The use of hot wires or hot films depended on the application. Hot films have less error due to flow disturbance around the sensor supports, and are more durable due to their larger physical size. Hot wires, however, provide faster time response and finer spatial resolution. The time response and spatial resolution required for wind tunnel measurements was met by a hot film. As discussed later, the measurement of velocity across the outlets of model stacks required the use of a hot wire to obtain as fine a spatial resolution as possible.

2.3 Concentration Measurements

The buoyant plumes modelled in the present study required a stack gas comprised of helium and air so that the proper stack gas density could be obtained. Helium also acted as the tracer gas for concentration measurements in the plume.

The concentration detector was a four-arm thermal conductivity bridge which aspirated samples continuously from the wind tunnel. To compensate for the buildup of helium causing background concentration levels in the wind tunnel, a reference line was placed upstream of the stack. The sample line was attached to a probe mounted on a motor driven traverser and passed through the plume. The net concentration

in a plume was reflected by a bridge imbalance resulting from concentration differences between the sample and reference streams. A chart recorder was used to continuously display bridge output, which was simultaneously averaged on a Hewlett Packard 5326B counting voltmeter with a resolution several orders of magnitude greater than the accuracy of the concentration calibration. Low noise amplifiers were used when concentration levels were small. For typical concentration measurements of 1000 ppm the amplifiers had a noise level of about 10 ppm. Gains of 1, 10, 100 and 1000 were used. The equipment for generating model plumes and measuring their concentration is shown by the schematic in Fig. 2-3.

By using calibrated rotameters to mix helium and air, streams of known concentration were introduced into the sample line and the bridge output measured. The results showed that the relation between concentration levels and voltage output from the bridge was linear within $\pm 0.5\%$. Including errors from all sources the accuracy of concentration measurements was about $\pm 3\% \pm 20$ ppm.

To measure concentration in the wind tunnel within $\pm 10\%$ of the mean value required 400 second time averages. A zero reading was taken before and after each concentration measurement to compensate for any zero drift in the detector.

2.4 Volume Flow Measurements

In preliminary experiments rotameters were used to set the flow rates of helium and air, and the total flow rate

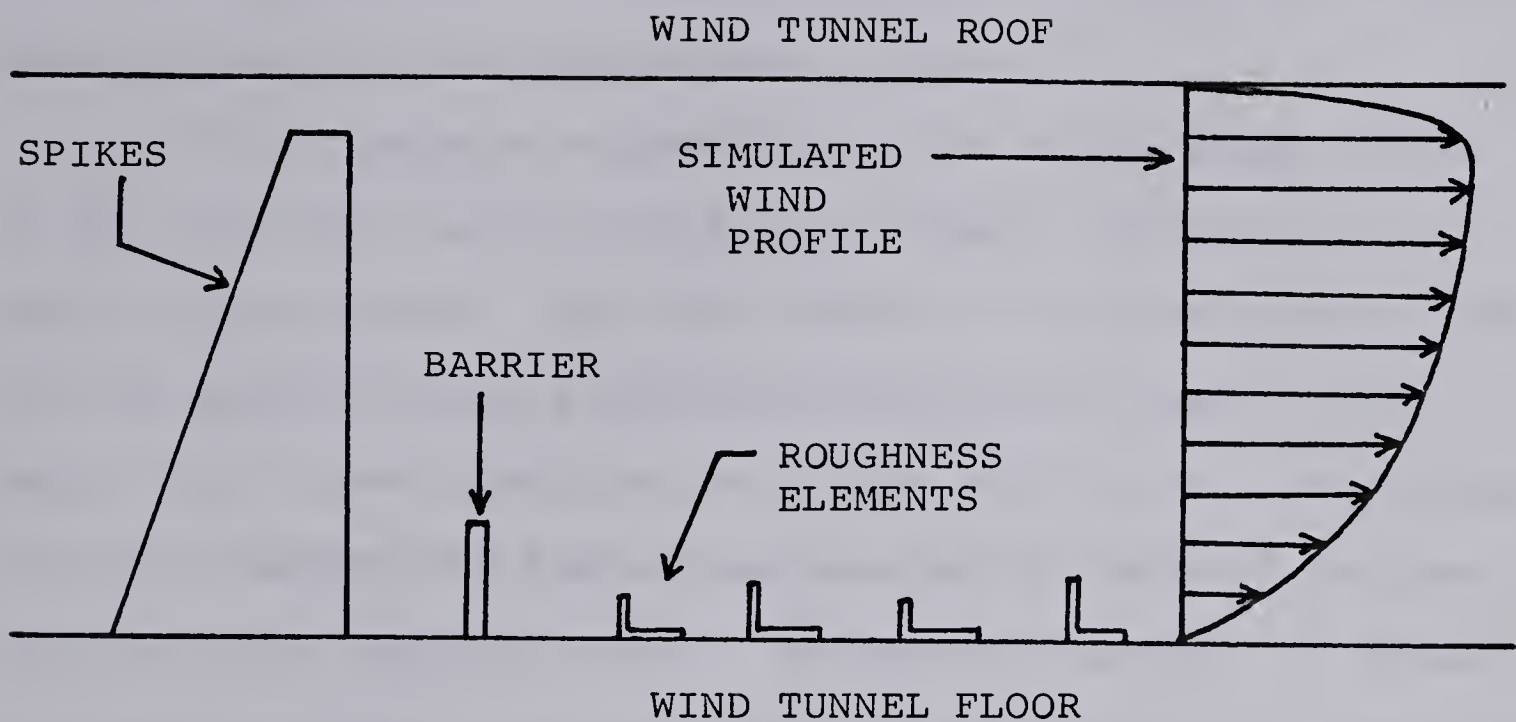
was checked by a dry gas meter as shown in Fig. 2-3. However, for the last half of tests performed, the rotameters were replaced by dry gas meters to improve the resolution and accuracy of volume flow.

The Singer model DTM-115 dry gas meters were checked for calibration using a gasometer. The gasometer used positive displacement of oil from a container of known volume to indicate volume flow. A Precision Scientific Wet Test Meter was used as a second check. Results agreed within 0.5% for flow rates between 1 and 20 liters per minute.

Fig. 2-4 illustrates the apparatus for measurements of volume flow, velocity and concentration.

2.5 Simulation of the Atmospheric Boundary Layer

The modeling of buoyant plumes in the laboratory requires the simulation of the atmospheric boundary layer if results are to apply to full scale plumes. To obtain the correct combination of velocity shear, turbulent velocities and flow uniformity requires the trial and error adjustment of the elements shown in the following sketch. The process is not totally random, however, if the dominant effects of each element is understood.



The triangular turbulence generators or spikes interact with the approach flow to form turbulent vortex motions with vertical axes of rotation. These spikes are sufficiently high to generate turbulence in the upper portion of the boundary layer. Adjusting the angle of attack for each of the seven spikes used in this study proved to be effective in establishing lateral uniformity.

The barrier wall consists of a wall topped with a coarse wire mesh. The barrier is a source for turbulent vortex motions in the crosswind direction and is about $1/7$ of the height of the spikes. This is a formidable obstruction in the approach flow and causes the high turbulence levels and large momentum losses required for rapid development of the boundary layer near the wind tunnel floor. The height of the barrier wall is

adjusted to produce the correct velocity shear and turbulent shear stresses in the region near ground.

The roughness elements are flat sharp edged plates of two different heights that are randomly distributed on 1.2 meter square panels. The same number of elements were placed on each panel so that a pseudorandom pattern results when panels are placed side-by-side in the wind tunnel. The elements provide a source for turbulence generation downwind and can also influence the velocity shear. Adjustment consists of adding or removing roughness elements. Variation in height may also be required. The sharp edges on roughness elements result in separation points and wake structure being insensitive to changes in Reynolds number.

Due to a Reynolds number mismatch, the size of roughness elements is exaggerated to produce a proper match in turbulence properties. The geometric scale of 800:1 and the velocity scale of 30:1 results in a Reynolds number mismatch by a factor of about 24,000 between model and fullscale. Small scale turbulent eddies are not modelled in the wind tunnel due to the large differences in Reynolds number. Fortunately, these eddies are not expected to actively participate in the diffusion of a plume.

The configuration of spikes, barrier, and roughness for the present study is illustrated in Fig. 2-5.

In order to match the boundary layer in the wind tunnel with that in the full scale requires some information

on the magnitude of quantities as they exist in the atmosphere. Wilson (unpublished) uses the full scale data of Counihan (1975) to compare with the simulated boundary layer in the present study. As shown in Table 2-1 the comparison consists of matching parameters that uniquely identify the characteristics of a turbulent flow, for a given roughness length z_o . Agreement is good in all cases except for the magnitude of crosswind and vertical fluctuation levels, which are smaller in the wind tunnel. This is partially due to the restraining effect of the wind tunnel walls, but values are still lower than expected. As shown in Chapter V, the deficit in crosswind and vertical fluctuations has no noticeable influence on dispersion results.

Fig. 2-6 shows the mean velocity and turbulence structure for the simulated atmospheric boundary layer in the present study. The variation in data for Reynolds stress suggests that the averaging time was too short to define the cross correlation. Averaging times of 100 seconds were used for all quantities shown in Fig. 2-6.

2.6 Wind Tunnel Experiments Behind Grids

The apparatus for plume rise experiments in grid wake turbulence is illustrated in Fig. 2-7.

To investigate the effects of velocity shear on plume behaviour required an approach flow with uniform mean velocity and turbulent fluctuation levels similar in magnitude to those in the boundary layer. An approach flow with these

TABLE 2-1

COMPARISON OF WIND TUNNEL BOUNDARY LAYER WITH FULL
SCALE ATMOSPHERIC DATA OF COUNIHAN (1975)
FROM WILSON (UNPUBLISHED)

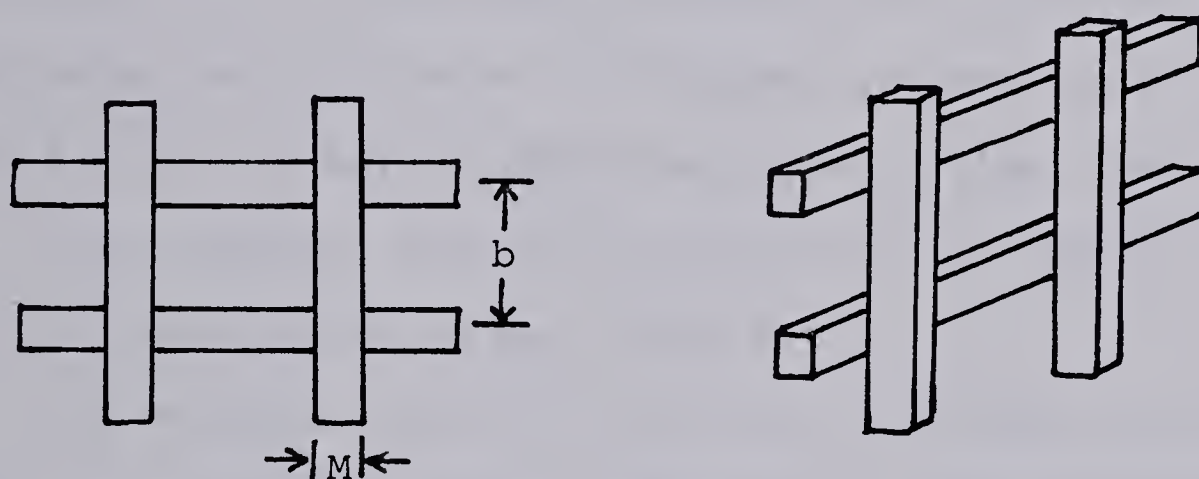
Parameter	Wind Tunnel 800:1 Scale	Full Scale Neutral Stability with same Z_0
Roughness height, Z_0	0.4m	Fixed at 0.4m
Mean velocity power, n	0.18 $Z < 160m$ 0.28 $Z > 160m$	0.20 ± 0.30
Boundary layer thick- ness, δ	600 - 700m	600m (approx.)
$\overline{\left(\frac{u}{u_w}\right)^2}^{0.5}$ @ 30m	1.94	1.9
$\overline{\left(\frac{v}{u}\right)^2}^{0.5}$ @ 30m	0.53	0.75 ± 0.15
$\overline{\left(\frac{w}{u}\right)^2}^{0.5}$ @ 30m	0.41	0.50 ± 0.1
$\frac{C_f}{2} = \frac{\overline{uw}}{U_\delta^2}$ @ 30m	0.00236	0.00251 ± 0.005
$\sqrt{\frac{u}{U}}^2$ @ 30m	0.17	0.20 ± 0.03
Integral Scale, Λ_X	150m @ $Z = 30m$ 180m @ $Z = 160m$	$130m \pm 50$ $200m \pm 50$
$\frac{\overline{uw}}{\overline{u^2} + \overline{v^2} + \overline{w^2}}$ @ 100m	0.17	$0.14^1 \pm 0.01$

¹Data from Hinze (1975) p. 729.

characteristics was obtained by placing bars in a grid pattern across the wind tunnel.

The flow behind grid networks is well documented in the literature. In the present study the results of Baines and Peterson (1951) were used to design a grid with the required characteristics.

The experiments of Baines and Peterson applied to grids with square bars and a square mesh as shown in the following sketch. The bar width is "b" and "M" is the mesh length.



The data in Fig. 2-11 indicates that the turbulence intensity $\sqrt{\bar{u}^2}/U$ is about 0.12 at stack height in the atmospheric boundary layer. Grid dimensions were computed using correlations of Baines and Peterson (1951) to produce approximately this value at a distance of 10 mesh lengths downstream, which is a minimum distance for flow development. A large bar size was required to generate this level of turbulence at typical downwind distances in the wind tunnel. This in turn led to substantial

blockage of the wind tunnel as reflected by solidity ratio "S" which relates the total area of the bars to the total area of the screen. The relevant grid dimensions were chosen as $b = 7.6$ cm. and $M = 30.5$ cm. so that $S = 0.44$ and the calculated turbulence intensity becomes 0.10 at 10 mesh lengths downstream.

One compromise was made in the grid construction. The use of heavy 7.6 cm. square bars was judged as impractical and unnecessary for the present study. The alternative was to use plywood strips of standard 1.9 cm thickness so that the bars become rectangular in cross-section. The grid dimensions are shown in Fig. 2-9. The figure indicates that data for longitudinal decay of turbulence is in good agreement with the predicted curve of Baines and Peterson with their data scatter shown. This suggests that the turbulent field behind a grid is relatively insensitive to bar thickness.

The solidity ratio $S = 0.44$ had no effect on flow uniformity due to possible flow instability. Fig. 2-10 shows that mean velocity in the plume layer was reasonably constant. LT012 is used to classify the data plotted on this graph. The regions of higher velocity fluid outside the plume layer indicate that in fact the shear was slightly negative in the plume layer.

Fig. 2-11 shows the turbulence intensity profiles in the simulated atmospheric boundary layer and at the stack location in grid wake turbulence. Because the plume rises about 16 cm through the boundary layer, the local turbulence intensity was observed to decrease from 0.13 to about 0.10.

This occurs over a downwind distance of about 2 meters from the stack and corresponds to a normalized downwind distance of about $x/b = 60$ behind the grid. Fig. 2-9 shows that turbulence intensity drops from 0.10 to about 0.06 in this region. This is somewhat more than the change of 0.03 that occurred as the plume rose through the boundary layer. The diffusion study in Chapter V, however, indicates that this had no significant effect on plume dispersion.

2.7 Velocity Measurements Across Stack Exit

The correct modeling of stack gas momentum effects required the measurement and adjustment of velocity profiles across the model stack exit.

As the model stack diameter was only 1.0 cm it was important to have good spatial resolution of probe position. For this reason hot wire probes rather than hot film probes were used to measure velocity. The stack was clamped in a horizontal position and vertical sweeps were made across the stack exit by mounting the hot wire probe on a vernier traversing mechanism. A resolution of about 0.01 cm. in probe position was achieved.

The stack was enclosed in a chamber with 30 cm x 30 cm cross-section to prevent errors in velocity measurement due to drafts in the laboratory.

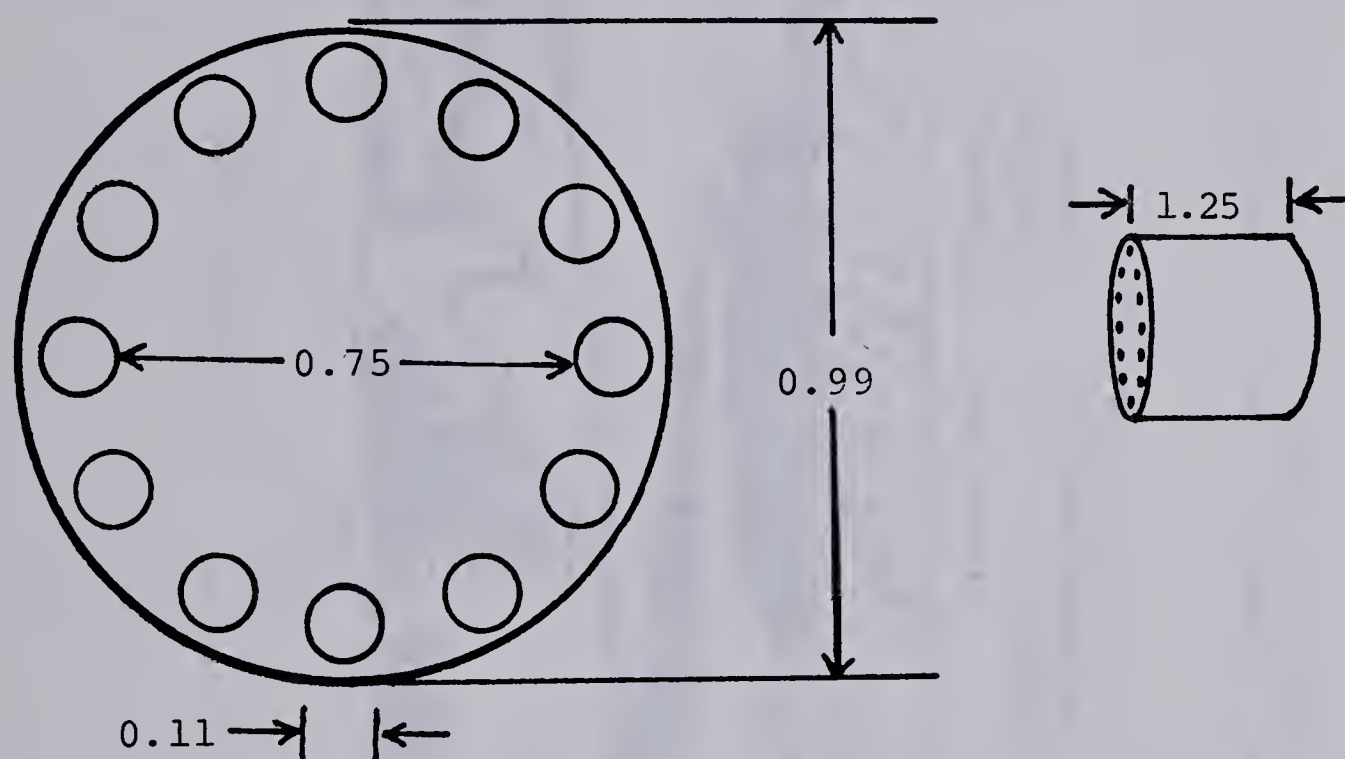
Experiments with model plumes required a stack gas comprised of a helium-air mixture. The hot wires, however,

were calibrated in air and are sensitive to changes in fluid properties which affects the heat transfer around the probe. To avoid this problem pure air was used as the stack gas during the velocity profile measurements. The mean velocity of the stack gas was kept the same so that using pure air gave Reynolds numbers about twice as high the value of 300 for model tests with helium-air mixtures. Both cases are well within the laminar flow regime for pipes.

To check the accuracy of measurements, velocity data were obtained for $R_e = 600$ in the model stack. Comparison of data to the known parabolic shape of a laminar velocity profile showed good agreement and supported the accuracy of probe positioning. Once satisfied that profile shape could be experimentally determined, efforts were made to make the velocity profile more uniform across stack exit to simulate a turbulent stack gas. The procedure adopted was initially suggested by Hewett et al. (1971) who used a circular plate with 4 small holes to form turbulent jets that expanded to fill the cross-section. Fig. 2-8 shows various plugs tested in this study. Small wire screens with varying solidity ratio were also tested, but they did not perform as well as the plugs.

Experiments soon indicated that plugs with very small holes near the stack wall gave the best results when placed 3.5 diameters from the stack exit. Plugs with large holes, disks centered on flow straighteners and screens were sensitive to

alignment and produced unsymmetrical velocity profiles. The final plug design is shown in the following sketch. The plug was placed in the stack and the distance to stack exit adjusted to produce the desired velocity profile.



DIMENSIONS IN CM

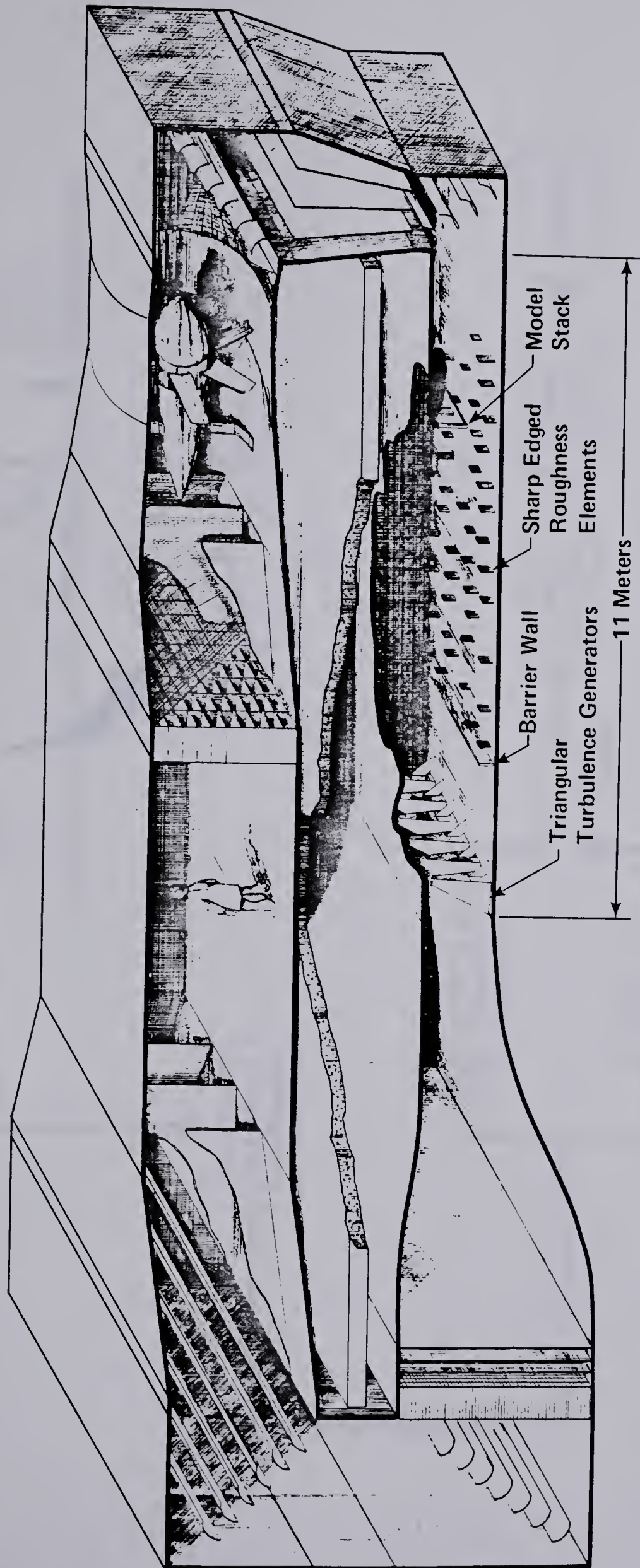


Fig. 2-1 Wind Tunnel Facility and Elements Used to Generate a Simulated Atmospheric Boundary Layer

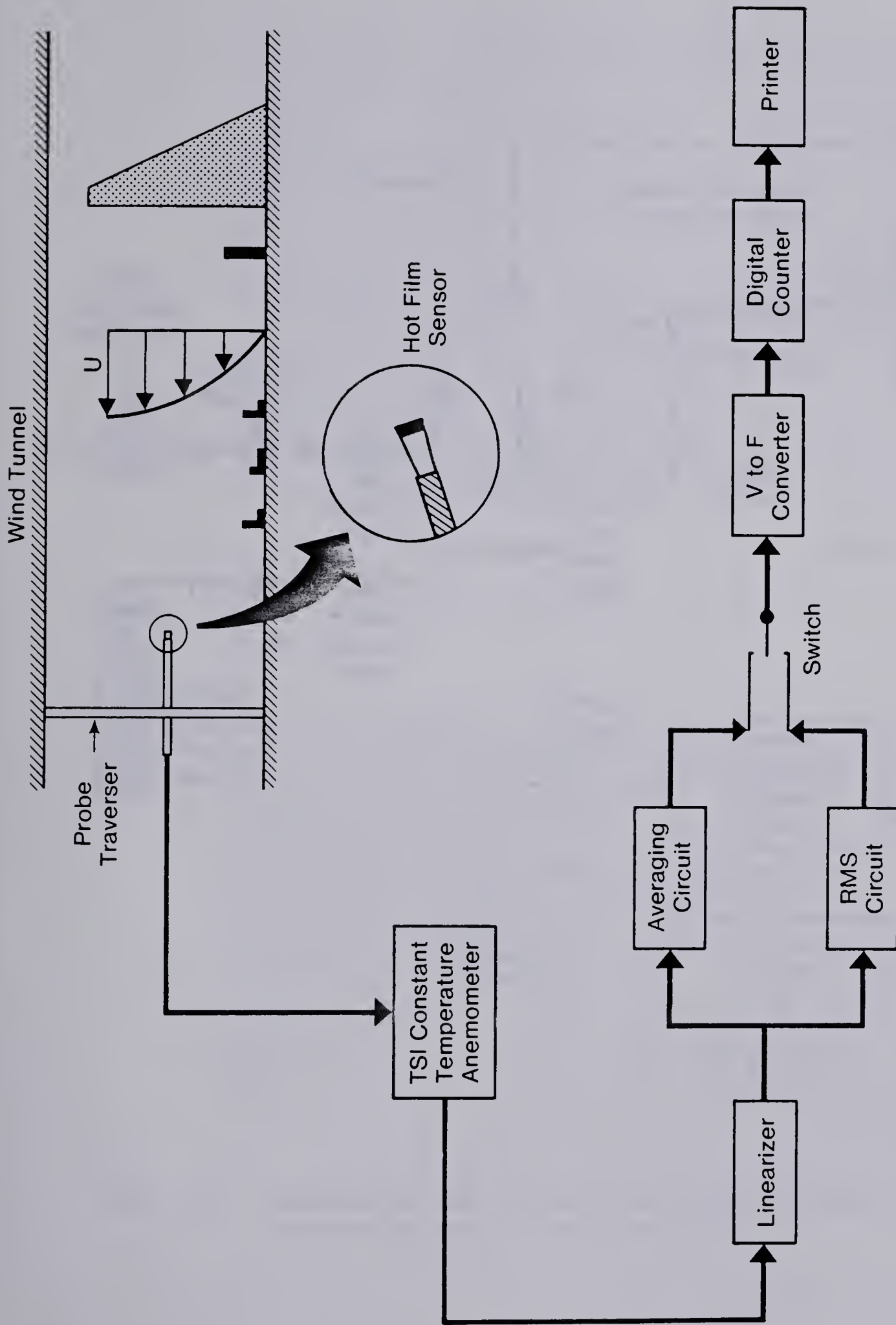


Fig. 2-2 Apparatus for Measurement of Mean and Turbulent Velocities

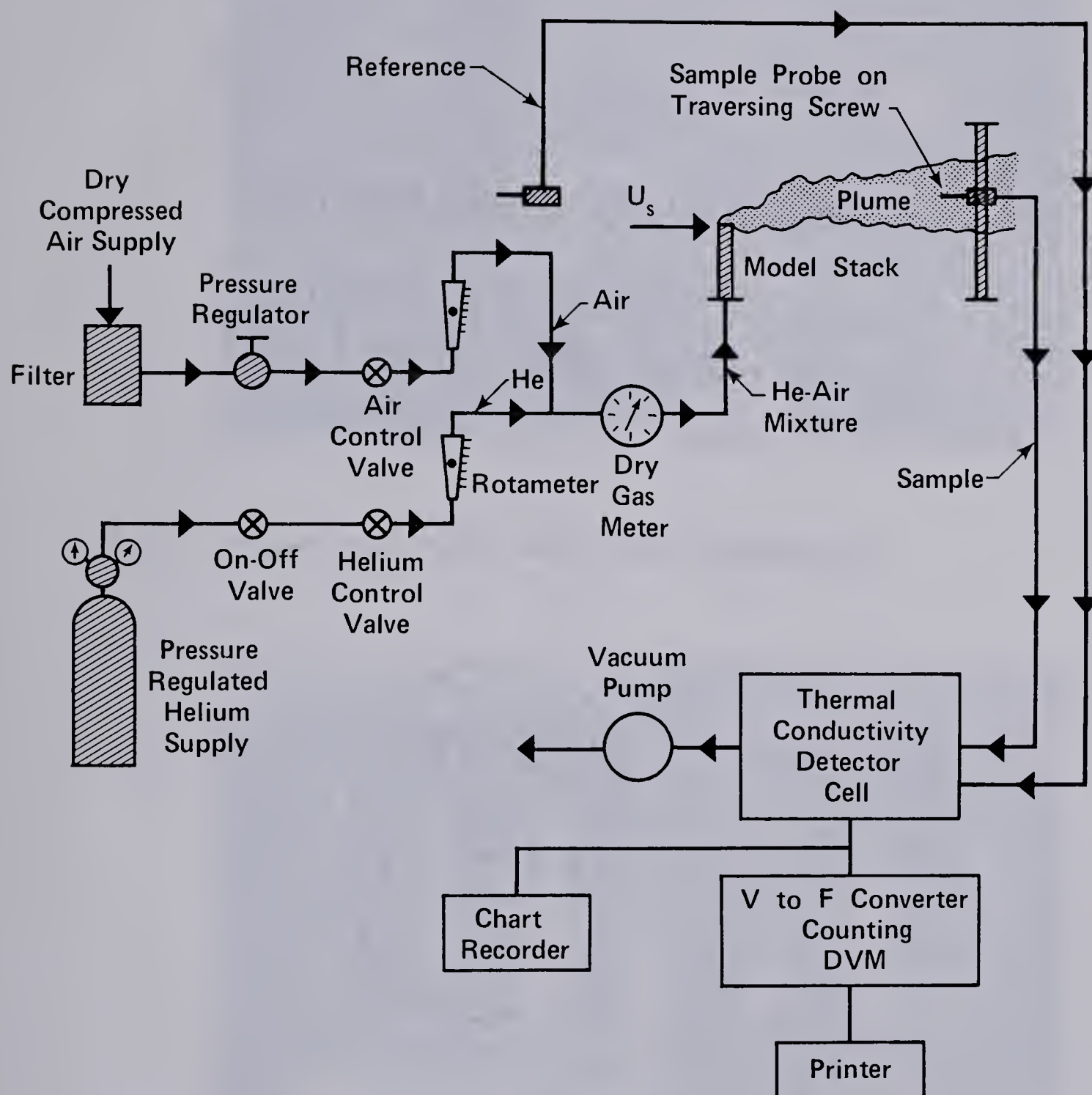
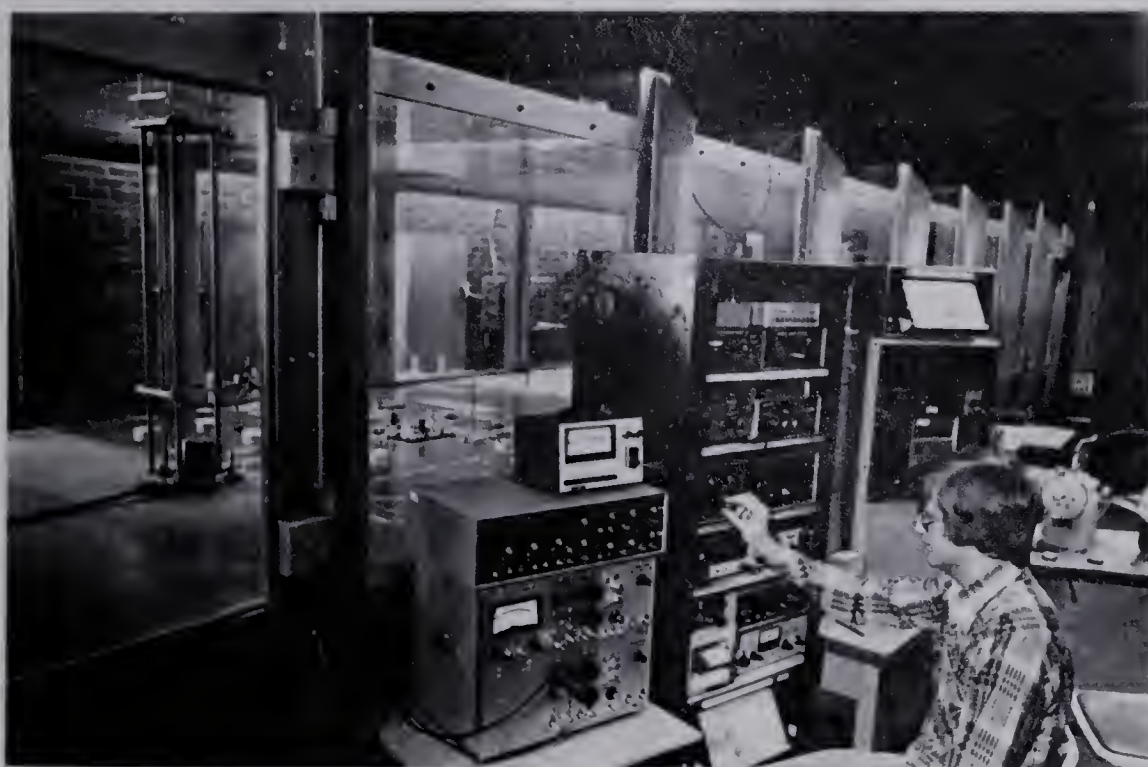
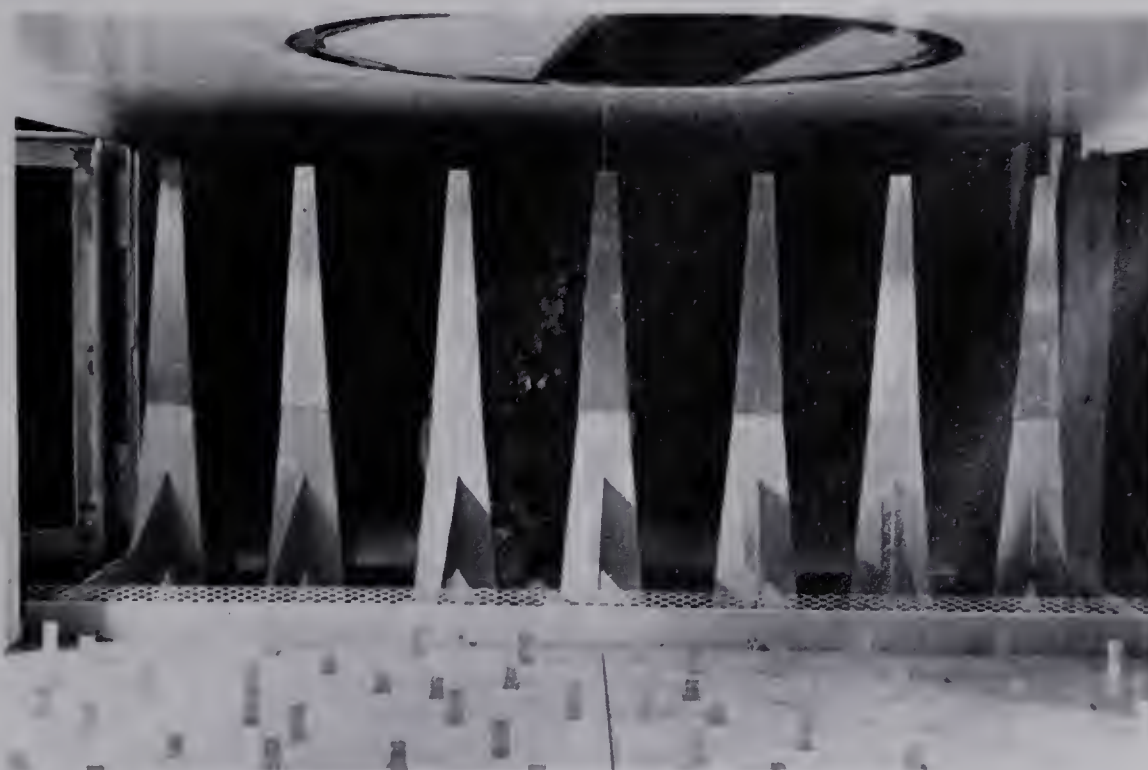


Fig. 2-3 Apparatus for Generating Model Plumes and Measuring Their Concentration



2-4 Probe Traverser and Instrumentation



2-5 Spikes, Barrier and Roughness used in the Simulation of an Atmospheric Boundary Layer

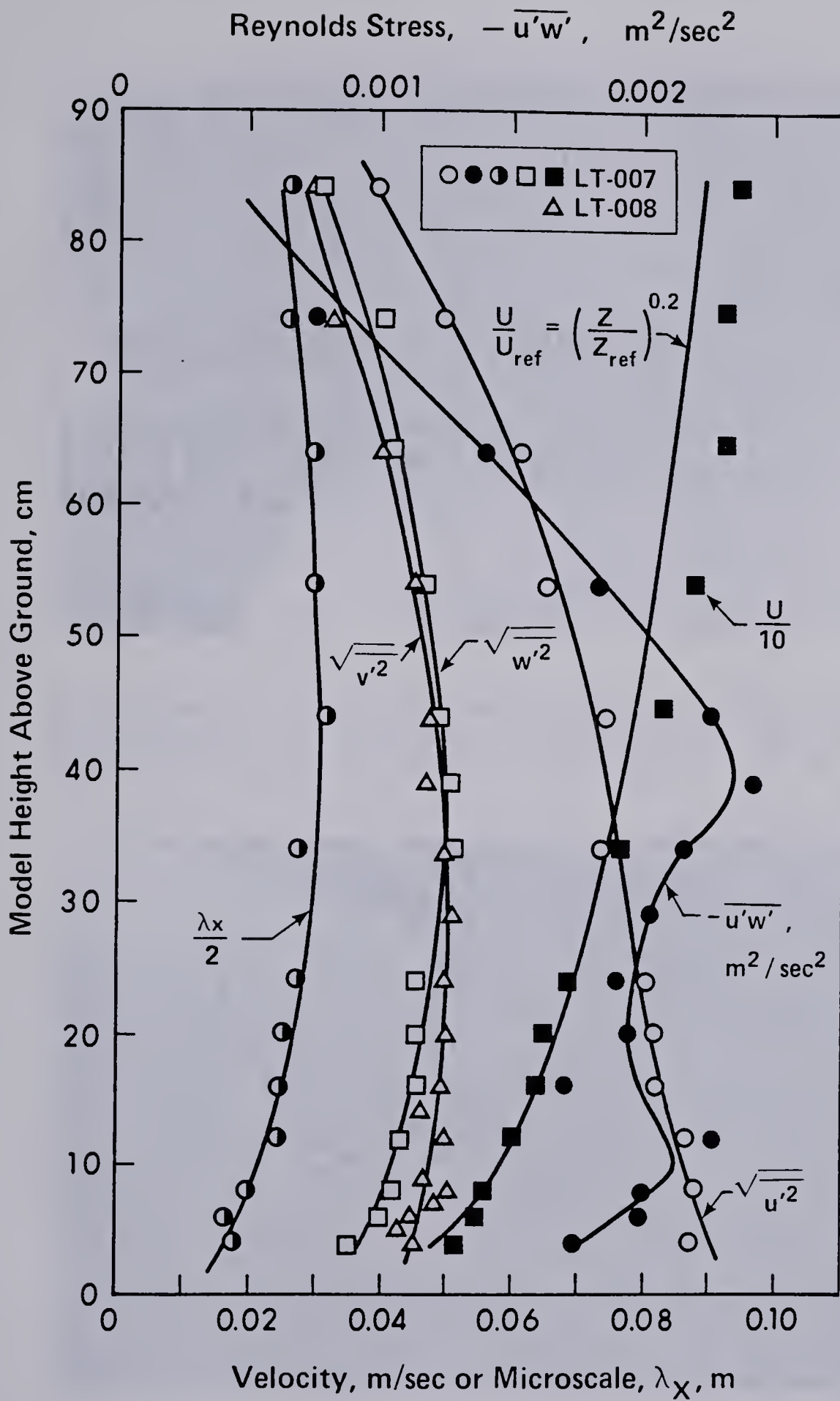
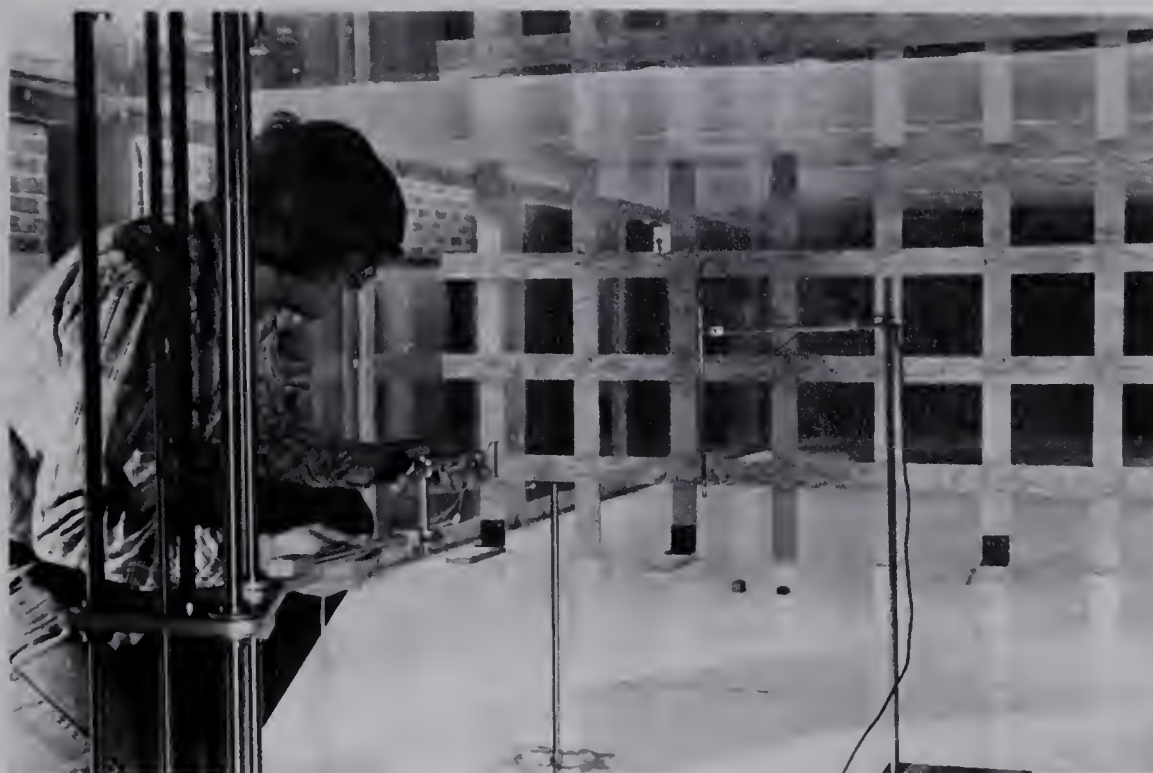


Fig. 2-6 Mean Velocity and Turbulence Structure of Simulated Atmospheric Boundary Layer



2-7 Adjustment of Concentration Sample Probe for Experiments in Grid Wake Turbulence. The Kurtz Hot Film Probe is Shown to the Right of the Stack.



2-8 Plugs Used in Modifying the Velocity Profiles of the Stack Gas

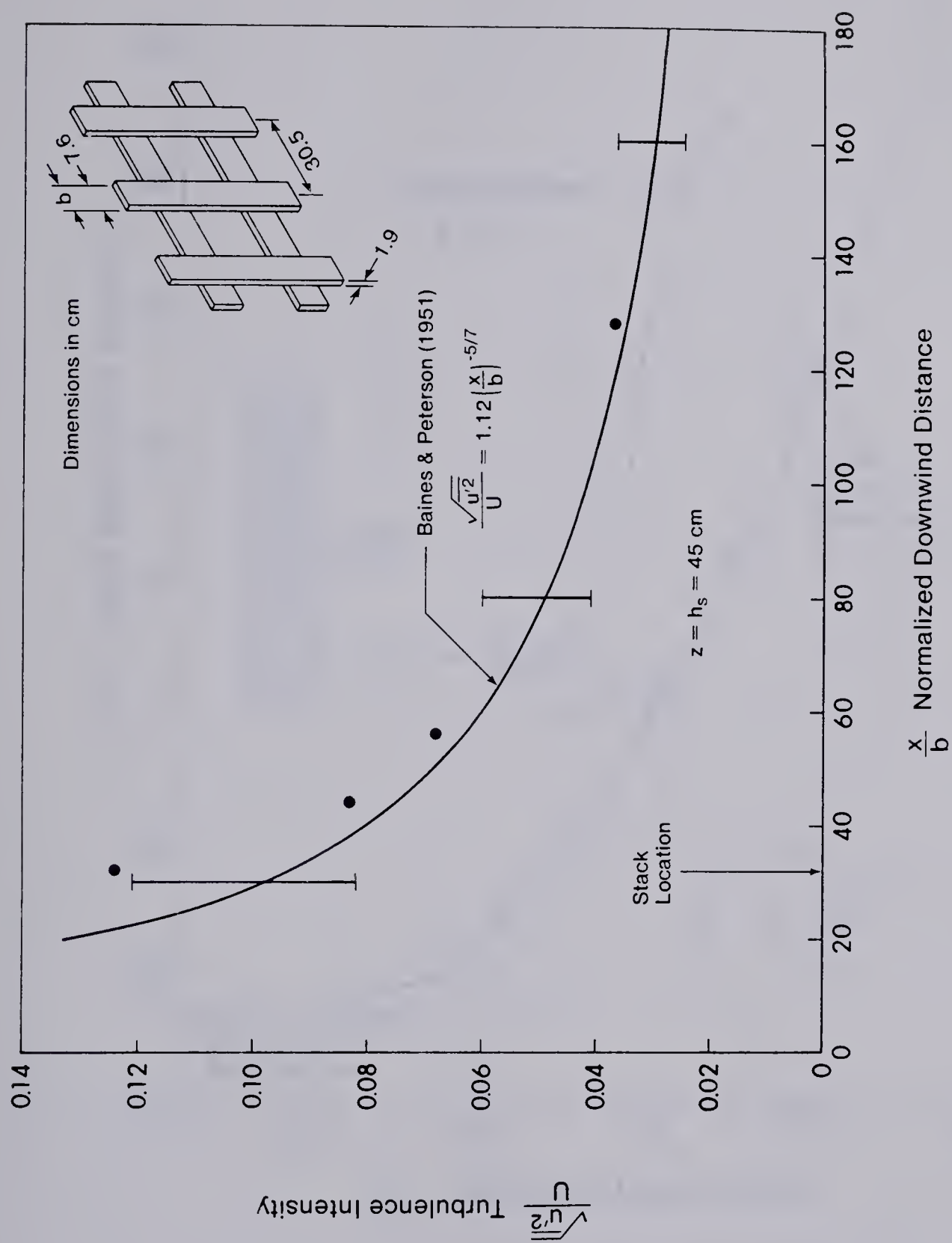


Fig. 2-9 Decay of Grid Wake Turbulence

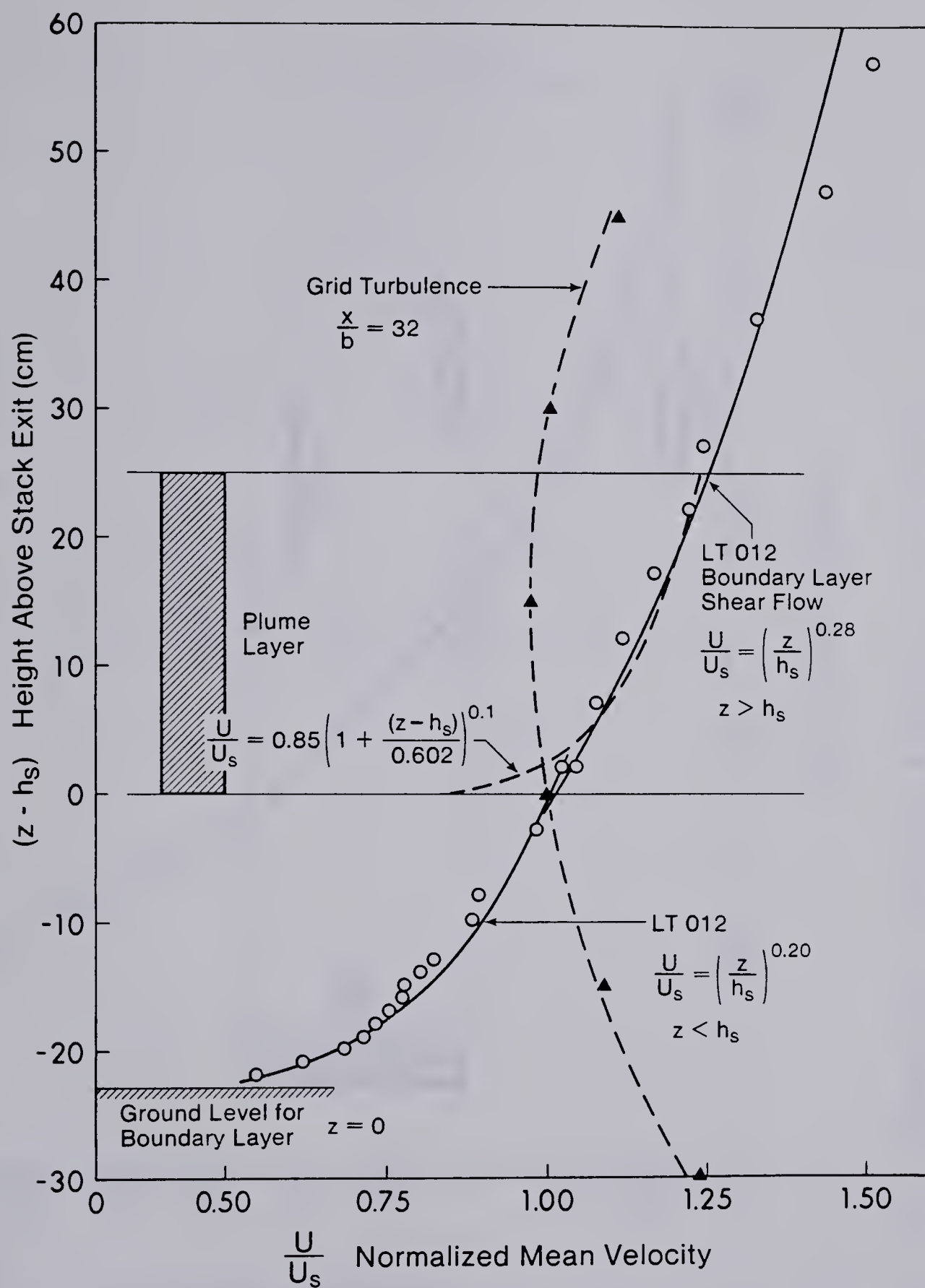


Fig. 2-10 Mean Velocity Profiles in Boundary Layer Shear Flow and Grid Wake Turbulence

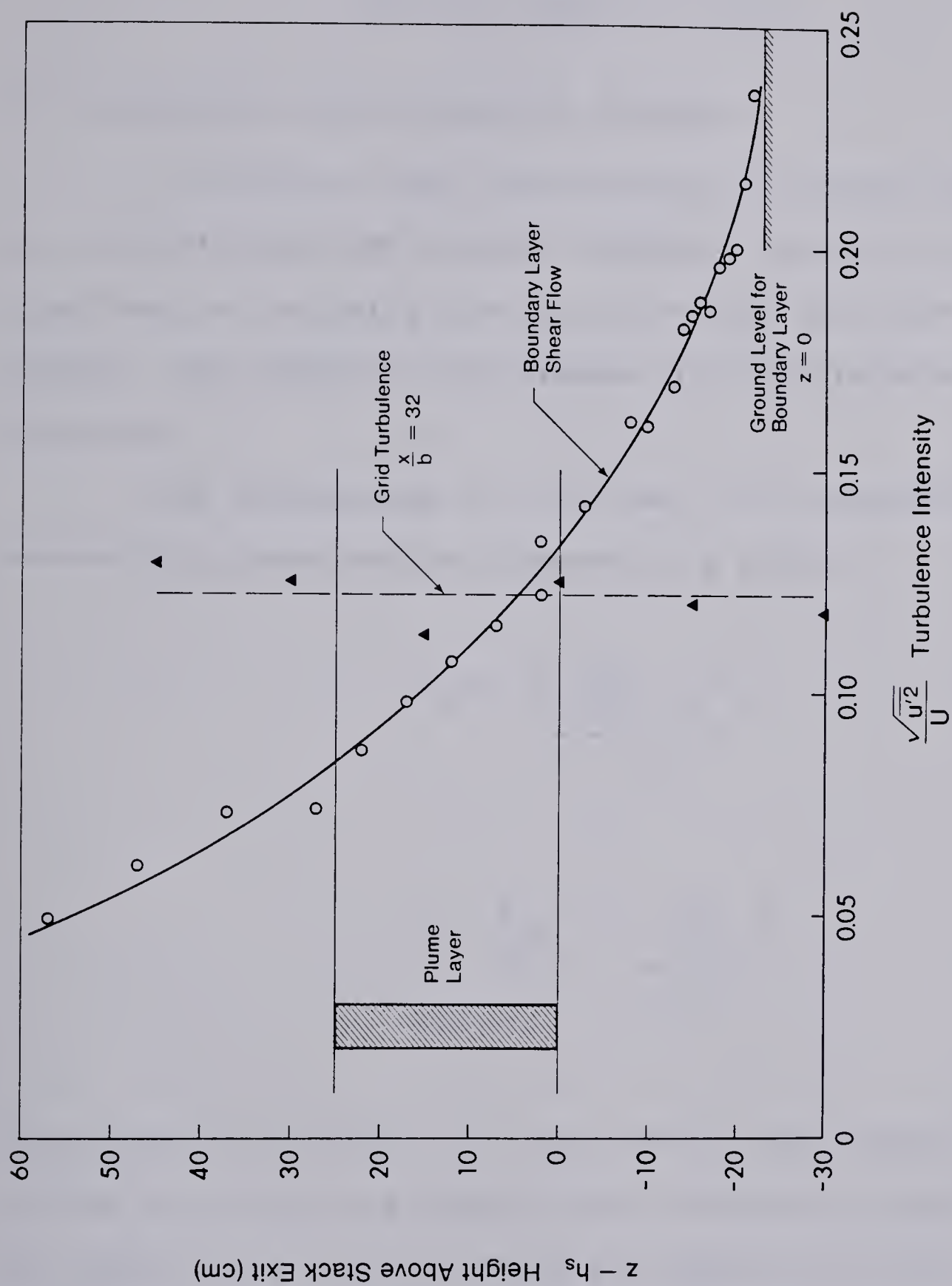


Fig. 2-11 Turbulence Intensity Profiles in Boundary Layer Shear Flow and Grid Wake

CHAPTER III

MODELING BUOYANT PLUMES

3.1 Similarity Parameters for Buoyancy

In Chapter I the introduction to buoyant plume modeling demonstrated that several different parameters were important in obtaining similarity between model and fullscale plumes. The physical significance of these parameters will now be discussed.

The expressions in (3-1) and (3-2) represent parameters that describe the buoyancy in a plume.

$$\phi_B = \frac{g \left(\frac{\Delta \rho}{\rho_a} \right) W_s R_s}{U_s^3} \quad (3-1)$$

$$R_i = \frac{1}{F_r^2} = \frac{g \left(\frac{\Delta \rho}{\rho_a} \right) d}{U_s^2} \quad (3-2)$$

Note that the buoyancy of a full scale plume largely depends on the high stack gas temperatures lowering the density. In the wind tunnel the same stack gas density is used, obtained by using a light gas such as helium. The implied assumption is that self-generated turbulence due to buoyancy is the same

whether the buoyancy is due to differences in molecular weight or temperature differences. In other words, temperature transports identically as concentration in a turbulent flow. Hewett et. al. (1971) support this with laboratory measurements of plume rise for heated air plumes and air-helium plumes. No difference in plume behaviour was observed.

The buoyancy flux parameter ϕ_B in (3-1) is the ratio of stack gas buoyant force to stream inertia force per unit time for a mixture of stack gas and entrained air in a volume. This parameter also implies that sufficient entrainment of air occurs to make the concentrations in the plume small, resulting in the density of the plume being close to ambient, ρ_a , in the region of buoyant rise. Equation (3-1) derives its name from the buoyancy flux F_B of a plume where

$$F_B = g \left(\frac{\Delta\rho}{\rho_a} \right) W_s R_s^2 \quad (3-3)$$

F_B represents the buoyant force per unit time per unit mass due to the density difference $\Delta\rho$ between a parcel of stack gas and the ambient fluid. The buoyancy flux is referenced to the ambient density ρ_a .

The buoyancy flux parameter in (3-1) can be thought of as a length ratio. A simple dimensional analysis combines the buoyancy flux F_B and the freestream velocity U_s to form a buoyancy length L_B .

$$L_B = \frac{F_B}{U_s^3} \quad (3-4)$$

Normalizing L_B by a typical length in the model such as the stack radius R_s produces (3-1) so that

$$\phi_B = \frac{L_B}{R_s} \quad (3-5)$$

Equation (3-5) shows that the plume buoyancy may be related to a length L_B which scales in the same way as any other length in the geometry.

The bulk Richardson number R_i in (3-2) can be written as the inverse square of the densimetric Froude number. Multiplying and dividing the expression in (3-2) by $\rho_a A$ shows that R_i is the ratio of buoyant and inertial forces in a volume, in contrast to the force per unit time related by the buoyancy flux parameter. Here "A" represents an arbitrary area.

3.2 Similarity Parameters for Momentum and Mass

The parameter in (3-6) is the ratio of momentum flux per unit area in the freestream to that of the stack gas. The parameter assumes that the velocity profile is uniform for the stack gas and has mean velocity W_s .

$$\phi_v = \frac{\rho_s}{\rho_a} \left(\frac{W_s}{U_s} \right)^2 \quad (3-6)$$

This parameter derives its name from the momentum flux F_v of a plume which is referenced to the ambient density ρ_a .

$$F_v = \frac{\rho_s}{\rho_a} W_s^2 R_s^2 \quad (3-7)$$

The momentum flux F_v can also be combined with the freestream velocity U_s to form a length. The resulting momentum length L_v is given by

$$L_v = \frac{\sqrt{F_v}}{U_s} \quad (3-8)$$

so that

$$\phi_v = \left(\frac{L_v}{R_s} \right)^2 \quad (3-9)$$

The plume momentum length also scales as any other length in the system.

If the efflux momentum of a plume is not high enough the plume can be sucked down the stack by the low pressure region in the stack wake. This is known as downwash. The momentum flux parameter in (3-6) is often called the downwash parameter because it indicates the relative strength of the stack efflux momentum as compared to that in the freestream. The result of downwash is to bring stack effluent closer to

ground so that the effective stack height is reduced. Wilson (1977) recommends that criteria that $\phi_v \geq 2.0$ to prevent downwash. The ability of a model to simulate downwash is discussed later.

The mass flow rate parameter in (3-10) relates the ratio of mass flux in the freestream to that of the stack. "L" is any typical length in the geometry except for the stack diameter d.

$$\phi = \frac{\rho_s}{\rho_a} \frac{W_s}{U_s} \left(\frac{d}{L}\right)^2 \quad (3-10)$$

3.3 Comparison of Modeling Techniques

If the stack gas to ambient density ratio is the same in model and fullscale the similarity requirements in (3-1), (3-2), (3-6) and (3-10) are all satisfied. Cermak (1975) cites the matching of this density ratio as a requirement for exact similarity. However, matching the density ratio requires very low freestream velocities, beyond the capabilities of most wind tunnels. Due to equipment limitations, researchers are then forced to vary the density ratio with the result that not all of the similarity parameters can be satisfied.

The modeling techniques of Melbourne and Gartshore (1975) match the Richardson number, the momentum flux parameter and the mass flux parameter in model and fullscale. This

results in the distortion of length scales between the model and its fullscale counterpart because the stack diameter is scaled differently than other objects in the system. The most serious problem with this approach concerns the modeling of the momentum flux parameter ϕ_v as given in (3-6). Melbourne and Gartshore keep ϕ_v constant in model and fullscale but the parameter ϕ_v requires consistent geometric scaling of length. For distortion of length scales $\phi_v \left(\frac{d^2}{L^2}\right)$ must stay constant so their method is invalid if momentum effects are at all important. The different scaling of stack diameter with respect to the geometry could also misrepresent wake effects behind a stack.

Hoult et. al. (1977) employ a modeling scheme that satisfies both the buoyancy parameters given in (3-1) and (3-2). The method requires that the velocity ratio W_s/U_s is matched in model and fullscale. A serious difficulty with this method is that momentum effects are not considered. The momentum contribution to plume rise and the effect of downwash is not modelled. As a result this method can only be applied to buoyancy dominated plumes with no downwash as for this case errors introduced in the mismatch of momentum flux are relatively small.

The investigations of Isyumov and Tanaka (1979) and Ludwig and Skinner (1976) both employ the momentum flux parameter in (3-6) but differ in the choice of buoyancy parameter. This choice reflects the modeling of either buoyant forces

per unit volume of plume or buoyant forces emitted per unit time. One incentive for the use of the buoyancy flux parameter is the success in characterizing plume rise with buoyancy length as shown in Chapter IV.

3.4 Correction For Non-Uniform Flow at Stack Exit

The momentum flux parameter in (3-6) assumes a constant velocity in the approach flow and across stack exit. The implication is that the average velocity across a section can be used in the calculation of momentum flux. For an approach flow with shear the variation in freestream velocity over the height where momentum rise dominates is usually small and the wind velocity at stack height is appropriate for momentum flux calculations. For the momentum flux of the stack, however, the error in using the average velocity depends on the velocity profile across stack exit.

The kinetic energy correction factor α , as defined in (3-11), must be used to correct the momentum flux when the average velocity across stack exit is used. "A" is the efflux area and w is the velocity at different positions across the stack exit.

$$\alpha = \frac{1}{A} \int_A \left(\frac{w}{W_s} \right)^3 dA \quad (3-11)$$

Fig 3-1 compares α for different velocity profiles. As discussed in Chapter II, the data in this figure is the result of experiments carried out in the present study to determine the magnitude of α .

For the expected fullscale turbulent velocity profiles $\alpha \cong 1.03$, so that it is often neglected in momentum flux calculations. This implies a uniform flow across the stack, so that $\alpha = 1.0$. The modeling of buoyant plumes, however, requires very low freestream and stack efflux velocities for similarity. In wind tunnel experiments α can have a value as high as 2.0 for the laminar flow of the stack gas as shown at the top of Fig. 3-1. In the model special attention must then be given to the velocity profile across stack exit if the momentum contribution is to be modelled correctly.

The parameters ϕ_v , F_v , and L_v all assume a uniform flow across stack exit. To accurately model the momentum flux in a plume requires the use of α in momentum calculations. For the momentum flux parameter in (3-6) substitution of α gives

$$\phi_M = \alpha \frac{\rho_s}{\rho_a} \left(\frac{W_s}{U_s} \right)^2 = \alpha \phi_v \quad (3-12)$$

similarly

$$F_M = \alpha \frac{\rho_s}{\rho_a} W_s^2 R_s^2 = \alpha F_v \quad (3-13)$$

and

$$L_m = \left(\alpha \frac{\rho_s}{\rho_s} \right)^{1/2} \frac{W_s}{U_s} R_s = \alpha^{1/2} L_v \quad (3-14)$$

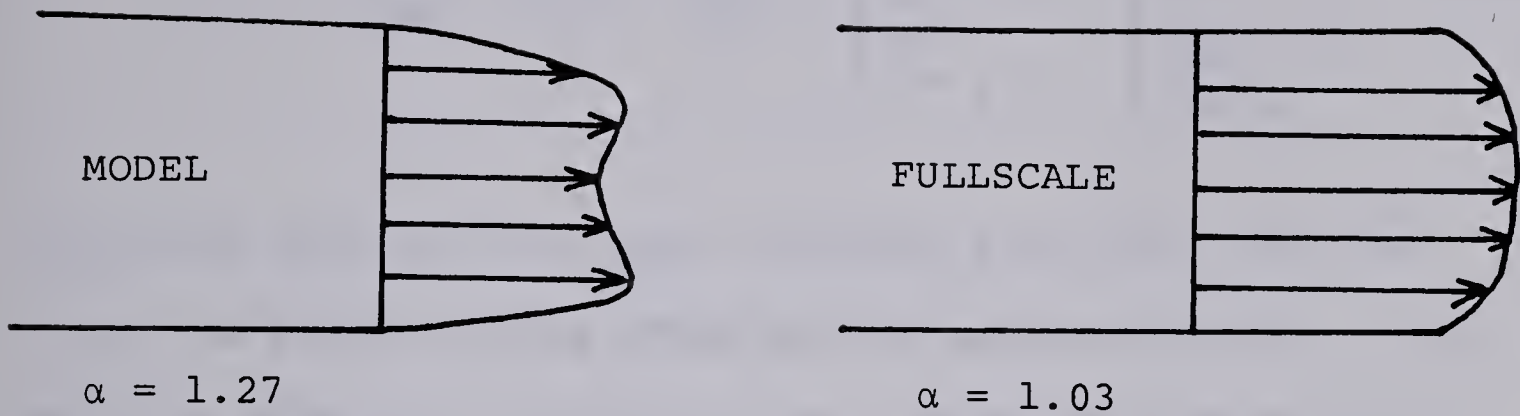
Note that the downwash of a plume is now characterized by ϕ_M , not ϕ_v .

In some modeling investigations the similarity of stack exit velocity profiles were considered. The major concern was that flow in the wind tunnel stack was often laminar where it should have been turbulent. To compensate for this Cermak (1974) suggested roughening the inner surface of the stack to achieve a turbulent exhaust flow. Hewett et. al. (1971) used a circular plate with four small holes to form turbulent jets that expand to fill the cross-section. Their results showed good agreement in plume rise for different stack Reynolds numbers ranging from 156 to 573. However, Hewett et. al. employed the same method as Hoult et. al. (1977) so that momentum flux was not modelled and the study was restricted to highly buoyant plumes. Melbourne (1968) used a sudden expansion 4 diameters from stack exit and covered it with a wire mesh in an attempt to form a uniform and turbulent velocity profile. No data was given to support this approach. Isyumov and Tanaka (1979) used a tip contraction with inside diameter as required by the geometric scaling. However, no value of α was given for the resulting velocity profile and α was not included in momentum flux calculations.

In the present study the velocity profiles were measured at stack exit. Measured velocity profiles are shown in Fig. 3-1 for R_{ed} of about 600. As discussed in Chapter II, different methods were used in an attempt to make the velocity profile more uniform. A plug with 12 small equally spaced holes near the stack wall gave the best results. This velocity profile is the "turbulent model" in Fig. 3-1. The region of slow moving fluid that persists near the stack walls still produces a larger value of $\alpha = 1.27$ than the expected full scale value of 1.03.

The value of $\alpha = 1.27$ is large enough that it must be included in momentum flux calculations. For this reason ϕ_M in (3-12) is used as the momentum flux parameter in the present study. This, however, leads to the result that matching the stack gas to ambient density ratio in model and full scale no longer guarantees exact similarity.

The incorporation of α in the momentum flux parameter requires α to be the same in model and fullscale for exact similarity. As shown in the following sketch fullscale values of α can be matched by forming a saddle-type velocity profile in the model. Unfortunately, it is also important to model the shape of the velocity profile as is discussed later. The turbulent model in Fig. 3-1 is a compromise between velocity profile shape and α .



3.5 Modeling Techniques in the Present Study

The Richardson number and the buoyancy flux parameter cannot both be satisfied when ϕ_M is used as the momentum flux parameter and α is not the same in model and fullscale. In the present study the buoyancy flux parameter in (3-1) is used as the similarity variable for the effects of buoyancy in a plume. The choice reflects the importance of dynamic similarity for a continuous plume in crossflow. Further, the success in characterizing plume rise with the buoyancy length implies that it must scale as any other length in the geometry. Equality of ϕ_M and ϕ_B between model and fullscale produces the following modeling equations. The subscripts "m" and "f" denote model and fullscale values respectively.

$$\frac{U_{sf}}{U_{sm}} = \left[\frac{d_f}{d_m} \right]^{1/2} \left[\frac{\alpha_m}{\alpha_f} \right]^{1/4} \left[\frac{\frac{\rho_s}{(\rho_a)_m}}{\frac{\rho_s}{(\rho_a)_f}} \right]^{1/4} \left[\frac{\frac{(\Delta\rho)}{\rho_a}_f}{\frac{(\Delta\rho)}{\rho_a}_m} \right]^{1/2} \quad (3-15)$$

$$\frac{W_{sf}}{W_{sm}} = \left[\frac{d_f}{d_m} \right]^{1/2} \left[\frac{\alpha_m}{\alpha_f} \right]^{3/4} \left[\frac{\left(\frac{\rho_s}{\rho_a} \right)_m}{\left(\frac{\rho_s}{\rho_a} \right)_f} \right]^{3/4} \left[\frac{\left(\frac{\Delta \rho}{\rho_a} \right)_f}{\left(\frac{\Delta \rho}{\rho_a} \right)_m} \right]^{1/2} \quad (3-16)$$

Previous studies have been concerned with the liberties taken in adjusting the stack gas to ambient density ratio and the subsequent exaggeration of stack efflux velocity with respect to the freestream velocity. In the present study this ratio is matched and concern now shifts to the exaggeration of freestream velocity with respect to stack efflux velocity when α is not the same in model and fullscale. This is shown in Table 3-1 which summarizes the similarity parameters used in different studies.

3.6 The Influence of Stack Exit Conditions on Modeling Buoyant Plumes

The effect of stack exit velocity profile was investigated experimentally by using a plug inserted in the stack to produce the turbulent model in Fig. 3-1. A plume trajectory was measured after which the plug was removed and another plume trajectory measured for the resulting laminar model. Except for α all source conditions were the same for both plumes implying that the uniform flow momentum flux parameter ϕ_v in (3-6) was matched. A comparison of plume rise for the turbulent model and the laminar model with matched ϕ_v is shown in Fig. 3-2.

TABLE 3-1

SIMILARITY PARAMETERS MODELLED IN DIFFERENT STUDIES

Parameters	Exact Simulation	Present Study	Isyumov and Tanaka (1979)	Ludwig and Skinner (1976)	Hoult, O'Dea, Touchton, Ketterer (1977)	Melbourne and Gartshore (1975)
Density Ratio	Yes	Yes	No	No	No	No
Bulk Richardson Number $R_i = \frac{g \left(\frac{\Delta \rho}{\rho_a} \right) d}{U_s^2}$	Yes	No	Yes	No	Yes	Yes
Buoyancy Length Ratio $\frac{L_B}{R_s} = \frac{g \left(\frac{\Delta \rho}{\rho_a} \right) R_s W_s}{U_s^3}$	Yes	Yes	No	Yes	Yes	No
Uniform Flow Exit Momentum Ratio $\frac{\rho_s}{\rho_a} \left(\frac{W_s}{U_s} \right)^2$	Yes	No	Yes	Yes	No	Yes
Mean Exit Momentum Ratio $\alpha \frac{\rho_s}{\rho_a} \left(\frac{W_s}{U_s} \right)^2$	Yes	Yes	No	No	No	No
Plume Kinetic Energy Factor α	Yes	No	No	No	No	No
Plume Velocity Ratio $\frac{W_s}{U_s}$	Yes	No	No	No	Yes	No
Mass Flow Rate $\frac{\rho_s}{\rho_a} \left(\frac{W_s}{U_s} \right) \frac{d^2}{L^2}$	Yes	No	No	No	No	Yes, by distorting d
Stack Exit Velocity Profile Shape	Yes	No	No	No	No	No

Isyumov and Tanaka (1979) report that improved modeling of the stack exhaust flow has only a small effect on plume behaviour. In contrast, the results in Fig. 3-2 show that the laminar stack gas produces substantially more rise than the turbulent stack gas. This is to be expected because with identical average exit velocities the laminar plume has about 60% more exit momentum than the turbulent plume. The initial plume rise due to momentum is then larger for the laminar stack gas. In Chapter IV the momentum rise of a plume is found to vary as $L_m^{2/3}$.

Fig. 3-3 compares concentration profiles 5 cm. downstream of the source for the laminar and turbulent models. The turbulent stack gas produces a concentration profile that is symmetrical about centerline. As discussed in Chapter V, this profile has a Gaussian distribution of concentration which corresponds to that observed in the atmosphere. The laminar stack gas, however, produces a skewed concentration profile but with higher plume rise. This is due to the relatively large amounts of very high and very low momentum fluid present in a laminar velocity profile. The high momentum fluid produces the large plume rise. The low momentum fluid is sucked downward and entrained by the stack wake. This causes the observed skewness which lowers the plume center of gravity.

The character of dispersion as well as plume rise was affected by the velocity profile across stack exit. The

effects on dispersion soon disappear as one moves farther downstream where profiles of Gaussian character are observed in each case.

The large differences in plume behaviour when α is not taken into account supports the use of ϕ_M and not ϕ_V as the momentum flux parameter. To test this a plume trajectory was taken for a laminar plume with matched ϕ_M of the turbulent model. A comparison is shown in Fig. 3-2. This figure indicates that α alone cannot compensate for the effects of different velocity profiles across the stack exit. In this case the low pressure region in the stack wake produces forces which pull the slow-moving laminar fluid down.

As stated previously a mismatch in α exaggerates the freestream velocity with respect to the stack efflux velocity. Even though ϕ_M is still the same the physical interaction between the plume and the stack wake then changes.

A final problem was the high turbulence intensity of 20% at centerline for the turbulent model stack gas. Hinze (1975) uses the experimental results of Laufer for turbulent flow in pipes and shows the turbulence intensity to be about 3% at centerline.

To investigate the mismatch in turbulence intensity the dispersion of the laminar and turbulent models with matched ϕ_V in Fig. 3-2 are compared. Both plume trajectories show that the plumes had sufficient momentum to escape suction due

to the stack wake. Also, the plumes have the same buoyancy and exit in the same approach flow. At about 20 stack diameters downstream the skewing of concentration profiles due to a laminar velocity profile is no longer apparent. From this point on the concentration profiles are again symmetrical and Gaussian. As the turbulence intensity was 20% for the turbulent model and zero for the laminar model the effect should be evident by examining the spreading rates for each plume as shown in Table 3-2.

TABLE 3-2

COMPARISON OF VERTICAL DISPERSION, σ_z , FOR PLUMES
WITH LAMINAR AND TURBULENT VELOCITY PROFILES
AT STACK EXIT

Downwind Distance x (cm)	Laminar Model σ_z (cm)	Turbulent Model σ_z (cm)
20	2.5	2.4
50	4.8	4.9
100	7.8	7.9

The good agreement for vertical dispersion in Table 3-3 suggests that the turbulence intensity in the stack has little influence in enhancing plume growth. As discussed in Chapter

V, the dispersion is dominated by other forms of turbulence.

This result is contrary to that found in Chapter IV where a dependence of entrainment in the buoyant rise region on initial stack conditions is suggested.

In summary, the stack exit velocity profile significantly affects the total plume rise. The character of dispersion near the source is also affected. It was also found that ϕ_M did not fully describe the downwash effects behind a stack. The ratio of stack efflux to freestream velocity, W_s/U_s , is also important in determining how a plume interacts with stack wake. The intensity of turbulence in the stack had no apparent effect on dispersion.

3.7 The Effects Of Stack Gas Density Ratio

Once satisfied that momentum effects are properly modelled, it was possible to investigate the significance of stack gas density ratio on plume behaviour.

The model plume used in this experiment had $\phi_M = 2.57$, so that no downwash was expected to influence the results. Lowering the stack gas density for the same ϕ_M increases the ratio of W_s/U_s so that there was no danger of downwash for the test plumes. Any effects were solely due to changes in stack gas density.

The plume rise and the vertical dispersion are shown for different density ratios in Figs. 3-4 and 3-5. No significant trend is apparent in either case, given the scatter in

data. The good agreement supports the use of buoyancy flux and momentum flux parameters ϕ_B and ϕ_M from (3-1) and (3-6) in obtaining similarity.

The comparisons in Fig. 3-4 and 3-5 imply that density ratio can be altered to allow higher wind tunnel speeds. This is very important for other investigators with facilities incapable of reaching the low speeds normally required for modeling of buoyant plumes.

Note there is some effect on momentum rise of ρ_s/ρ_a predicted in Chapter IV by (4-18). However, a factor of 3 variation in ρ_s/ρ_a , for the same ϕ_M , predicts a change of less than 10% in plume rise, so this effect is small enough to be obscured by data scatter.

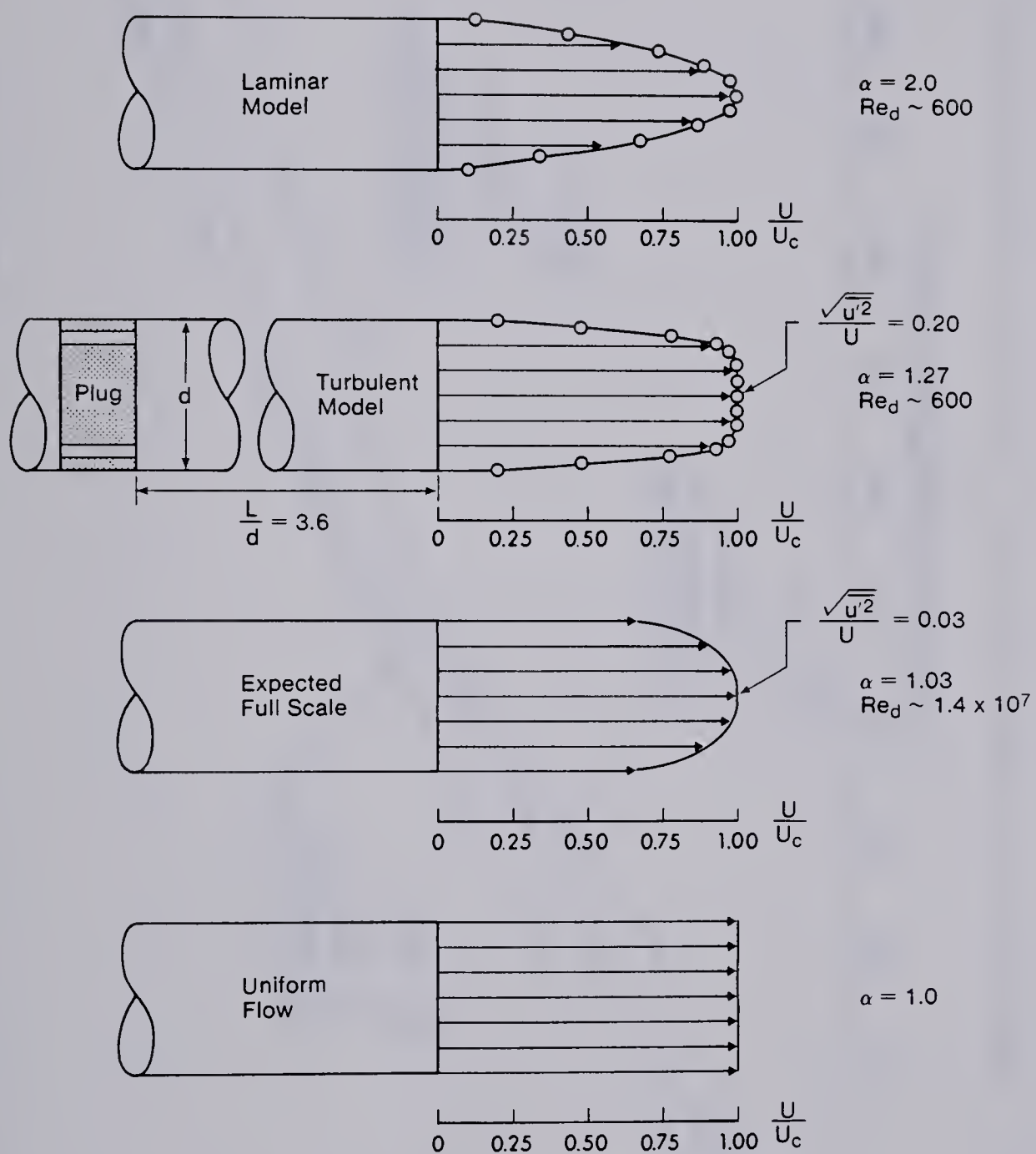


Fig. 3-1 Comparison of Measured and Theoretical Velocity Profiles at Stack Exit

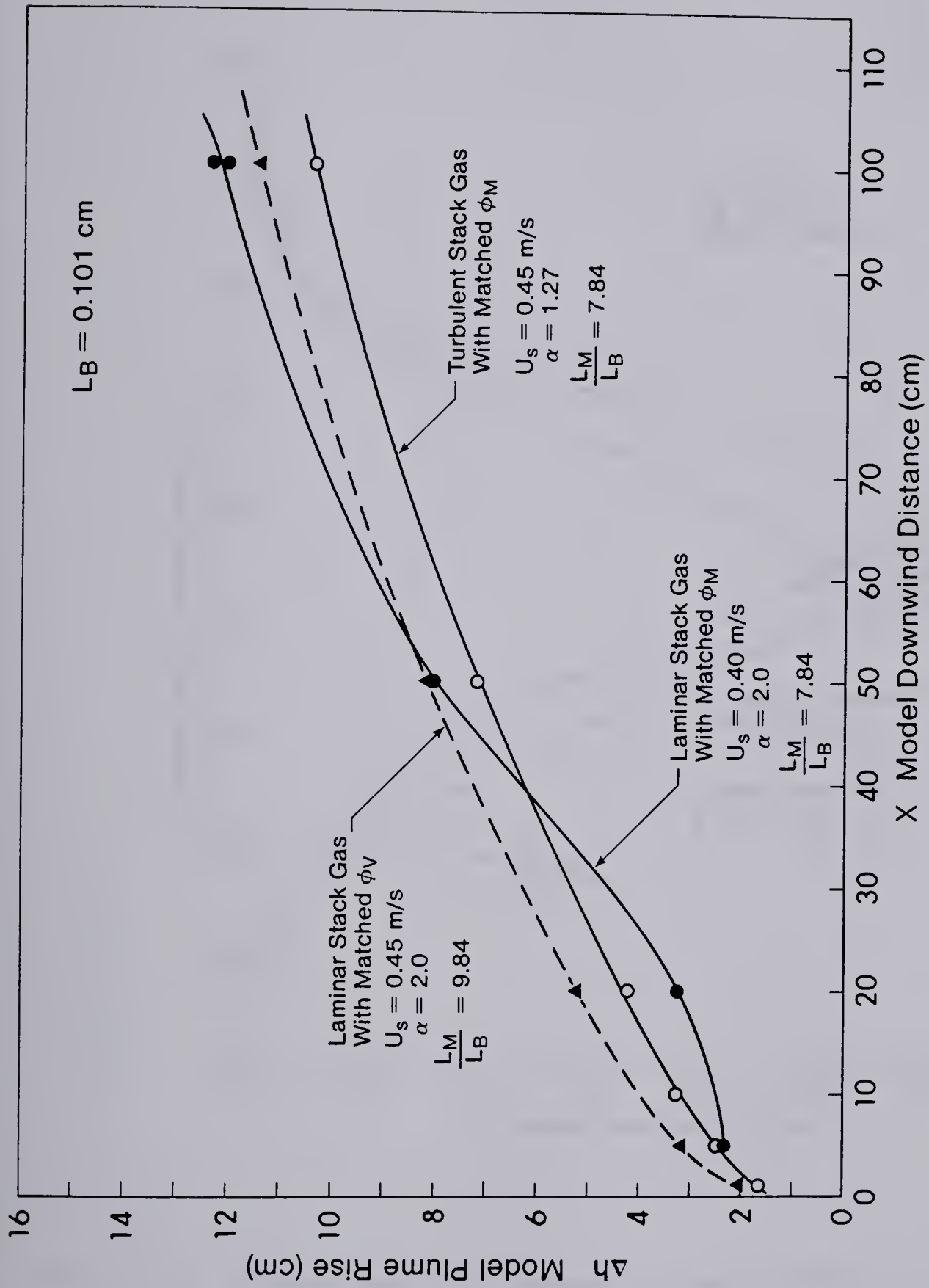


Fig. 3-2 Comparison of Plume Rise for Different Momentum Effects

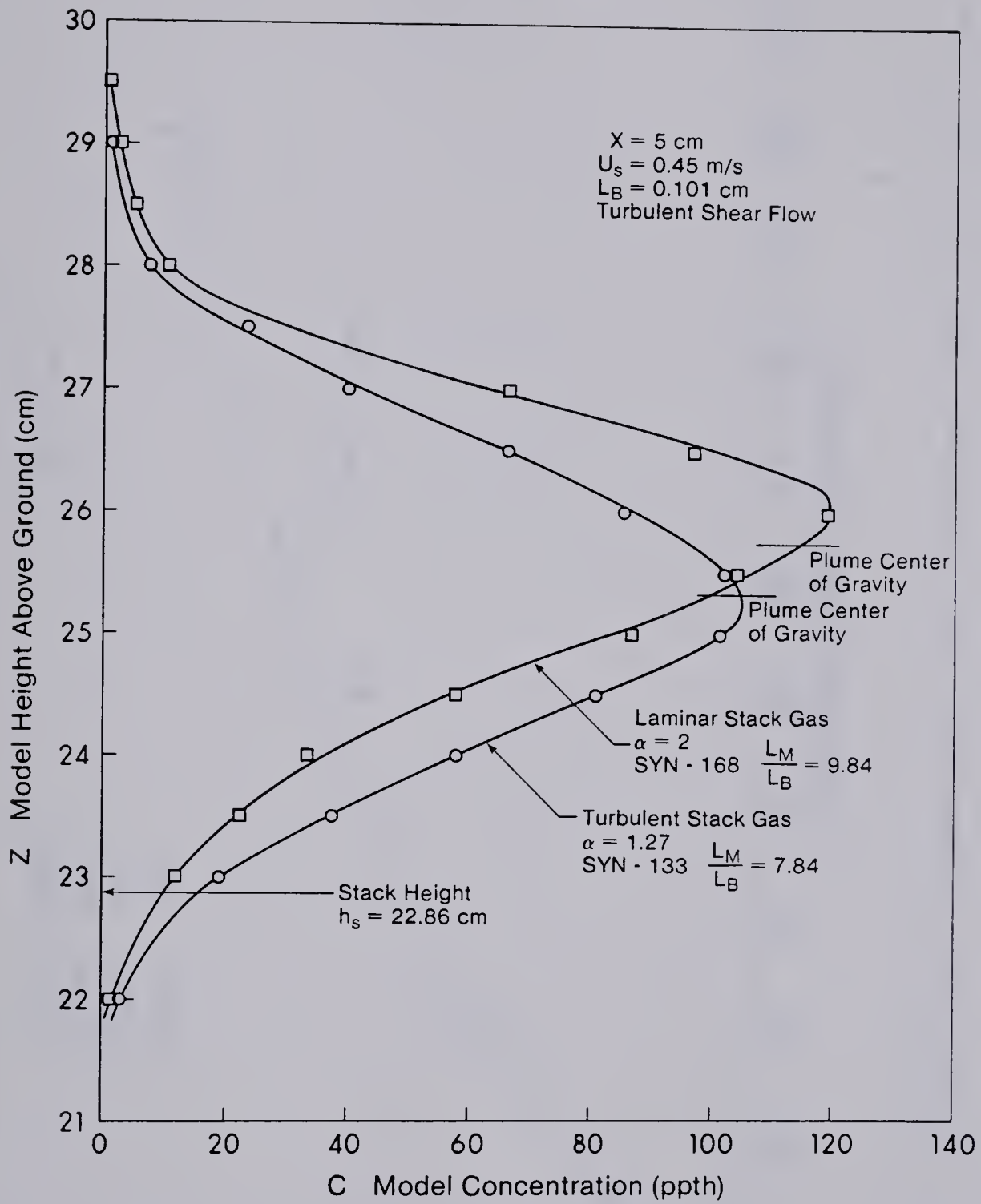


Fig. 3-3 Comparison of Concentration Profiles for a Laminar and Turbulent Stack Gas

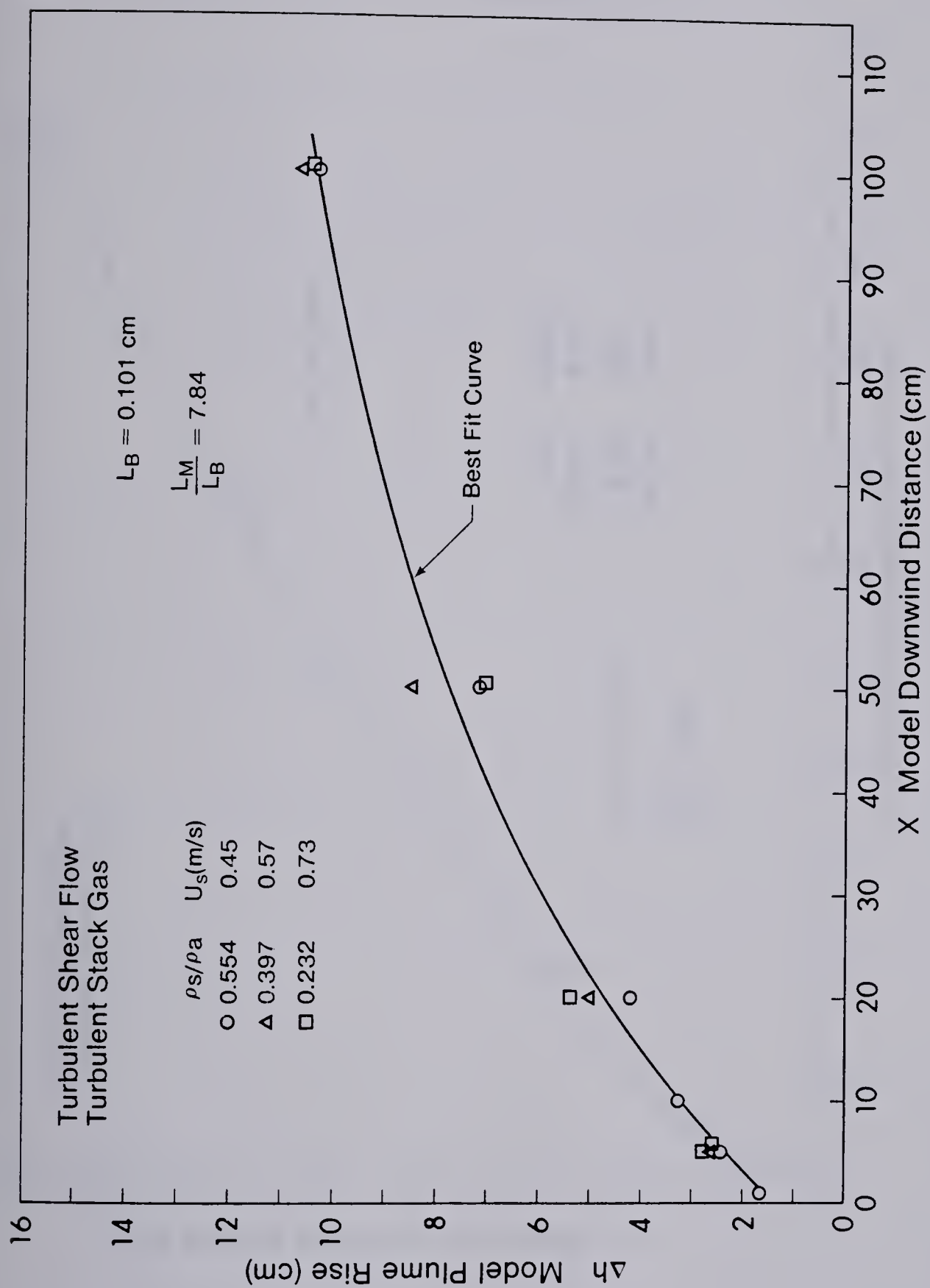


Fig. 3-4 Comparison of Plume Rise for Different Stack Gas Densities

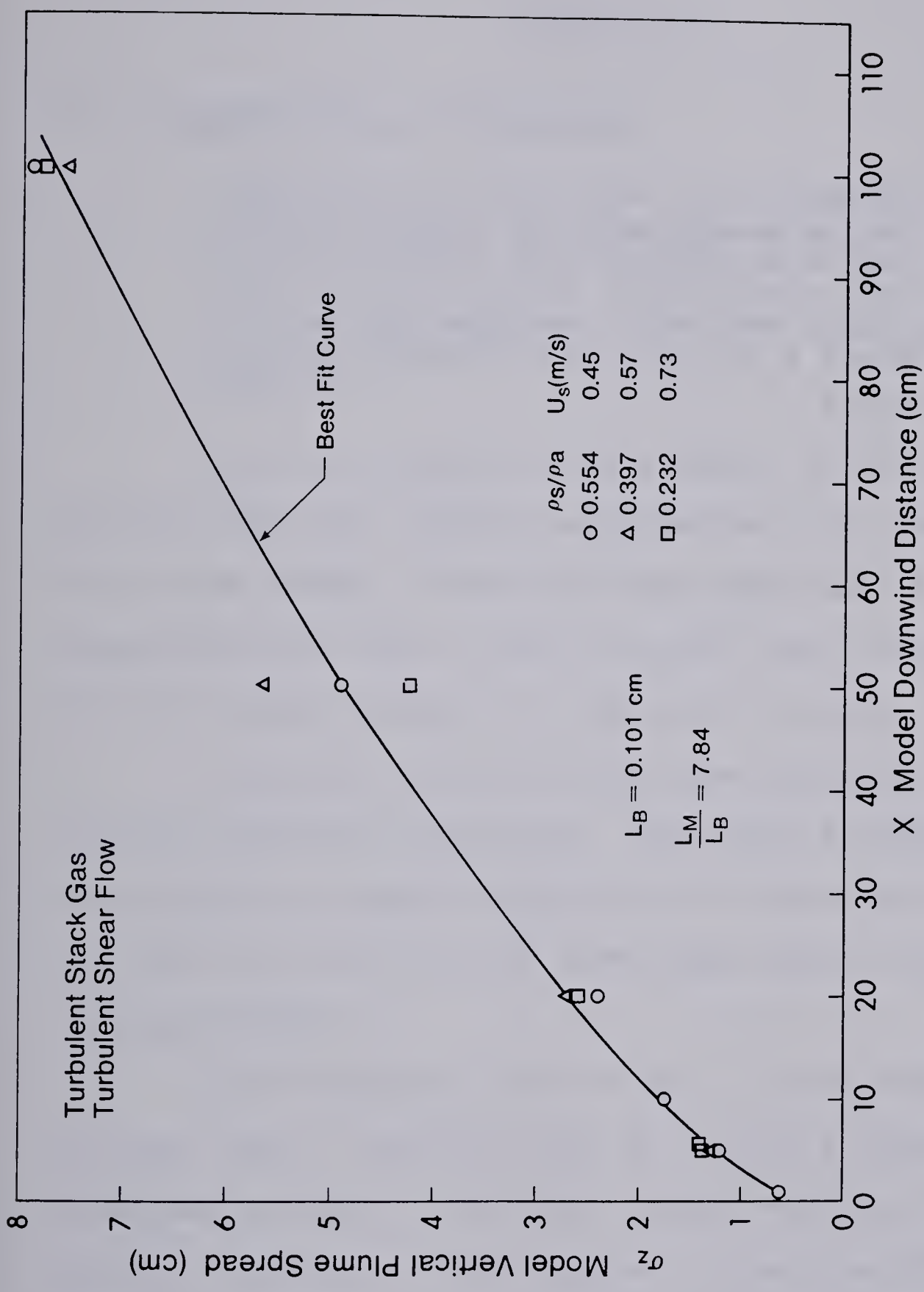


Fig. 3-5 Comparison of Vertical Plume Spread for Different Stack Gas Densities

CHAPTER IV

PLUME RISE

4.1 Introduction to Plume Rise

"There are over 30 plume rise formulas in the literature, and new ones appear at the rate of about 2 a year. All require empirical determination of one or more constants and some formulas are totally empirical. Yet the rises predicted by various formulas may differ by a factor greater than 10."

Briggs (1969)

The rise formulas Briggs refers to are usually derived from site specific experimental data for existing full scale stacks. These formulas agree well with experimental data but due to their specific application, often fail for plumes outside the particular study.

A general study of plume rise requires the consideration of different mechanisms. The first is momentum rise, due to the initial upward momentum of the stack gas. Secondly, any stack gas with density less than ambient will rise due to buoyant forces.

The entrainment of air into a plume reduces the rate of plume rise. Momentum rise is initially dominant but decreases rapidly as the plume moves downstream. Though usually negligible in the region of momentum effects, buoyant forces act constantly as the plume rises. When momentum rise ceases to be important the forces due to

buoyancy dominate plume rise for the remaining downwind travel.

The most commonly used plume rise formulas were derived by Briggs (1969). The rise of a jet, including the effect of stack gas density on momentum, is given by (4-1). Equation (4-2) is the Briggs 2/3 law for buoyant rise. Each formula is applied separately at the appropriate downwind locations where momentum or buoyancy effects dominate plume rise.

$$\Delta h_M = 2.3 \frac{F_V^{1/3}}{U^{2/3}} x^{1/3} \quad (4-1)$$

$$\Delta h_B = 1.6 \frac{F_B^{1/3}}{U} x^{2/3} \quad (4-2)$$

U is defined by Briggs (1969) as the average windspeed at stack level. The present study uses the windspeed U_s at stackheight as a suitable value.

4.2 The Combination of Momentum Rise and Buoyancy Rise

For plumes with significant momentum and buoyancy there is a transition region where momentum rise and buoyant rise are both important. An equation which includes rise in the transition region is given by Briggs (1975) as:

$$\Delta h = \left[\frac{3}{\beta^2} \frac{F_V}{U_s^2} x + \frac{3}{2\beta^2} \frac{F_B}{U_s^3} x^2 \right]^{1/3} \quad (4-3)$$

Equation (4-3) was derived for a bent over plume in a uniform crossflow. The initial stack radius was assumed to be zero. β is the entrainment constant resulting from the application of the Morton, Taylor, Turner (1956) entrainment assumption to a bent over plume. This assumption relates the entrainment velocity to the vertical velocity of a plume with β , resulting in a linear growth of plume radius with plume rise. Neiman (1979) shows that for a finite source radius R_s (4-3) becomes

$$\Delta h = \left[\frac{3}{\beta^2} \frac{F_v}{U_s^2} x + \frac{3}{2\beta^2} \frac{F_B}{U_s^3} x^2 + \left(\frac{R_s}{\beta} \right)^3 \right]^{1/3} - \frac{R_s}{\beta} \quad (4-4)$$

A serious liberty taken by Briggs in deriving (4-3) was the use of source conditions, where the plume was vertical, as boundary conditions for a bent over plume. The formula, however, offers an alternative to considering the momentum rise and buoyant rise separately.

Briggs used the data of Fan (1967) to justify the use of different entrainment constants for the momentum and buoyancy terms in (4-3). For the momentum rise term Briggs recommends

$$\beta = \beta_1 = 0.33 + \frac{U_s}{W_s} \quad (4-5)$$

and for the buoyancy rise term the data of Fan indicates

$$\beta = \beta_2 = 0.5 \quad (4-6)$$

The wind tunnel experiments in the present study will also support the use of different entrainment constants but not the ones suggested by Briggs.

The modeling discussion in Chapter III showed that the momentum flux F_v , defined in (3-7), assumes a uniform velocity profile across stack exit. The kinetic energy correction factor α defined in (3-11) is used to correct the momentum flux when the average velocity across stack exit is used. For full scale turbulent velocity profiles $\alpha \approx 1.03$, so that it is often neglected in momentum flux calculations. In wind tunnel experiments α can have a value as high as 2.0 for laminar flow of the stack gas. For this reason the momentum flux F_M , used in this study, includes α as was shown in (3-13).

$$F_M = \alpha F_v = \alpha \frac{\rho_s}{\rho_a} W_s^2 R_s^2 \quad (3-13)$$

Another result from Chapter III was the formation of a buoyancy length L_B with buoyancy flux F_B and the freestream velocity U_s .

$$L_B = \frac{F_B}{U_s^3} \quad (3-4)$$

Similarly a momentum length L_M was found to be

$$L_M = \sqrt{\frac{F_M}{U_s}} \quad (3-8)$$

Both the momentum and buoyancy length were found to scale as any other geometric length in the modeling scheme adopted.

Using different entrainment constants and substituting L_M and L_B , (4-4) becomes

$$\Delta h = \left[\frac{3}{\beta_1^2} L_M^2 x + \frac{3}{2\beta_2^2} L_B x^2 + \left(\frac{R_s}{\beta_1} \right)^3 \right]^{1/3} - \frac{R_s}{\beta_1} \quad (4-7)$$

Though not rigorous in its derivation (4-7) with the source radius terms negligible shows how the momentum rise Δh_M combines with the buoyant rise Δh_B to form the total plume rise Δh . Equation (4-7) with $R_s = 0$ may be written as

$$\Delta h = [\Delta h_M^3 + \Delta h_B^3]^{1/3} \quad (4-8)$$

The character of the combined rise formula is illustrated in Fig. 4-1. In this figure both plume rise and downwind distance are normalized with buoyancy length. Normalizing (4-7) with the buoyancy length and neglecting source radius terms gives

$$\frac{\Delta h}{L_B} = \left[\frac{3}{\beta_1^2} \left(\frac{L_M}{L_B} \right)^2 \frac{x}{L_B} + \frac{3}{2\beta_2^2} \left(\frac{x}{L_B} \right)^2 \right]^{1/3} \quad (4-9)$$

The ratio L_M/L_B that results indicates the relative contribution of momentum and buoyancy in a plume.

If the momentum rise is considered separately from (4-4) the Briggs (1969) equation (4-1) results if $\beta_1 = 0.5$. Similarly for buoyant rise (4-2) is obtained if $\beta_2 = 0.6$.

4.3 Final Rise of a Buoyant Plume

The rise of a buoyant plume is limited in a turbulent environment. Atmospheric turbulence limits rise by two processes.

The first is a passive process where entrainment lowers the plume buoyancy to nearly zero. As buoyant forces are small the atmospheric turbulence dominates the plume motion so that it gradually rises or levels off completely.

Another possibility discussed by Briggs (1975) is defined as plume breakup. Turbulent eddies break apart the plume so that it is no longer continuous. The buoyant forces associated with the resulting individual parcels of stack gas are small compared to those associated with the entire plume. As a result the motion of these parcels is rapidly dominated by atmospheric turbulence. The breakup of a continuous plume also increases the rate of entrainment.

Plume rise data for 7 different plumes, from the present wind tunnel experiments, are shown in Fig. 4-2. The data shows a rapid transition to the final rise stage.

Regardless of the process causing final rise, it is important to determine where it occurs because plume rise is very important in determining maximum ground level concentration. The downwind location for final rise of a plume has a large influence on the critical windspeed, which produces the largest ground level concentrations, in that the effective stack height is fixed beyond this point.

Briggs (1975) presents a final rise expression for buoyant plumes. The transition to final rise was assumed to occur when the dissipation rate of turbulence in the plume equals that of atmospheric turbulence. The resulting equation is

$$\Delta h_{Bf} = \left[\frac{0.474}{\beta_2} \right] \left[\frac{F_B}{U_s u_*} \right] \left[1 + \frac{h_s}{\Delta h_{Bf}} \right]^{2/3} \quad (4-10)$$

$(h_s + \Delta h_{Bf})$ is the effective stack height at final rise for a buoyant plume. u_* is the friction velocity. As indicated by (4-7) and (4-8) the buoyant rise of a plume is given by

$$\Delta h_B = \left(\frac{3}{2\beta_2} \right)^{1/3} \frac{F_B^{1/3} x^{2/3}}{U_s} \quad (4-11)$$

Substituting (4-10) into (4-11) and solving for x , the downwind location x_f where final rise occurs is

$$x_f = \frac{0.40}{\beta_2} \left(\frac{F_B}{U_s} \right) \left(\frac{U_s}{u_*} \right)^3 \left(1 + \frac{h_s}{\Delta h_{Bf}} \right) \quad (4-12)$$

Fig. 4-2 shows plume rise data from wind tunnel experiments in the present study. The range of values for L_M/L_B indicates the many different momentum and buoyancy combinations tested. The data shows that plume rise terminates at a normalized downwind distance of about 2200. Theoretical combined rise curves with $\beta_1 = 1.1$ and $\beta_2 = 1.2$ are drawn for varying L_M/L_B with final rise at this point. Because data were normalized with buoyancy length, the downwind position of final rise was found to be

$$x_f = 2200 L_B \quad (4-13)$$

The result in (4-13) is supported by Neiman (1979) who shows a linear plot in Fig. 4-4 of his report.

A simple and widely used criterion for final rise is given by the A.S.M.E. Task Group (1973). They recommend the termination of plume rise 10 stack heights downwind of the source.

$$x_f = 10 h_s \quad (4-14)$$

A comparison of the different final rise criterion is shown in Table 4-1 for a plume with known entrainment constants. The determination of entrainment constants is discussed later. The plume is sufficiently buoyant that momentum rise is negligible in the final rise region.

TABLE 4-1

COMPARISON OF FORMULAS FOR FINDING
DOWNWIND POSITION OF FINAL RISE

Study	x_f (cm) *
A.S.M.E. Task Group (1973)	229
Briggs (1975)	376
Present Study	223

* The plume used has the following source terms and entrainment constants.

$$\begin{array}{ll}
 L_M = 0.7939 \text{ cm} & \beta_1 = 0.87 \\
 L_B = 0.1012 \text{ cm} & \beta_2 = 0.87 \\
 h_s = 22.9 \text{ cm} &
 \end{array}$$

In Table 4-1 the measured value of x_f is given for the present study. The A.S.M.E. Task Group (1973) recommendation in (4-14) agrees well with the measured value of x_f . The Briggs (1975) equation gives a high estimate of x_f . The result is equivalent to terminating plume rise at $x_f = 3700 L_B$ as opposed to $2200 L_B$ in (4-13).

4.4 Entrainment Constants for Momentum Rise Of a Plume

The entrainment constant for momentum rise found from experiment varies for different plumes. An expression where

β_1 is related to source conditions is given by Briggs (1975). Using the data of Fan (1967), Briggs obtains:

$$\beta_1 = B + \frac{U_s}{W_s} \quad (4-15)$$

where $B = 0.33$ and U_s/W_s reflects the effect of crossflow on entrainment.

Wilson (unpublished) revised (4-15) to be consistent with the findings of Ricou and Spalding (1960) and the present study. Ricou and Spalding found the entrainment of jets to depend on the ratio of stack gas to ambient density. For jets released in a quiescent environment β_1 is given as

$$\beta_1 = B \left(\frac{\rho_s}{\rho_a} \right)^{1/2} \quad (4-16)$$

where $B = 0.28$ compared to the value of 0.33 suggested by Briggs.

The added complication of a crossflow can cause the plume to be sucked down into the stack wake. Briggs uses the ratio U_s/W_s to compensate for downwash effects on β_1 . The present study, as discussed in Chapter III, found that the degree of downwash is dependent on ϕ_M where

$$\phi_M = \frac{L_M^2}{R_s^2} = \alpha \frac{\rho_s}{\rho_a} \left(\frac{W_s}{U_s} \right)^2 \quad (4-17)$$

Downwash increases as ϕ_M decreases.

Using the results in (4-16) and (4-17) Wilson rewrites (4-15) as

$$\beta_1 = 0.33 \left(\frac{\rho_s}{\rho_a} \right)^{1/2} + \frac{1}{\sqrt{\phi_M}} \quad (4-18)$$

where $B = 0.33$ is chosen because it applies for data taken in crossflows. Equation (4-18) reflects the increase in entrainment by crossflow momentum effects for decreasing ϕ_M .

Fig. 4-3 shows plumes with different values of β_1 computed from (4-18). Substituting these values in the combined rise equation (4-9) gives theoretical plume rise curves that are in good agreement with experimental data.

The curves in Fig. 4-3, however, use a value of β_2 that best fits the data in the buoyant rise region. Fortunately, minor variations in β_2 have little influence on plume rise for normalized downwind distances less than 200. The successful match of theory to data in this region is governed by β_1 and good agreement suggests (4-18) is the correct form. The implications of fitting β_2 to the data are discussed later.

The values of β_1 were also fit to several plumes in the momentum rise region. Table 4-2 shows that values of β_1 calculated from (4-18) are in good agreement with fitted values.

TABLE 4-2

COMPARISON OF CALCULATED AND FITTED VALUES
OF β_1 FOR DIFFERENT PLUMES

L_M (cm)	$\frac{\rho_s}{\rho_a}$	ϕ_M	Best Fit of β_1 in Range $20 < \frac{x}{L_B} < 200$	β_1 From (4-18)
0.79	0.554	2.57	0.84	0.87
1.00	0.397	4.11	0.76	0.70
1.36	0.652	6.38	0.54	0.66

The theoretical plume rise curves in Fig. 4-3 are computed from (4-4) with $R_s = 0$. If the source radius terms are included, the fit of theory to data is worse because computed curves always fall farther below data near the source. As the effect of R_s is only important near the source, it is neglected. Plume behavior is not well defined in this region anyway.

4.5 The Effect Of Turbulence and Velocity Shear On Plume Rise

To investigate the effects of shear and turbulence on plume rise required wind tunnel measurements in three different approach flows. The same plume was released in a laminar crossflow, uniform grid wake turbulence and a simulated

atmospheric boundary layer. Fig. 2-10 shows the amount of shear in the boundary layer.

The resulting plume rise data in Fig. 4-4 shows that the presence of shear in the approach flow reduces plume rise by about 20%. The agreement between data taken in a laminar crossflow and data taken in a crossflow with grid turbulence indicates that plume rise is insensitive to background turbulence in the region where buoyant rise is dominant.

Because the same plume was used in the different approach flows, values of β_1 , L_B and \bar{L}_M/L_B remain fixed. Any change in plume rise is then reflected by changes in the best fit value of β_2 . For example, consider the plume rise measurements in a laminar crossflow and in grid wake turbulence in Fig. 4-4. For normalized downwind distances greater than 200 both cases agree with the combined rise formula if $\beta_2 = 0.87$. The introduction of wind shear as it occurs in an atmospheric boundary layer (see Fig. 2-10) requires a value of $\beta_2 = 1.4$ for the combined rise formula to fit the plume rise data. However, the same plume is not likely to have two different entrainment constants for buoyant rise, as discussed in the next section. Instead the increase in wind velocity with height is responsible for the reduction in plume rise.

As a simple attempt to correct for shear effects the local windspeed at the height of the plume centerline may be used in the combined rise equation. This procedure is to correct existing terms in the combined rise equation using the

factor

$$\lambda = \frac{U_s}{U_{\text{local}}} \quad (4-19)$$

For example, the local buoyancy length is given by

$$L_{B_{\text{local}}} = \frac{F_B}{U_s^3} \left(\frac{U_s}{U_{\text{local}}} \right)^3 = \frac{F_B}{U_s^3} \lambda^3 = L_B \lambda^3 \quad (4-20)$$

Similarly for the local momentum length

$$L_{M_{\text{local}}} = \frac{\sqrt{F_M}}{U_s} \left(\frac{U_s}{U_{\text{local}}} \right) = \frac{\sqrt{F_M}}{U_s} \lambda = L_M \lambda \quad (4-21)$$

Substituting the local values of L_M and L_B into the combined rise equation (4-4) gives

$$\Delta h = \left[\frac{3}{\beta_1^2} L_M^2 x \lambda^2 + \frac{3}{2\beta_2^2} L_B x^2 \lambda^3 + \left(\frac{R_s}{\beta_1} \right)^3 \right]^{1/3} - \frac{R_s}{\beta_1} \quad (4-22)$$

Equation (4-22) must not be viewed as a solution but as a rough correction for shear effects. The solution to (4-22) is iterative in that λ requires the plume rise Δh to compute U_{local} . The result of using (4-22) to correct the uniform wind plume rise data is shown in Fig. 4-4. The measured reduction in plume rise due to shear was greater than that predicted by the correction.

Another method of correcting for wind shear effects is given by Djurfors and Netterville (1978). This method applies only to the buoyant rise of a plume. However, Djurfors (unpublished) has extended the analysis to include momentum rise.

Djurfors and Netterville find the buoyancy and momentum conservation equations for a plume can be solved for a wind velocity profile of the form

$$\frac{U}{U_s} = M \left[1 + \frac{\Delta h}{\left(\frac{R_s}{\beta_*} \right)} \right]^\gamma \quad (4-23)$$

where M is a constant and

$$\beta_* = \frac{\beta}{1 + \frac{\gamma}{2}} \quad (4-24)$$

This profile is fitted to the wind tunnel velocity profile in Fig. 2-10. The profile described by (4-23), with $M = 0.85$ and $\gamma = 0.1$, agrees well with the data in the top 80% of the plume layer. The differences in the lower 20% of the plume layer are likely unimportant as the plume spends little time in this region.

The buoyancy and momentum conservation equations for a plume were solved with the velocity profile given by (4-23). Including a finite source radius in the analysis Djurfors

obtains

$$\begin{aligned} \frac{\Delta h(t)}{L_B} = & \left[\frac{3+\gamma}{\beta_*^2} \left(\frac{R_S}{\beta_*} \right)^\gamma \left(\frac{L_M}{L_B} \right) \frac{2(U_S t)}{L_B^{1+\gamma}} + \frac{3+\gamma}{2\beta_*^2} \frac{(U_S t)^2}{L_B^{2+\gamma}} + \right. \\ & \left. + \left(\frac{R_S}{\beta_* L_B} \right)^{3+\gamma} \right] \frac{1}{3+\gamma} - \frac{R_S}{\beta_* L_B} \end{aligned} \quad (4-25)$$

The downwind distance x for a corresponding travel time t is found by numerical integration of

$$x = \int_0^t U(t) dt = M U_S \int_0^t \left[1 + \frac{\Delta h(t)}{\left(\frac{R_S}{\beta_*} \right)} \right]^\gamma dt \quad (4-26)$$

Fig. 4-5 compares plume trajectories obtained from the application of different shear corrections. To be consistent with the recommendations of Djurfors and Netterville, the source radius $R_S = 0.5$ cm. has been included in the calculation of theoretical curves. The combined rise curves with source terms negligible can be retained by adding about 0.5 cm. to the curves in Fig. 4-5.

The comparison of plume trajectories in Fig. 4-5 shows the Djurfors and Netterville theory accurately predicts

the final rise of the plume in shear flow. At all other downwind locations the theory predicts values consistently lower than the plume rise data. The local windspeed correction undercorrects for the effects of shear so that plume rise estimates are generally higher than observed.

4.6 Entrainment Constants for Buoyant Plume Rise

The entrainment constants in the momentum rise region have been successfully related to source conditions. The entrainment constants for buoyant rise, however, are empirical in that they were determined by a best fit to the data. The present data suggests β_1 and β_2 are not true constants but vary with source conditions.

Both the Djurfors and Netterville (1978) correction shown in Fig. 4-5 and the local windspeed correction support the use of a single value of β_2 for a plume regardless of approach flow. The latter method uses the value of β_2 found directly from plume rise data in a uniform wind. The Djurfors and Netterville correction uses an effective entrainment constant β_* defined in (4-24). Because γ is typically 0.1 or less the value differs little from the actual entrainment constant. The empirical determination of β_2 from plume rise data taken in non-uniform wind conditions is invalid. The value of $\beta_2 = 1.4$ used in Fig. 4-4 is certainly not representative of a true entrainment constant for buoyant plume rise. Rather this must be considered as a curve fitting constant

valid only for a specific plume in shear flow.

Finding the true value of β_2 then requires the measurement of plume rise in a uniform crossflow. This places severe limitations on entrainment constants derived from full scale data, as wind shear is usually present in the approach flow for a neutral atmosphere. The plume rise data in Fig. 4-4 indicate that the buoyant rise of a plume is insensitive to turbulence in the approach flow.

The wind tunnel experiments support the dependence of β_2 on source conditions. This can be shown by first rewriting the combined rise expression as

$$\Delta h = [L_B \left(\frac{3}{\beta_1} \frac{L_I}{2} x + \frac{3}{2\beta_2} x^2 \right)]^{1/3} \quad (4-27)$$

where

$$L_I = \frac{L_M^2}{L_B} = \frac{\alpha}{g} \left(\frac{\rho_s}{\rho_a - \rho_s} \right) W_s U_s \quad (4-28)$$

The ratio of L_I/β_1^2 represents the effect of momentum relative to buoyancy on plume rise.

If plume rise data is taken in a uniform crossflow the physical value of β_2 is given by the value that best fits the data. Table 4-3 compares β_2 for three different plumes in a uniform laminar crossflow.

TABLE 4-3

COMPARISON OF β_2 FOR PLUMES WITH DIFFERENT SOURCE
CONDITIONS IN A UNIFORM CROSSFLOW

Flow Condition	α	β_1	β_2	L_M (cm)	L_B (cm)	$\frac{L_I}{\beta_1^2}$	$\frac{1}{\beta_2^2}$
Turbulent Stack Gas	1.27	0.87	0.87	0.79	0.10	8.25	1.32
Laminar* Stack Gas	2.0	0.66	0.52	1.36	0.18	23.6	3.70
Laminar* Stack Gas	2.0	0.76	0.48	1.09	0.036	57.1	4.34

* Data from Neiman (1979)

Table 4-3 shows a weak dependence of increasing values of $1/\beta_2^2$ with increasing L_I/β_1^2 for a laminar stack gas. For a turbulent stack gas the percentage decrease of $1/\beta_2^2$ with decreasing L_I/β_1^2 is much larger. This indicates that whether the stack gas is turbulent or laminar appears to strongly affect β_2 . In the fullscale this has little consequence as a turbulent stack gas always occurs. However, for wind tunnel experiments this shows that great care must be taken in modeling the initial stack conditions.

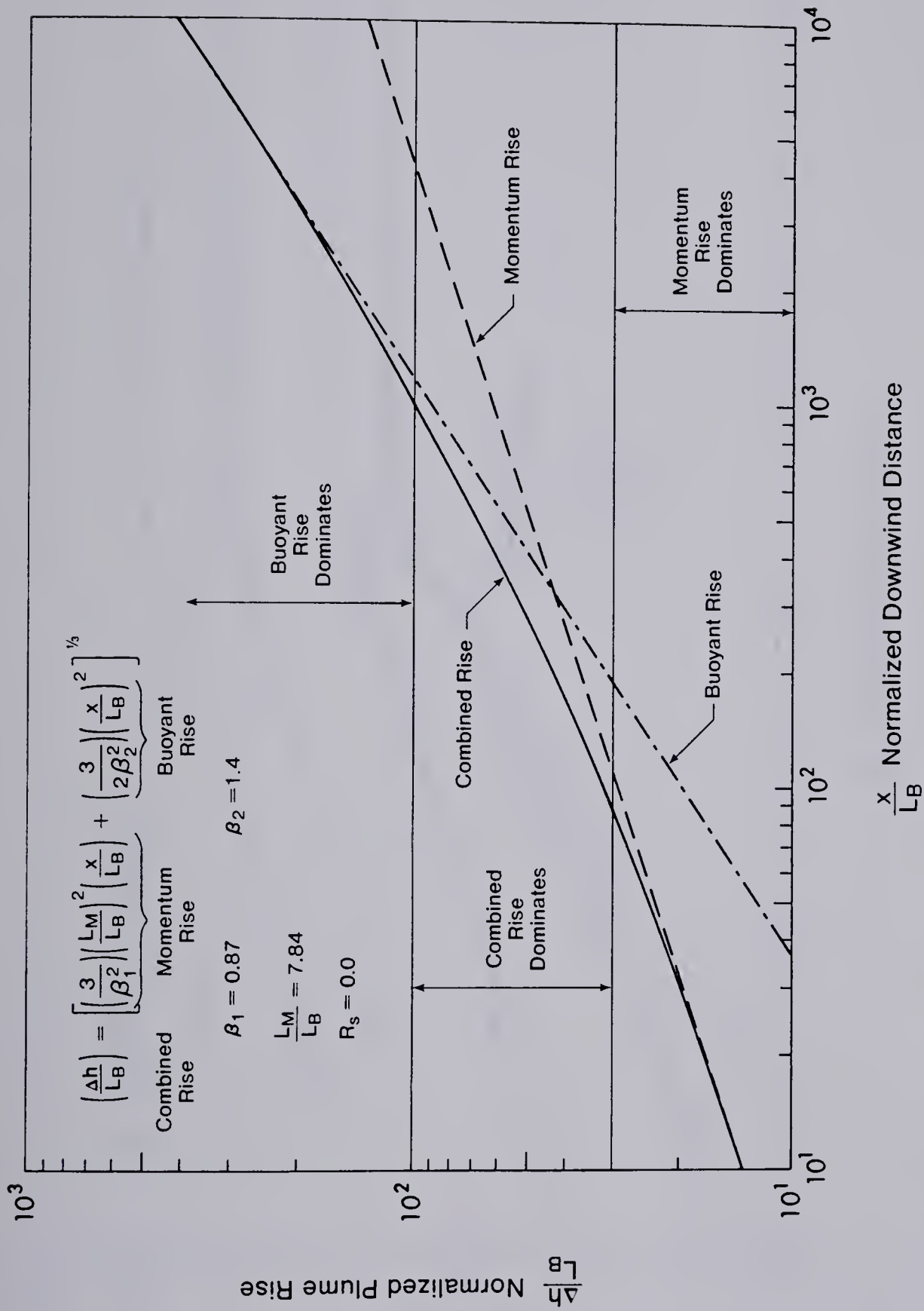


Fig. 4-1 Combination of Momentum Rise and Buoyant Rise

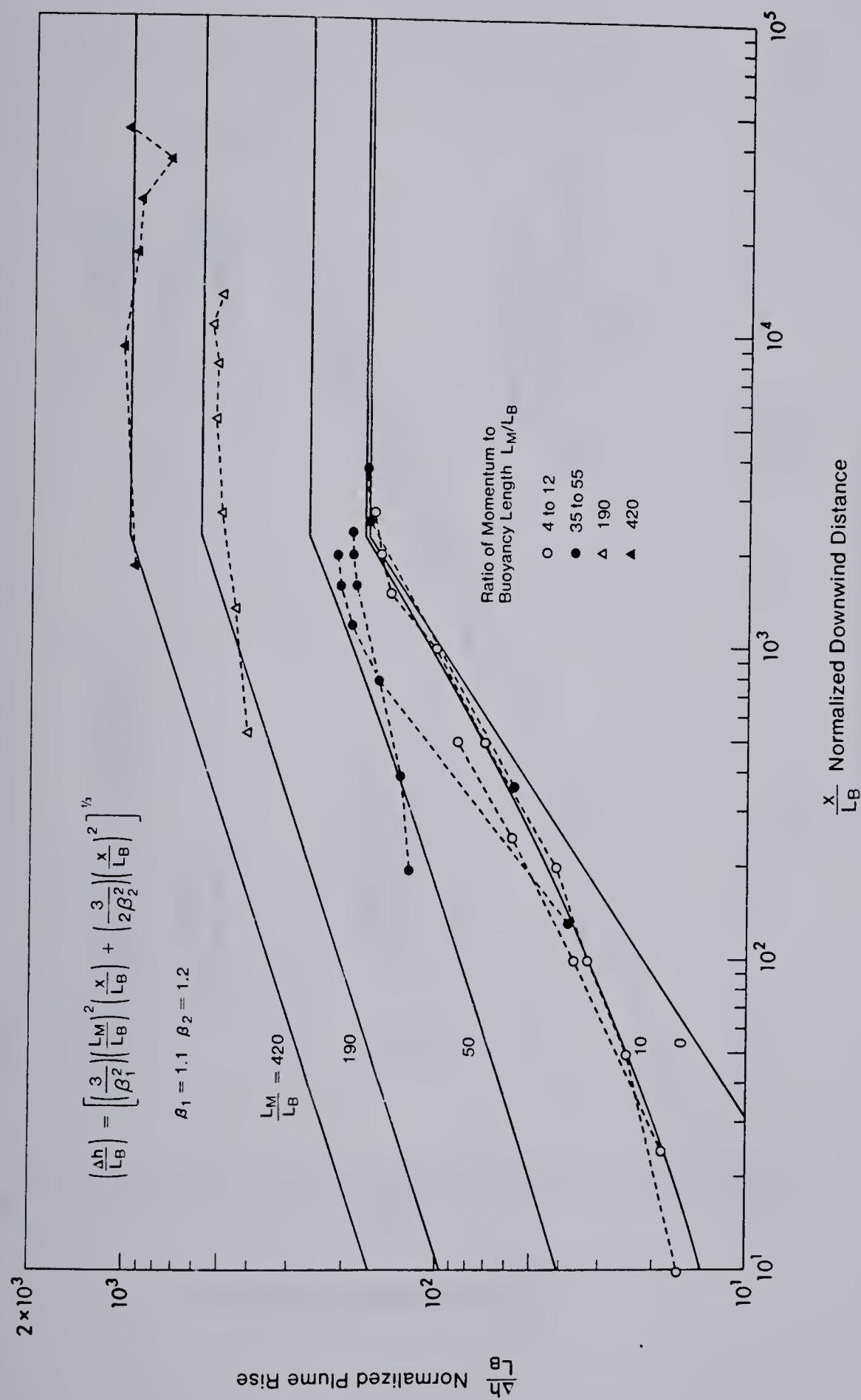


Fig. 4-2 Final Rise of Plumes

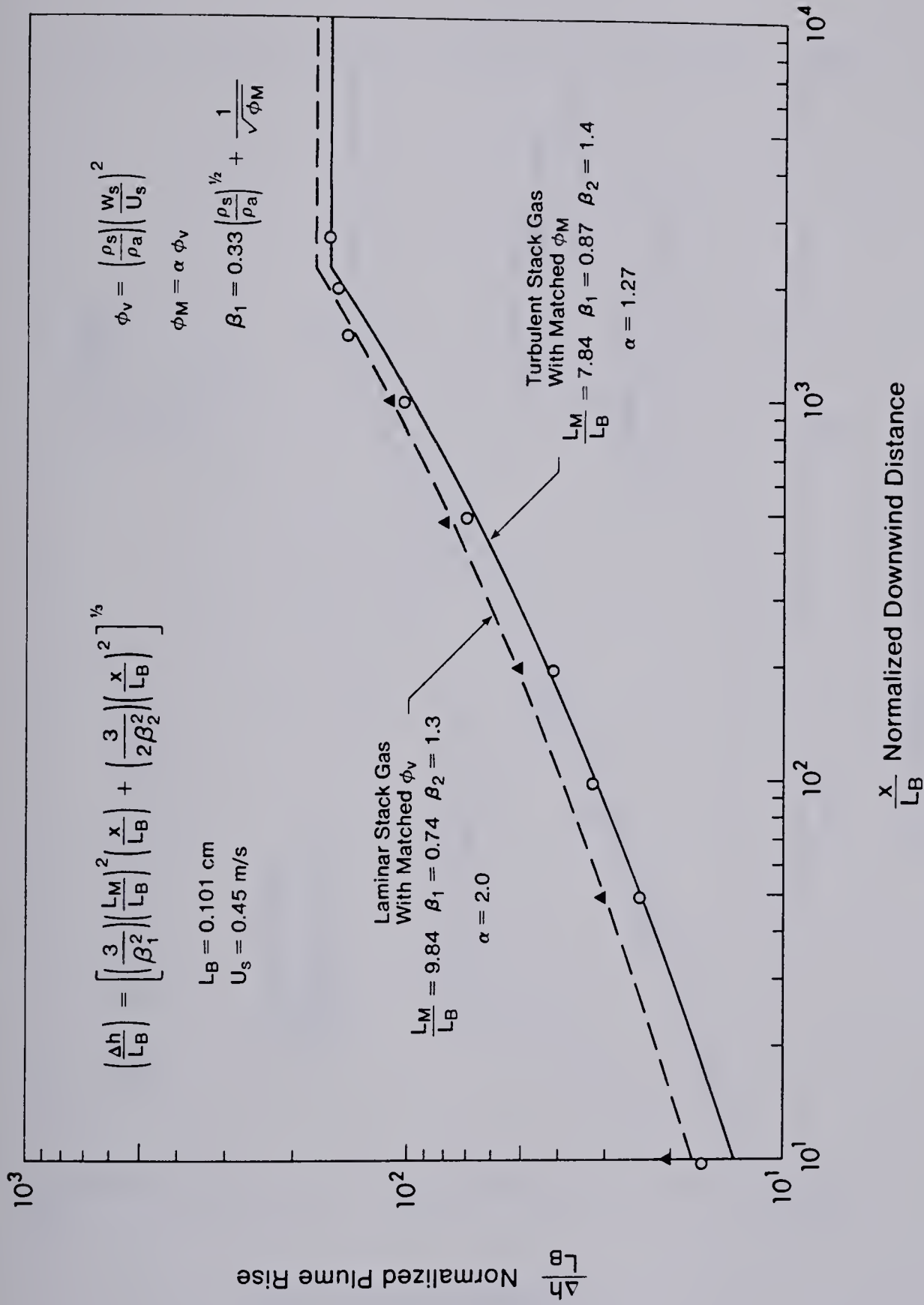


Fig. 4-3 Fitting the Combined Rise Expression for Calculated Values of β_1

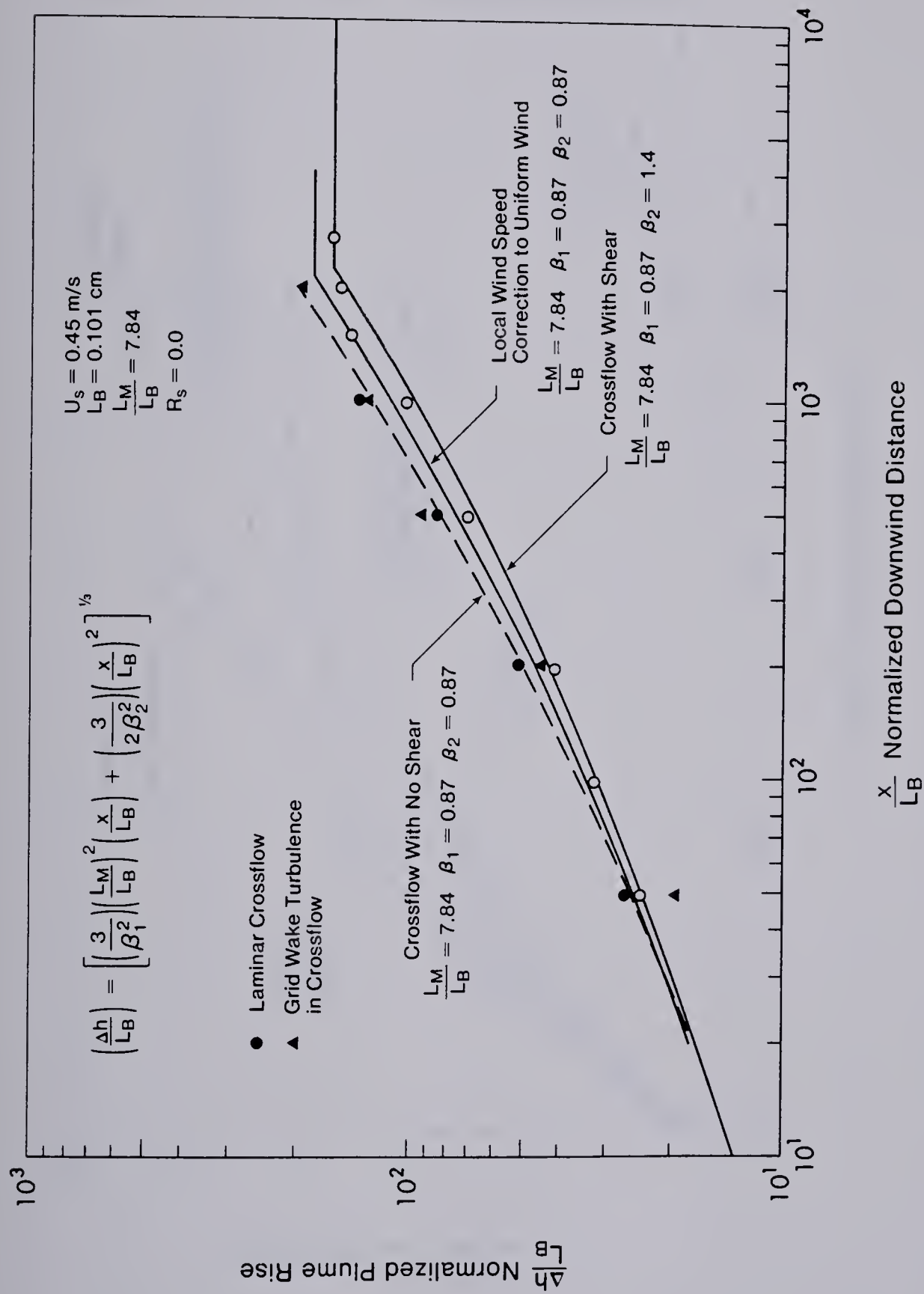


Fig. 4-4 Effects of Shear and Turbulence on Plume Rise

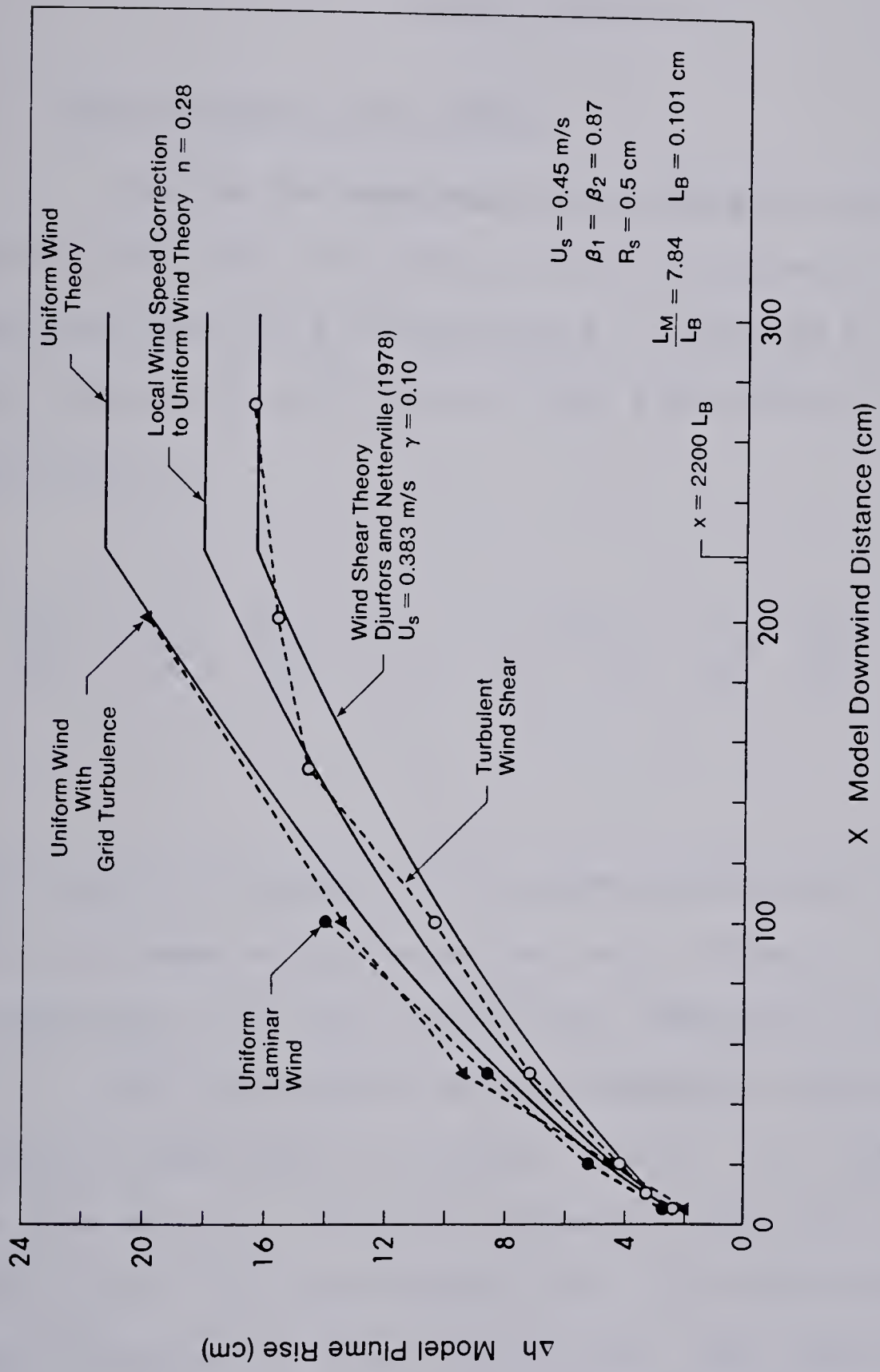


Fig. 4-5 Comparison of Different Shear Corrections

CHAPTER V

PLUME DISPERSION

5.1 The Gaussian Plume Model

Due to the complexities associated with turbulent flows the diffusive nature of the atmosphere is often characterized by a diffusivity K . Defining K_x , K_y and K_z as the diffusivities in the x , y and z directions, the diffusion equation is

$$\frac{\partial \chi}{\partial t} + U \frac{\partial \chi}{\partial x} + V \frac{\partial \chi}{\partial y} + W \frac{\partial \chi}{\partial z} = \frac{\partial}{\partial x} \left(K_x \frac{\partial \chi}{\partial x} \right) + \frac{\partial}{\partial y} \left(K_y \frac{\partial \chi}{\partial y} \right) + \frac{\partial}{\partial z} \left(K_z \frac{\partial \chi}{\partial z} \right) \quad (5-1)$$

The fluid is assumed to be incompressible and the concentration χ is the mass of pollutant per unit volume of fluid. U , V and W represent the mean wind in the component directions.

The application of the diffusion equation to a stack plume is discussed by Pasquill (1974). An important assumption is that any net turbulent transport along the mean wind direction, for a continuous plume, is comparatively small with diffusion in other directions. The implication of this is that turbulent velocities are small in comparison with the mean wind velocity as outlined by Frenkiel (1953). For a

single puff of pollutant, diffusion along the mean wind direction is important as air is entrained from all directions. For a steady flow with V and W zero and

$$K_x \frac{\partial \chi}{\partial x} \ll K_y \frac{\partial \chi}{\partial y}$$

(5-1) reduces to

$$U \frac{\partial \chi}{\partial x} = \frac{\partial}{\partial y} \left(K_y \frac{\partial \chi}{\partial y} \right) + \frac{\partial}{\partial z} \left(K_z \frac{\partial \chi}{\partial z} \right) \quad (5-2)$$

In attempting to solve (5-2) serious difficulties arise as the diffusivity is observed to vary with time of travel, position and scale of diffusion. Unfortunately (5-2) can be solved with only the simplest forms of variable diffusivity. Pasquill (1974) notes several solutions for a source at ground and a power law variation of diffusivity and mean wind with height.

The solution of the diffusion equation must satisfy several boundary conditions. The first condition (5-3) deals with mass conservation in that the amount of pollutant passing through any vertical plane must be constant and equal to the source strength m . This further implies that the pollutant be inert as reduction in concentration due to chemical reaction is not considered. Condition (5-4) also follows directly as the equal transport of pollutant through any vertical plane necessitates that the ground be a perfect reflection plane

with respect to concentration. The case of deposition or absorption of pollutant to ground is not treated. As indicated by (5-5), the point source has large concentrations near stack exit while concentration tends to zero at large downwind distances.

$$\int_{-\infty}^{\infty} \int_0^{\infty} U\chi(x,y,z) \, dz \, dy = m \quad (5-3)$$

$$\frac{\partial \chi}{\partial z} \rightarrow 0 \quad \text{as } x \rightarrow 0 \quad (5-4)$$

$$\chi \rightarrow \infty \quad \text{as } x \rightarrow 0 \quad (5-5)$$

$$\chi \rightarrow 0 \quad \text{as } x \rightarrow \infty$$

An alternative to solving for variable K_y and K_z is a more empirical approach where dispersion of pollutant is related to the travel time $t = x/U$. The distribution of pollutant in the y and z directions is represented by two arbitrary functions so that

$$\chi(x,y,z) = \frac{m}{U} E(y)F(z) \quad (5-6)$$

The problem is then reduced to finding the appropriate distribution functions, $E(y)$ and $F(z)$, that fit the character of

plume dispersion and satisfy the boundary conditions.

A Gaussian distribution of concentration from a point source is often observed to occur in the atmosphere. For a variable p the Gaussian distribution has a probability density function $G(p)$, with variance σ_p^2 and mean μ_p , defined as

$$G(p) = \frac{1}{\sigma_p (2\pi)^{1/2}} \exp \left[-\frac{(p - \mu_p)^2}{2\sigma_p^2} \right] \quad (5-7)$$

Assuming $E(y)$ and $F(z)$, in (5-7), to be Gaussian probability density functions like $G(p)$ results in the following solution for concentration.

$$\chi(x, y, z) = \frac{m}{2\pi U \sigma_y \sigma_z} \exp \left\{ -\frac{1}{2} \left[\frac{(y - \mu_y)^2}{\sigma_y^2} + \frac{(z - \mu_z)^2}{\sigma_z^2} \right] \right\} \quad (5-8)$$

It can be shown, Pasquill (1974), for constant K_y and K_z , that a Gaussian is also a solution to (5-2) with K related to the variance by

$$\sigma_y^2 = 2K_y t = 2K_y \frac{x}{U} \quad (5-9)$$

$$\sigma_z^2 = 2K_z t = 2K_z \frac{x}{U}$$

Putting $\mu_y = \mu_z = 0$ indicates the origin to be at stack height. The character of the solution in (5-8) is shown by Fig. 5-1. In this figure the origin is shifted to an effective stack height h_e to compensate for plume rise.

The final modification to (5-8) concerns the requirement of ground reflection as expressed by (5-4). This requires the mathematical mean of an image source as shown in Fig. 5-2. At location I in this figure, virtually no ground level reflection is present. To this point the analysis has assumed this, rightly implying that the bulk of pollutant is above ground. At position J, however, the model fails as it predicts that significant pollutant occurs below ground level. To correct for this an imaginary image source is located below ground. The conservation condition (5-3) requires the image source to have stack height h and source strength m equal to that of the real source. Superposition of both real and imaginary sources results in (5-10). The coordinate system has origin at ground level.

$$\chi(x, y, z) = \frac{m}{2\pi U \sigma_y \sigma_z} \left\{ \exp \left[\frac{-y^2}{2\sigma_y^2} \right] \right\} \left\{ \exp \left[\frac{-(z-h)^2}{2\sigma_z^2} \right] + \exp \left[\frac{-(z+h)^2}{2\sigma_z^2} \right] \right\} \quad (5-10)$$

Equation (5-10) is referred to as the Gaussian plume model for a continuous point source. It represents the most

common approach to dispersion modelling of stack plumes. Fig. 5-3 shows a ground level concentration profile for this model.

For wind tunnel studies it is often more convenient to define a volume concentration C in terms of the volume of pollutant per volume of mixture. Similarly the mass flow rate or source strength m is replaced by the volume flow rate Q . Substituting in C and Q the Gaussian plume model, when stack gas and ambient are at same temperature, is then written as

$$C = \frac{Q}{2\pi U \sigma_y \sigma_z} \left\{ \exp \left[-\frac{y^2}{2\sigma_y^2} \right] \right\} \left\{ \exp \left[-\frac{(z-h)^2}{2\sigma_z^2} \right] + \exp \left[-\frac{(z+h)^2}{2\sigma_z^2} \right] \right\}$$

(5-11)

5.2 Calculation of Plume Spread From Concentration Data

The Gaussian plume model predicts concentration levels that are strongly dependent on downwind distance. Though not explicit in (5-11), this strong dependence enters through the x dependence of the standard deviation in the vertical, σ_z , and crosswind, σ_y , directions. In order to predict a concentration field then requires information on the variation of plume spread with downwind distance. In this study plume spread is measured directly from concentration data taken in the wind tunnel.

To find plume spread for a concentration profile requires a method that is insensitive to the random scatter present in concentration data. This was achieved by using an integral quantity, such as the area bounded by a profile, as the criteria for best fit of the theory. Concentration data is smoothed using cubic splines and the area found by analytical expressions for integrated cubic splines. To find the area under theoretical curves requires integration of (5-11). The integration gives the area A (ppth cm) as

$$A = \sqrt{\frac{\pi}{2}} \sigma_z \left\{ \operatorname{erf} \left[\frac{z_2 - h_s}{\sqrt{2} \sigma_z} \right] + \operatorname{erf} \left[\frac{h_s - z_1}{\sqrt{2} \sigma_z} \right] + \right. \\ \left. + \operatorname{erf} \left[\frac{z_2 + h_s}{\sqrt{2} \sigma_z} \right] - \operatorname{erf} \left[\frac{z_1 + h_s}{\sqrt{2} \sigma_z} \right] \right\} \quad (5-12)$$

where

$$\operatorname{erf}(x) = \frac{2}{\sqrt{\pi}} \int_0^x e^{-t^2} dt \quad (5-13)$$

The contribution of each term in (5-12) to the total area is shown in Fig. 5-4. An iterative procedure was used to match theoretical to experimental areas and find the resultant plume spread.

One important input into (5-12) to find plume spread is the effective stack height. The predicted vertical spread is very sensitive to this quantity. For a plume with no sizeable ground reflection the concentration at stack height C_h coincides with the location of maximum concentration C_{\max} . Refer, for example, to position I in Fig. 5-2. At position K in the same figure, the effect of ground level reflection lowers the position of maximum concentration. In this case the location and magnitude of stack height is not readily discernable. Also, for plumes that rise or fall an effective stack height must be assumed from the data. Some iteration is required to find the correct stack height for these cases. The use of computer assisted interactive graphics greatly simplified the process of fitting data by allowing a visual check of fitted curves.

5.3 Accuracy and Validity of the Gaussian Plume Model

The observation that the dispersion of pollutants in the atmosphere has a Gaussian character led to the formulation of (5-11) for an elevated point source. To verify such an observation requires the comparison of theoretical to actual concentration profile shape.

To study profile shape it is useful to use the plume centerline concentration. Putting $y = 0$ and $z = h$ in (5-11) gives the centerline concentration C_{cr} as

$$C_{cr} = \frac{Q}{2\pi U \sigma_y \sigma_z} \left\{ 1 + \exp\left[-\frac{2h^2}{\sigma_z^2}\right] \right\} \quad (5-14)$$

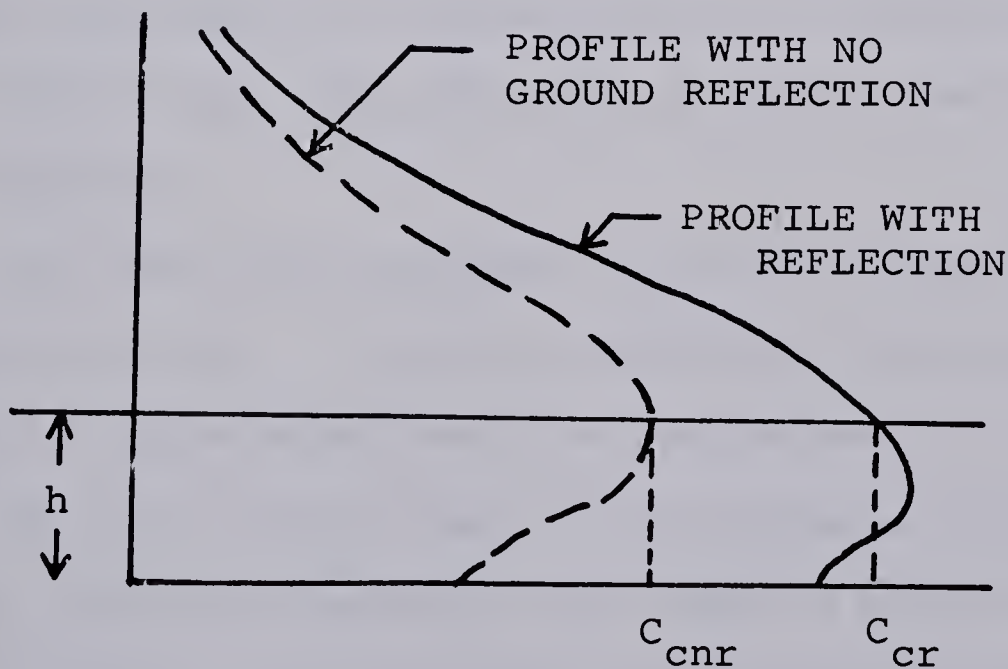
If the profile in question has no ground reflection the exponential term disappears and the centerline concentration becomes

$$C_{cnr} = \frac{Q}{2\pi U \sigma_z \sigma_y} \quad (5-15)$$

so that

$$C_{cnr} = \frac{C_{cr}}{\left\{ 1 + \exp\left[-\frac{2h^2}{\sigma_z^2}\right] \right\}} \quad (5-16)$$

The definitions of C_{cr} and C_{cnr} are shown in the following sketch.



Substituting C_{cnr} from (5-15) into (5-11) yields

$$C = C_{\text{cnr}} \left\{ \exp \left[\frac{-y^2}{2\sigma_y^2} \right] \right\} \left\{ \exp \left[\frac{-(z+h)^2}{2\sigma_z^2} \right] + \exp \left[\frac{-(z-h)^2}{2\sigma_z^2} \right] \right\} \quad (5-17)$$

Application of the fitting techniques described in section 5.2 allows the calculation of C_{cnr} , by (5-16), from concentration data alone. Since C_{cnr} was then fitted to a set of data, any further discrepancies are only due to profile shape. Examples of theoretical fits to concentration data are shown for two downwind locations in Figs. 5-5 and 5-6. Good agreement was obtained in both the crosswind and vertical directions. Fig. 5-19, which will be discussed later, illustrates that good agreement was also obtained for profiles with sizeable ground reflection. The character of concentration data was indeed Gaussian.

To check profile shape C_{cnr} was allowed to fit the concentration data. The next step was to investigate how well C_{cnr} can be calculated from a diffusion model.

To aid in this study, a more general form of a diffusion model for which the Gaussian is a special case is presented, Pasquill (1974). In this model the concentration has the more

general functional form

$$C(x, y, z) = a \exp[-(b|y|^r + e|z|^s)] \quad (5-18)$$

"b" and "e" are constants dependent on plume dimension. When $r = s = 2.0$ a Gaussian results. The constant "a" results from applying the continuity condition (5-3) for given values of "b" and "e". Applying boundary conditions and using the plume standard deviation σ as a measure of plume dimension, results in a general solution in terms of Gamma functions given by (5-19) and (5-20). No ground reflection is assumed.

$$C(x, y, z) = \frac{Q}{B_2 \sigma_y \sigma_z} \exp \left\{ - \left[\left(\frac{\Gamma(3/r)}{\Gamma(1/r)} \right)^{r/2} \left(\frac{y}{\sigma_y} \right)^r + \left(\frac{\Gamma(3/s)}{\Gamma(1/s)} \right)^{s/2} \left(\frac{z}{\sigma_z} \right)^s \right] \right\} \quad (5-19)$$

where

$$\frac{1}{B_2} = \frac{rs}{4\bar{u}} \frac{[\Gamma(3/r) \Gamma(3/s)]^{1/2}}{[\Gamma(1/r) \Gamma(1/s)]^{3/2}} \quad (5-20)$$

From these equations C_{cnr} becomes

$$C_{cnr} = \frac{Q}{B_2 \sigma_y \sigma_z} \quad (5-21)$$

This form of solution has the advantage that the calculation of C_{cnr} is now possible for any of a family of diffusion models. As an example note the assumption of a Gaussian model implies

$r = s = 2$. For this case

$$\left[\frac{\Gamma(\frac{3}{r})}{\Gamma(\frac{1}{r})} \right] \frac{r}{2} = \left[\frac{\Gamma(\frac{3}{s})}{\Gamma(\frac{1}{s})} \right] \frac{s}{2} = \frac{1}{2}$$

and

$$\frac{1}{B_2} = \frac{1}{2\pi U}$$

The Gaussian form of (5-11) is then recovered.

To calculate C_{cnr} from any one diffusion model first requires some input as to the downwind variation of plume spread. To provide this and also obtain centerline concentration data, profiles were taken in the crosswind and vertical directions at different downwind locations. The fitting procedures of section 5.2 were employed and the plume spreads found. The comparison of plume spread to downwind distance indicated a power law variation as shown below. A and B are constants.

$$\sigma = A x^B$$

The comparison of experimental centerline concentration data to that predicted by several different diffusion models is shown in Fig. 5-7. The figure indicates that the prediction of centerline concentration is fairly insensitive to the choice

of exponents r or s , given the scatter in the data. The Gaussian model does, however, provide a reasonably good fit over the entire range of data. This and the apparent insensitivity to exponents make the Gaussian model a viable choice for modeling atmospheric diffusion.

It is tempting to justify the Gaussian model on the basis of observed profile shape. However, profile shape is also only weakly sensitive to r and s between 1.75 and 2.5. For this reason the close agreement between a Gaussian and measured concentration, in Figs. 5-5 and 5-6, is no guarantee that $r = s = 2.0$ is the proper choice.

As a final consideration note that Pasquill (1974) cites the work of Roberts in solving the diffusion equation for a power law variation of velocity with height. The solution is given by (5-19) and (5-20) with $s = 2+n$ for $U \propto z^n$. In experiments in the present study $n = 0.28$ so that the exponents have values $r = s = 2.3$. Given the curves in Fig. 5-7, the change is again seen to be minor when compared to the Gaussian model.

5.4 Choosing An Average Plume Convection Speed

One difficulty with the Gaussian model is that the derivation assumes a uniform mean wind. This is not valid in the atmospheric boundary layer where the mean windspeed varies with height. The simplest choice for a velocity U , to use in the Gaussian plume equation, is the velocity U_s at source

height. This is the velocity used to generate the centerline concentration curves in Fig. 5-7. An alternative to this choice is the use of the average velocity over the plume layer, as suggested by Turner (1969). For ground level releases Högström (1963) uses a weighted value of velocity derived from numerical integration of the continuity condition (5-3). Using concentration measurements the sensitivity of concentration to different values of convection velocity can now be examined.

The nature of Fig. 5-7 is such that the curves shown could be obtained by assuming a Gaussian model ($r = s = 2.0$), and varying the velocity. This is shown in Table 5-1.

TABLE 5-1

EQUIVALENT VELOCITY VARIATION FOR FIG. 5-7

Value of r and s for Curves in Fig. 5-7	Values of U needed to generate this curve for Gaussian model ($r = s = 2.0$) (m/s)
1.5	0.31
2.0	0.45
2.5	0.55
3.5	0.66

Comparing Table 5-2 to Table 5-1 we note that the maximum effect of velocity is equivalent to changing the exponents r and s from 2.0 to about 2.5 in Fig. 5-7. For these experiments the centerline concentration is then only weakly sensitive to the choice of velocity. The velocity at source height does, however, fit the data best over the entire range.

There is no evidence to show that a more suitable value of velocity than that measured at source height should be used.

TABLE 5-2
MAGNITUDES OF CHARACTERISTIC VELOCITIES
FROM EXPERIMENTS

Definition of Characteristic Velocity	Magnitude of Characteristic Velocity from Experiments (m/s)
Velocity at Source Height	0.45
Average Velocity Over Plume Layer	0.50
Average Velocity Over Boundary Layer	0.56

5.5 Corrections for the Effect of Buoyancy On Plume Spread

The spread of a non-buoyant plume in the atmosphere is dependent only on the turbulent structure of the approach flow. If a plume is buoyant there is an added contribution

of velocity fluctuations due to buoyant production. This self generated turbulence greatly increases the initial growth of plume spread. Buoyancy induced growth of plume spread further prevents any form of comparison between data with different or no plume buoyancy.

A correction that accounts for the effects of buoyancy induced spread has been proposed by Pasquill (1976). For spread in either the crosswind or vertical direction

$$\sigma_b^2 = \sigma_{nb}^2 + (\eta \sigma_{self})^2 \quad (5-22)$$

where Pasquill suggests $\eta = 1.0$ and that

$$(\sigma_{self})^2 \approx \frac{(\Delta h)^2}{10} \quad (5-23)$$

The variances σ_b^2 and σ_{nb}^2 refer to the buoyant and non-buoyant cases respectively. Δh is the plume rise.

The correction for buoyancy in (5-22) enters through the plume rise in (5-23) as a sum of variances. If $\eta = 1.0$, the implication is that the effects of plume buoyancy are statistically independent of the processes normally occurring in a buoyant plume. However, turbulent fields do not add

linearly. Only a fraction ($\eta < 1.0$) of the total variance due to buoyancy is likely to contribute.

The origin of (5-23) follows from the Morton, Taylor, Turner (1956) entrainment assumption which produce

$$\frac{dr}{dz} = \beta \quad (5-24)$$

Here r denotes plume radius, z is the vertical rise and β is the entrainment constant for a bent over plume in a laminar crossflow.

Integrating equation 5-24 yields

$$r = \beta z + R_s \quad (5-25)$$

R_s is the constant of integration and represents the initial stack radius. Assuming R_s to be small in comparison with r for the bent over region of the plume gives

$$r = \beta z \quad (5-26)$$

The plume radius can arbitrarily be defined in terms of the plume spread as shown in (5-27)

$$r = \xi \sigma_{\text{self}} \quad (5-27)$$

where ξ is a constant. σ_{self} is due only to buoyancy induced

mixing as the plume is rising in a laminar crossflow. Adopting the previous convention for plume rise so that $z = \Delta h$, and combining equations 5-26 and 5-27 gives

$$\sigma_{\text{self}}^2 = \frac{\beta^2}{\xi^2} \Delta h^2 \quad (5-28)$$

Using the Briggs (1975) recommended value of $\beta = 0.6$ and assuming $\xi = 2$ produces the constant of 1/10 in (5-23).

The direct proportionality between plume rise and plume spread suggests the use of plume rise expressions developed in Chapter IV. The plume rise equation was found to be

$$\Delta h = \left[\frac{3}{\beta_1^2} L_M^2 x + \frac{3}{2\beta_2^2} L_B x^2 \right]^{1/3} \quad (5-29)$$

with $\beta_1 = \beta_2 = 0.87$ for no wind shear.

The entrainment constant β in (5-28) applies to the bent over region of the plume. In this area the buoyant rise is dominant so that by the conventions adopted in Chapter IV, $\beta = \beta_2$ should apply.

To attach physical significance to values of σ_{self} requires an approximation for the non-linear interaction between background and self generated turbulence. This first necessitates a new definition of plume radius. Rewriting (5-28) produces

$$\xi = \frac{\beta \Delta h}{\sigma_{\text{self}}} \quad (5-30)$$

Using measured values of σ_{self} from the laminar crossflow data in Fig. 5-8, the resulting radii are shown in Table 5-3 with Δh computed from (5-29). Using the mean value of plume radius from Table 5-3, of $\xi = 1.75$ gives

$$\sigma_{\text{self}}^2 = \left[\frac{3}{\beta_1^2} L_M^2 x + \frac{3}{2\beta_2^2} L_B x^2 \right]^{1/3} \left[\frac{\beta_2}{1.75} \right] \quad (5-31)$$

TABLE 5-3

DETERMINATION OF PLUME RADIUS

x (cm)	σ_{self} (measured) (cm)	$\xi = \frac{\beta \Delta h}{\sigma_{\text{self}}}$
5	1.20	1.88
20	2.6	1.70
50	3.95	1.88
100	7.0	1.63
		Mean $\xi \approx 1.75$

A comparison for shear effects on vertical plume spread is shown in Fig. 5-8. The data taken in shear flow and grid turbulence shows no consistent difference, given the

scatter in the data. Assuming a statistically independent process, this is equivalent to stating that there is no added variance to the plume due to shear.

The $\beta_2 = 1.4$ used for plume rise in shear flow is not a real entrainment constant because it includes variable windspeed effects. The $\beta_2 = 0.87$ for uniform windspeed with height is the appropriate value of β_2 for the correction.

To investigate the character of the correction two different plumes were used. The first plume had a significant amount of rise in both the momentum and buoyancy dominated regions. The second plume was obtained by doubling the free-stream velocity for the first case. The resulting effects of downwash and a much smaller buoyancy length produced a plume with no rise. However, σ_{self} is due to buoyant mixing and not the actual plume rise. When the plume is sucked into the stack wake by downwash, the buoyancy correction should still apply even if there is no actual rise.

The application of the correction to both plumes is shown in Figs. 5-9 to 5-12. For the high speed case the correction is small as expected for a plume with little buoyancy. For the low speed case the correction is significant and compensates for the large initial growth of plume spread due to buoyancy. It was found that $\eta^2 = 0.33$ in (5-22) best fit the experimental data. Equation (5-22)

then becomes

$$\sigma_b^2 = \sigma_{nb}^2 + 0.33 (\sigma_{self})^2 \quad (5-32)$$

The nonlinear relation between plume variances allows σ_{self} to physically describe plume spread in a laminar cross-flow. The results are shown in Table 5-4.

TABLE 5-4

COMPARISON OF MEASURED AND CALCULATED VALUES OF σ_{self}

$\eta^2 = 0.33$ AND $\xi = 1.75$ IN THE CALCULATION

x (cm)	σ_{self} (measured) (cm)	σ_{self} (calculated) (cm)
5	1.20	1.29
20	2.6	2.52
50	3.95	4.25
100	7.0	6.51

The combined effect on both plumes results in the corrected data forming a common variation of spread with downwind distance. One power law was then used to describe the non-buoyant spread of both plumes. To test this the correction was reversed and the corresponding buoyant values for each plume are generated. The results of this procedure are shown in Figs. 5-13 and 5-14.

The compromise of using a common power law for the non-buoyant spread of both plumes over corrects the low speed case and under corrects for the high speed case. Values of plume spread are, however, very successful when used in the Gaussian model to predict ground level concentrations. This is illustrated in Figs. 5-15 and 5-16.

An attempt was also made to improve the prediction of ground level concentrations by fitting σ_z to the lower half of the profile. As shown in Figs. 5-16 and 5-17, this value of σ_z makes no significant improvement over the value of σ_z from fitting the entire profile.

Referring to Fig. 5-14, note that for downstream distances of more than 100 cm the data for the higher windspeed shows consistently more crosswind spread. This may be due to increased meandering of the plume by a wake of shed vortices behind the stack. Vortex shedding occurs for Reynolds numbers based on outside diameter in the range of 60 to 5000, Schlichting (1968). For the high speed case ($Re = 680$) the plume has no rise and spends it's entire trajectory in the

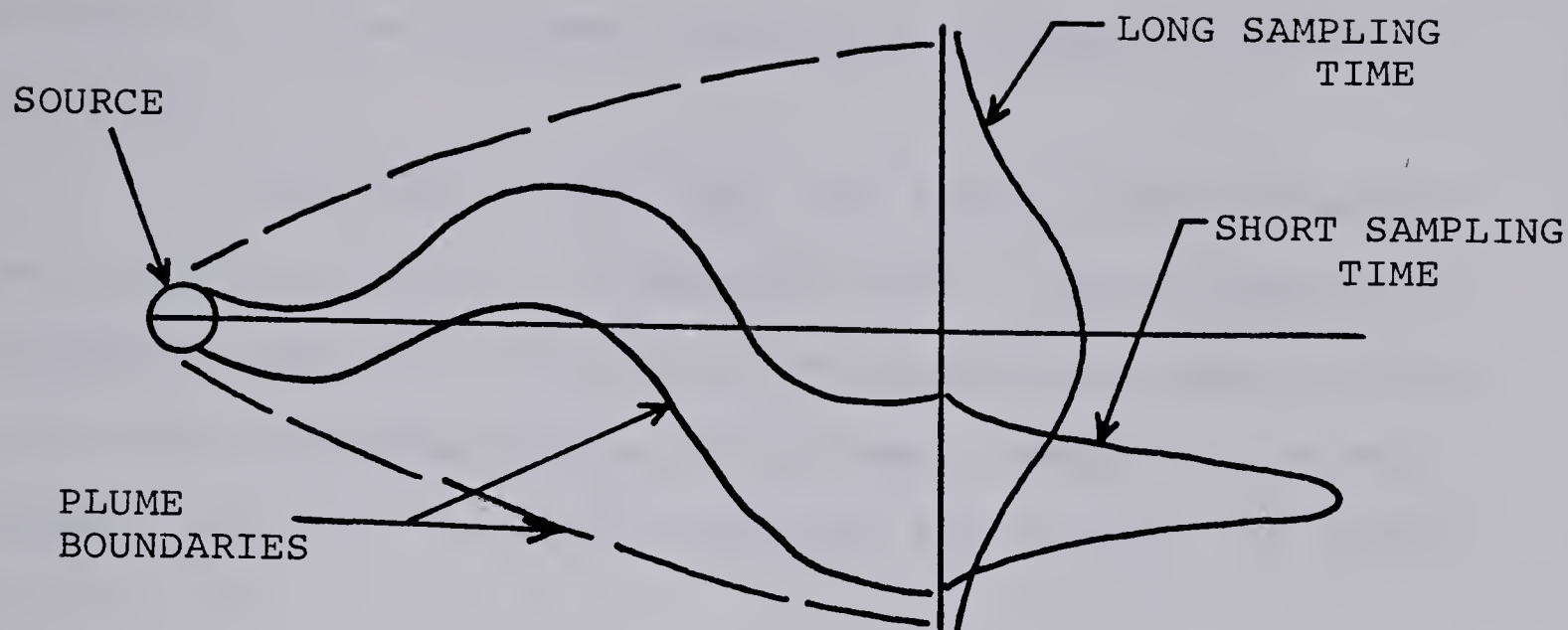
stack wake. However, for the low speed case ($R_e = 340$) the plume rises high enough that stack wake effects quickly become unimportant.

5.6 Comparing Measured Spread to Full Scale σ_y and σ_z

The buoyancy correction produces values of plume spread due to background turbulence alone. These values should agree with full scale studies of plume spread made with non-buoyant tracers. The resulting comparison is shown in Figs. 5-17 and 5-18. There are large differences between different full scale studies, perhaps due to dependence of plume spread on roughness length z_0 and sampling time t . To make a proper comparison the effects of z_0 and t are examined.

The effect on spread of surface roughness has been investigated by Smith in Pasquill (1974). Power law variations for vertical plume spread are given there for roughness lengths of 1, 10, and 100 cm. The effect of z_0 on crosswind spread is also discussed by Hanna et. al. (1977) who suggest a dependence of crosswind spread on $z_0^{0.2}$.

The correction for sampling time stems from the fluctuating nature of a plume. This is best observed in the following sketch.



The sketch also implies that the plume fluctuations are normally distributed about centerline.

To compensate for differences in sampling time the values of plume spread are corrected by the relation

$$\frac{\sigma_1}{\sigma_2} = \left(\frac{t_1}{t_2}\right)^p \quad (5-33)$$

An added complication is that the value of p differs for vertical and crosswind plume spread. This may be avoided by considering the proportionality

$$\chi \propto \frac{1}{\sigma_y \sigma_z} \quad (5-34)$$

so that

$$\frac{\chi_1}{\chi_2} = \left(\frac{t_1}{t_2}\right)^q \quad (5-35)$$

Values for q from different fullscale studies are shown in Table 5-5.

It is evident from Table 5-5 that no one correction yet exists to account for sampling time. For instance, two different curves for vertical plume spread are shown in Fig. 5-17 for a roughness length of 100 cm. Though the curves closely coincide the stated sampling times differ by factors of 10 to 30.

This leads to the subject of comparison of plume spread in general. Basically, the spread of a non-buoyant plume depends on atmospheric turbulence. This is in turn dependent on the thermal stability for convective turbulence and the wind speed for mechanical turbulence. The Pasquill stability and Brookhaven gustiness categories are an attempt to classify the state of turbulence in the atmosphere. This general description of atmospheric variables and the dependence of plume spread on these variables leads to the observed scatter in results. Efforts to correct for roughness length and sampling time may be obscured by the variability in other parameters. Hanna et. al. (1977) stress the importance of providing more detailed information on the atmospheric conditions during tests for determining plume spread.

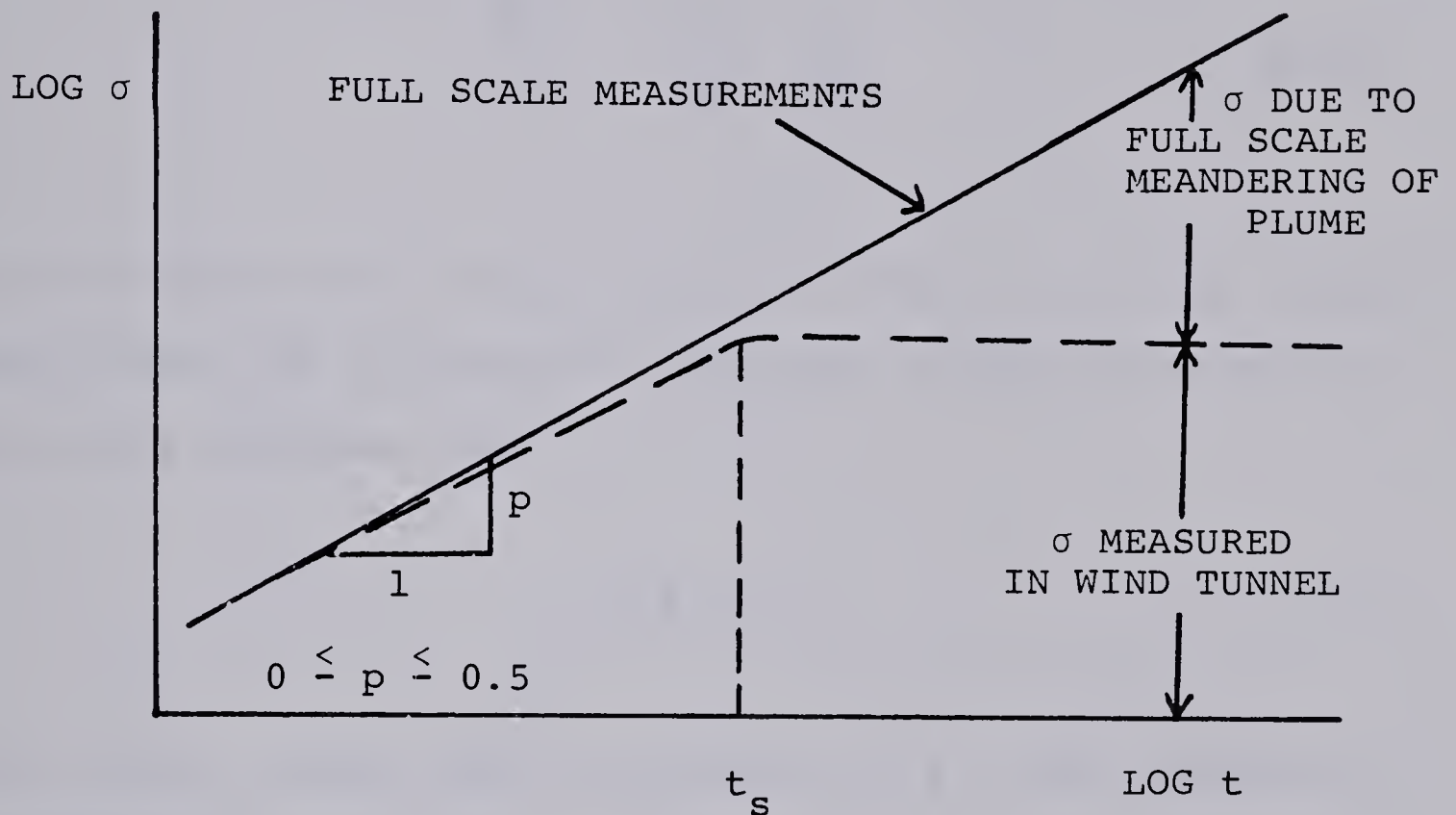
The determination of sampling time for a wind tunnel plume is complicated by restriction of the flow caused by sidewalls on the tunnel. After a sufficient averaging time no further reduction in concentration occurs and the plume

TABLE 5-5

INVESTIGATIONS ON THE EFFECT OF SAMPLE TIME
ON CONCENTRATION MEASUREMENTS

Study	q	Restrictions and Comments
Gifford (1960)	0.2	Centerline Concentrations (Ground Source)
	0.75	Off-Centerline Concentrations (Elevated Source)
Hinds (1969)	0.45	Centerline Concentrations (Ground Source)
Singer et. al. (1963)	0.6	Unstable Conditions
	0.45	Slightly Unstable Conditions
	0.3	Neutral Conditions
	0.15	Light to Heavily Wooded Surface
Turner (1970)	0.17-	t < 2 Hrs
	0.2	
A.S.M.E. Task Group (1973)	0.65	Very Unstable Conditions, t < 1 Hr
	0.52	Unstable Conditions, t < 1 Hr
	0.35	Neutral Conditions, t < 1 Hr
Hino (1968)	0.5	10 Min < t < 5 Hr
	0.2	t < 10 Min
		Ground Level Concentrations

spread is statistically stationary. The atmosphere has sufficient variability that this does not occur. To relate model spread to that in the atmosphere then requires one to determine when the model plume becomes statistically stationary (t_s). This is shown in the following sketch.



A typical concentration profile for the present study is shown in Fig. 5-19 for 100 and 400 second time averages. Though 400 second time averages were enough to well define the concentration profile, the scatter in the data indicates the plume is still non-stationary. However, the large scale variations in the wind tunnel probably do not simulate those in the atmosphere due to the restraining effect of the side-walls. Referring to Figs. 5-17 and 5-18, the 400 second averages in the wind tunnel are estimated to be like 60-90 minute

averages in the full scale. Periods longer than 90 minutes in the atmosphere are likely to show diurnal variation.

The mechanics of plume rise require that both velocity and length be scaled. This immediately leads to a time scale factor where

$$\frac{t_f}{t_m} = \left(\frac{L_f}{L_m}\right) \left(\frac{U_f}{U_m}\right) \quad (5-36)$$

Here the subscripts f and m denote fullscale and model values. Substituting the appropriate length and velocity scales for this study indicates that

$$t_f = 26.84 \ t_m \quad (5-37)$$

A 400 second average then corresponds to a 3 hour average in the fullscale.

The time scales in (5-37), however, relate to the self generated turbulence in a plume. When atmospheric turbulence is dominant for the majority of plume travel, the time scales in (5-36) are questionable.

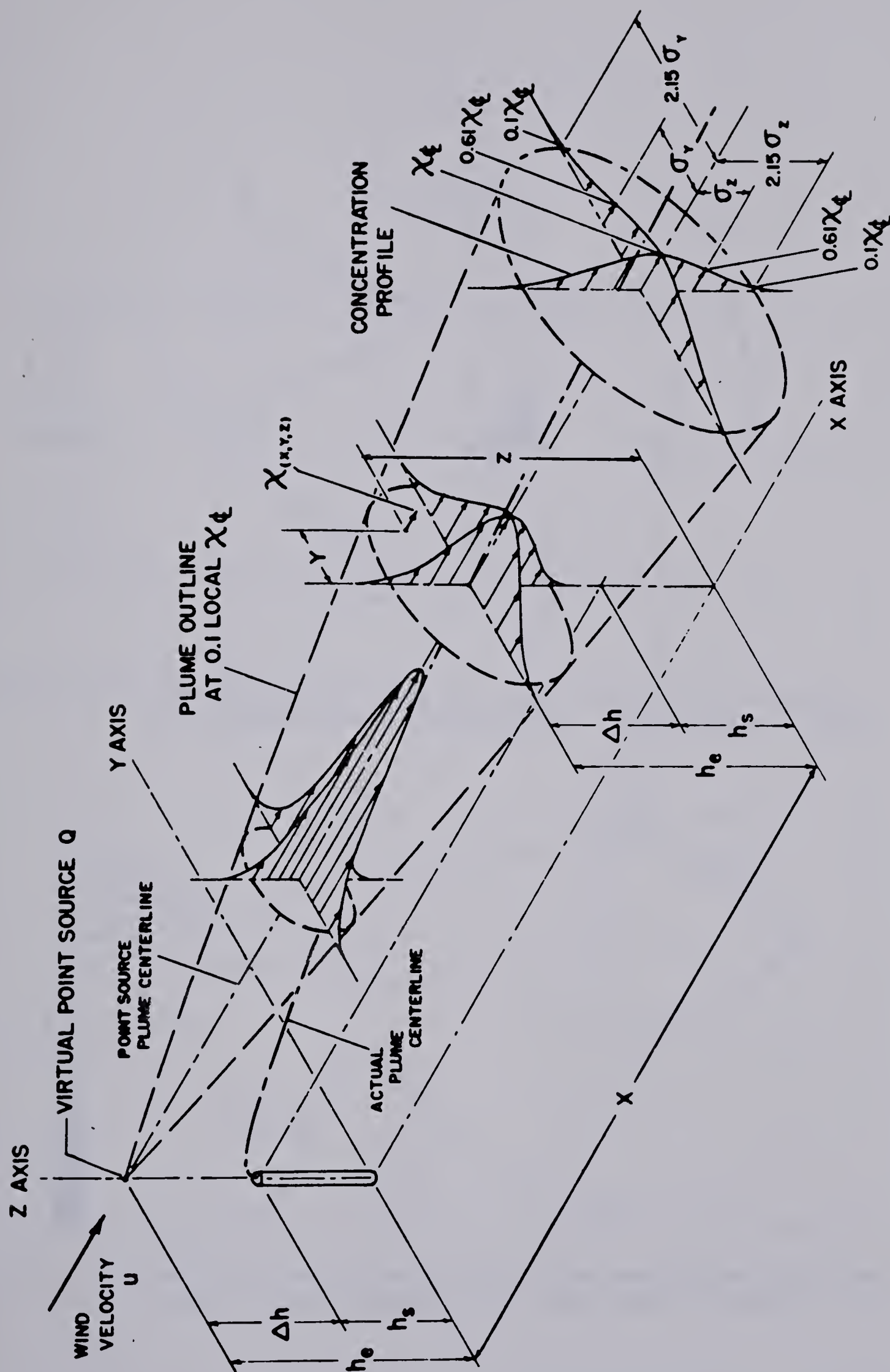


Fig. 5-1 Gaussian Plume Model for a Continuous Point Source. From Stern (1976)

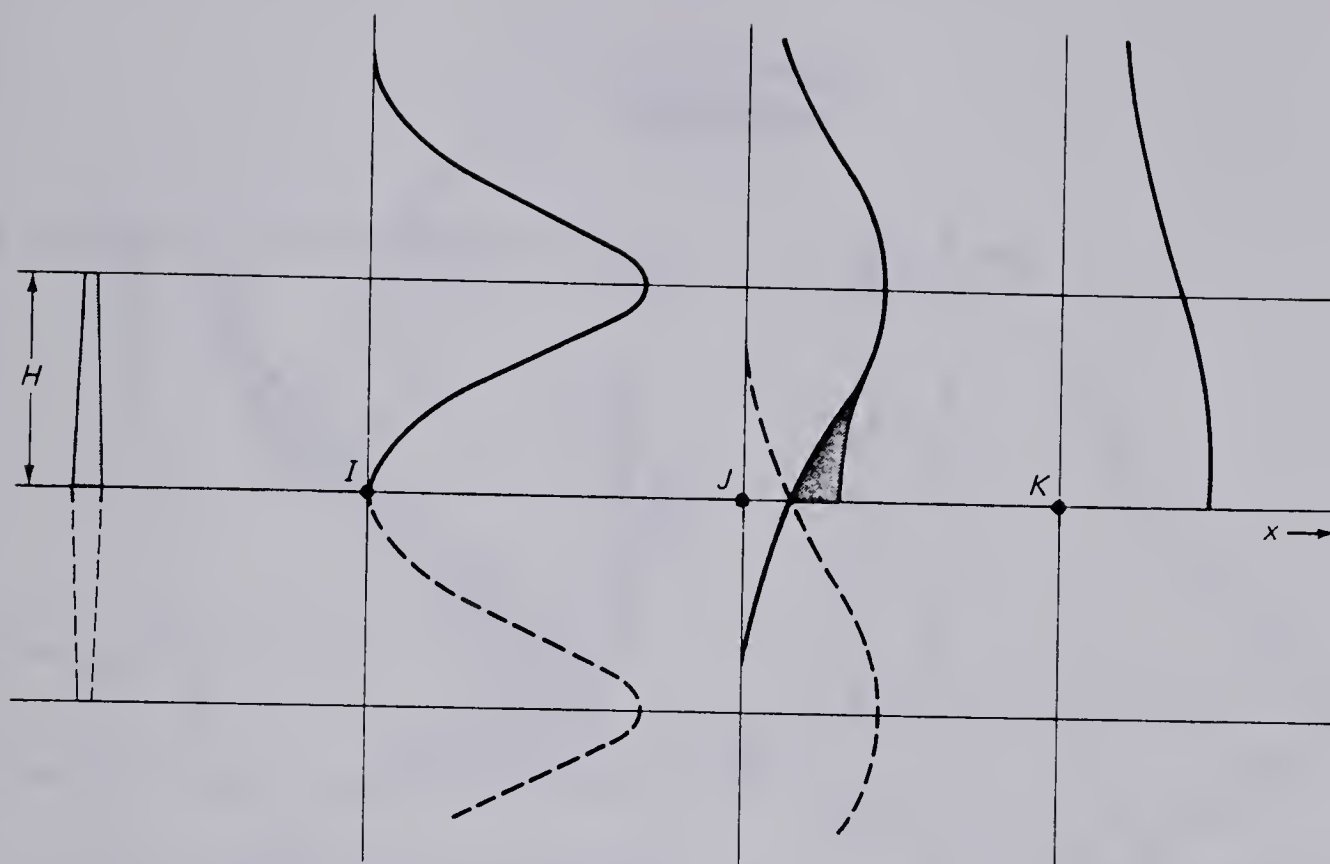


Fig. 5-2 The Application of an Image Source to Correct for Ground Level Reflection. From Stern (1976)

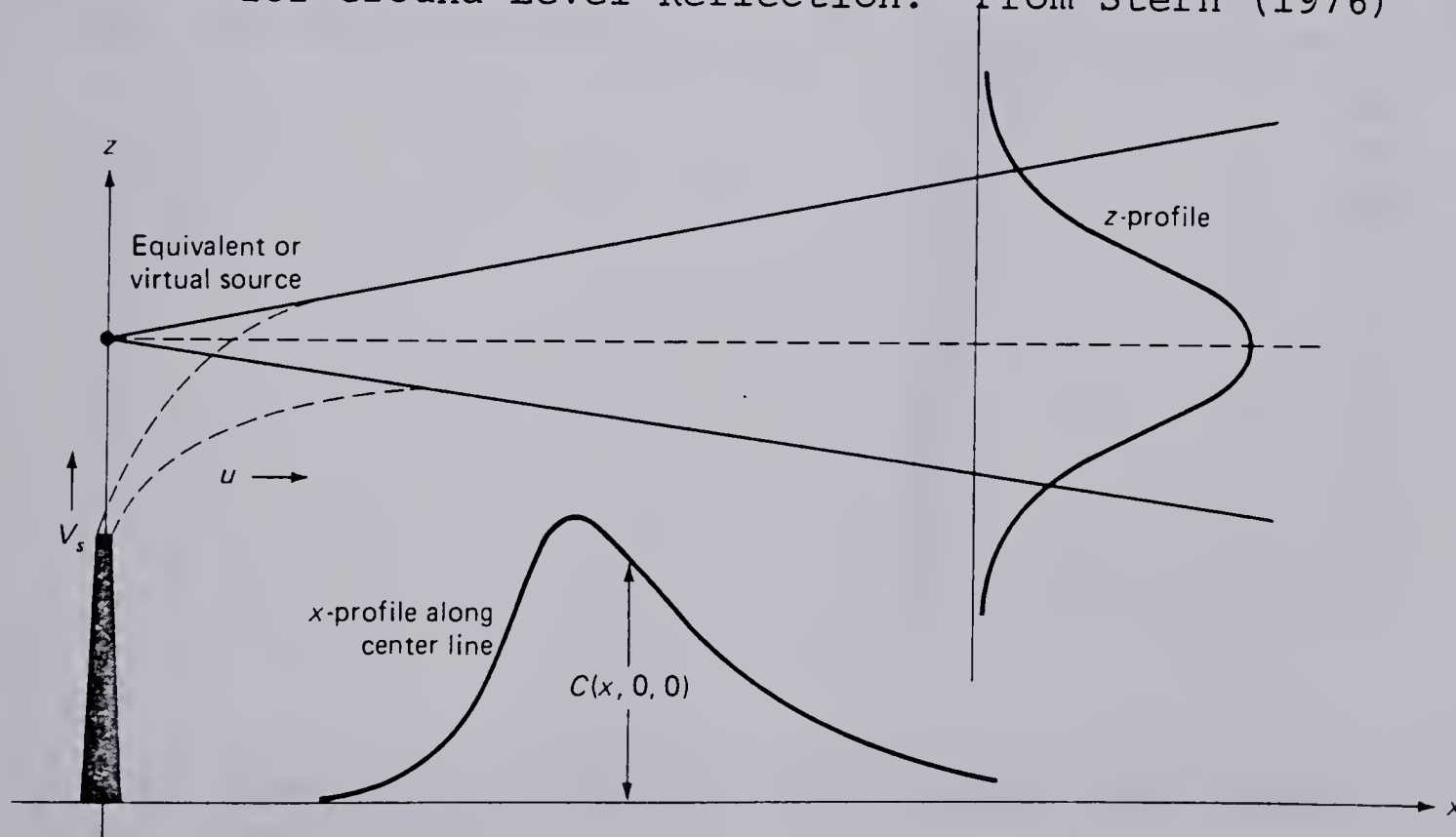


Fig. 5-3 Vertical and Ground Level Concentration Profiles Along Plume Centerline. From Stern (1976)

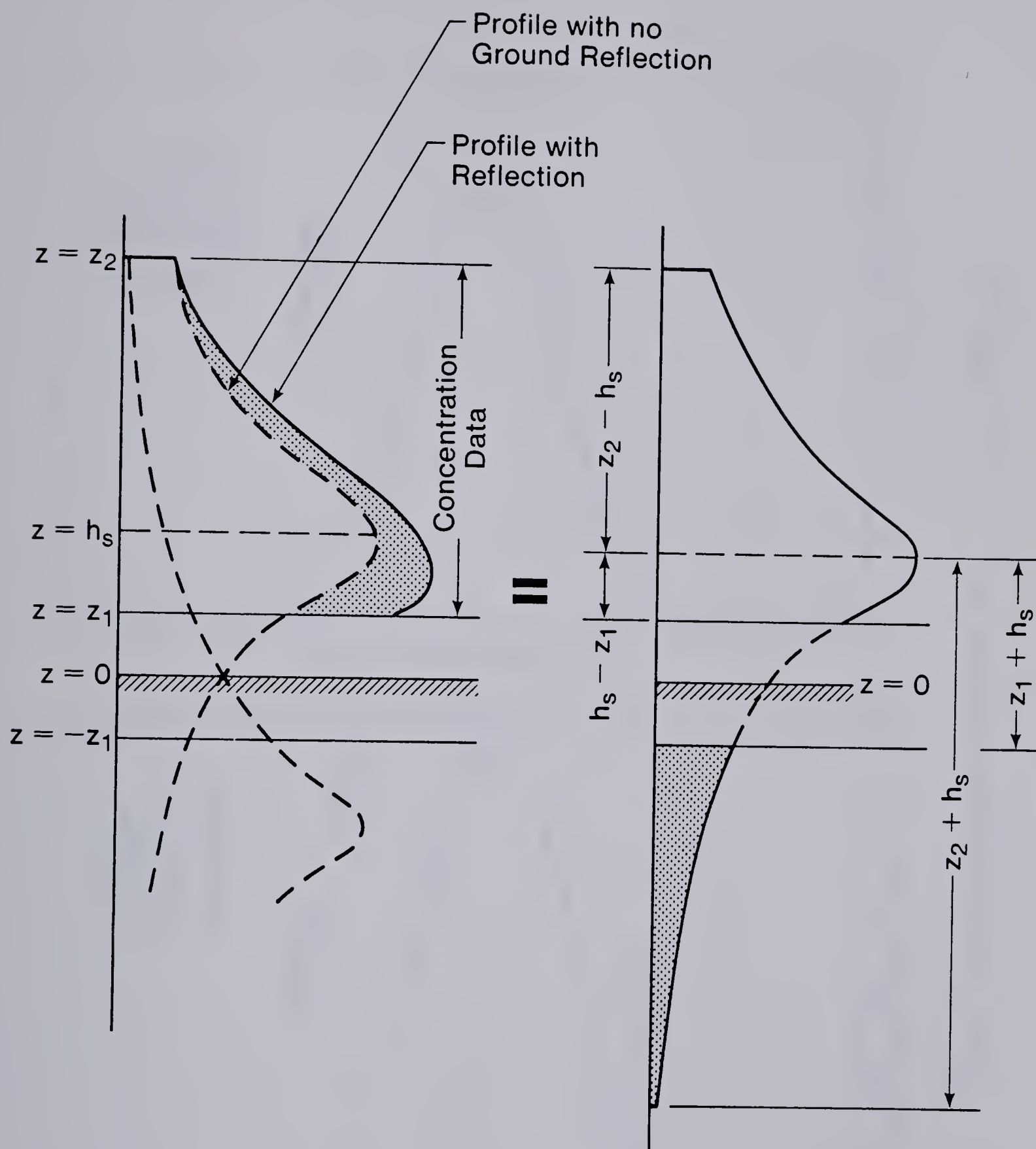


Fig. 5-4 Area Under a Concentration Profile with Ground Reflection

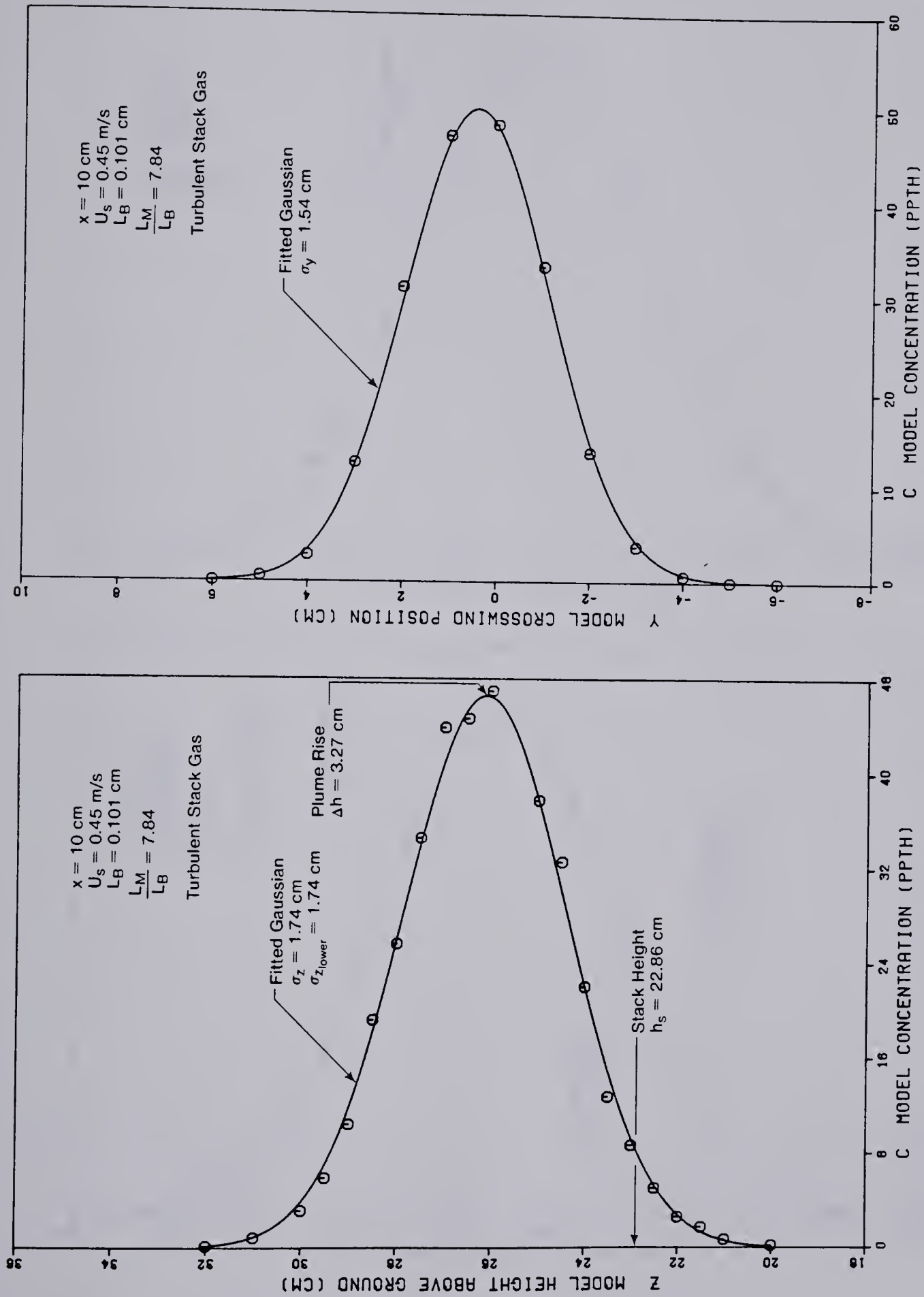


Fig. 5-5 Fitted Concentration Profiles at $x = 10 \text{ cm}$ Downwind

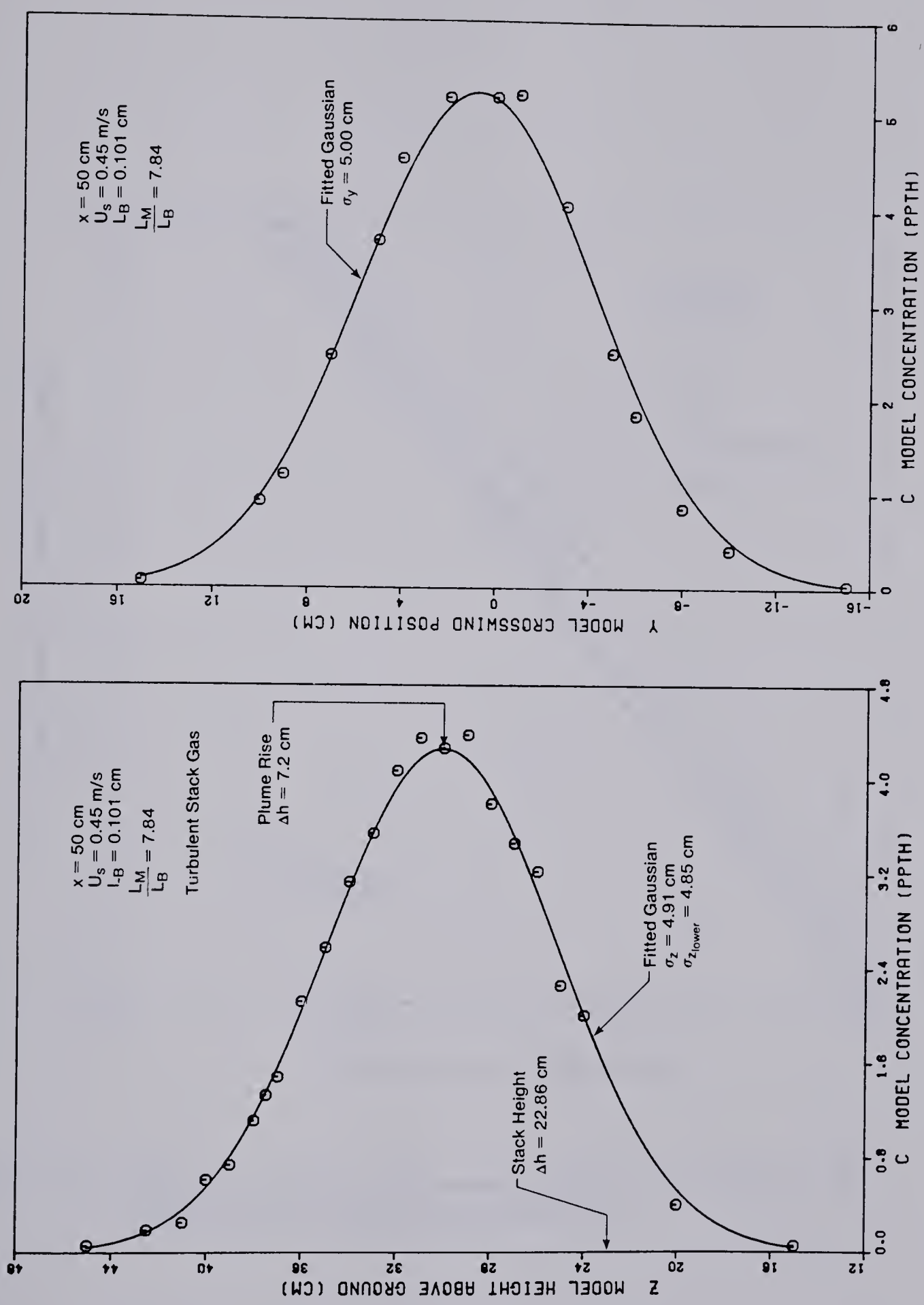


Fig. 5-6 Fitted Concentration Profiles at $x = 50 \text{ cm}$ Downwind

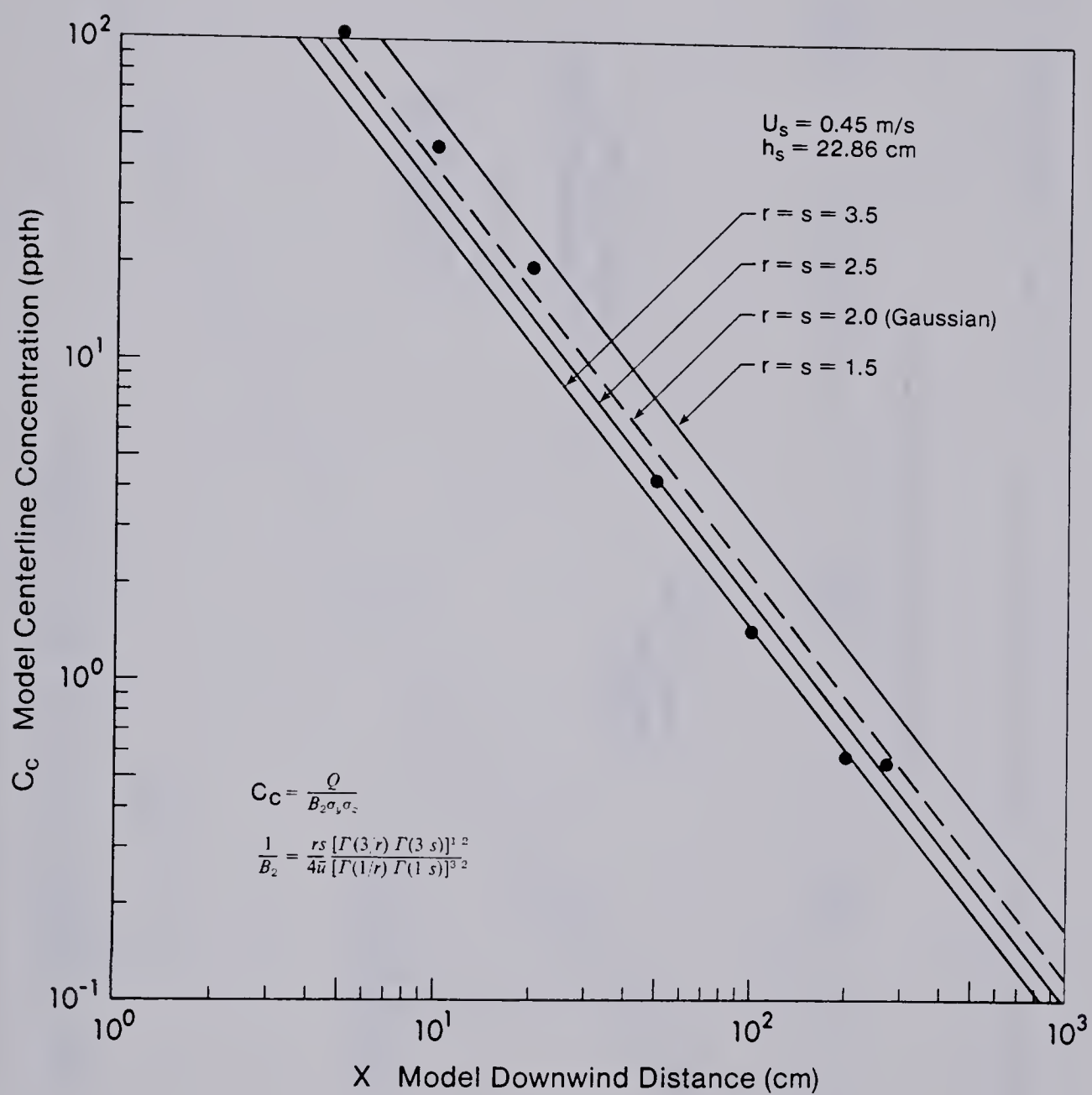


Fig. 5-7 Comparison of Different Diffusion Models to Centerline Concentration Data

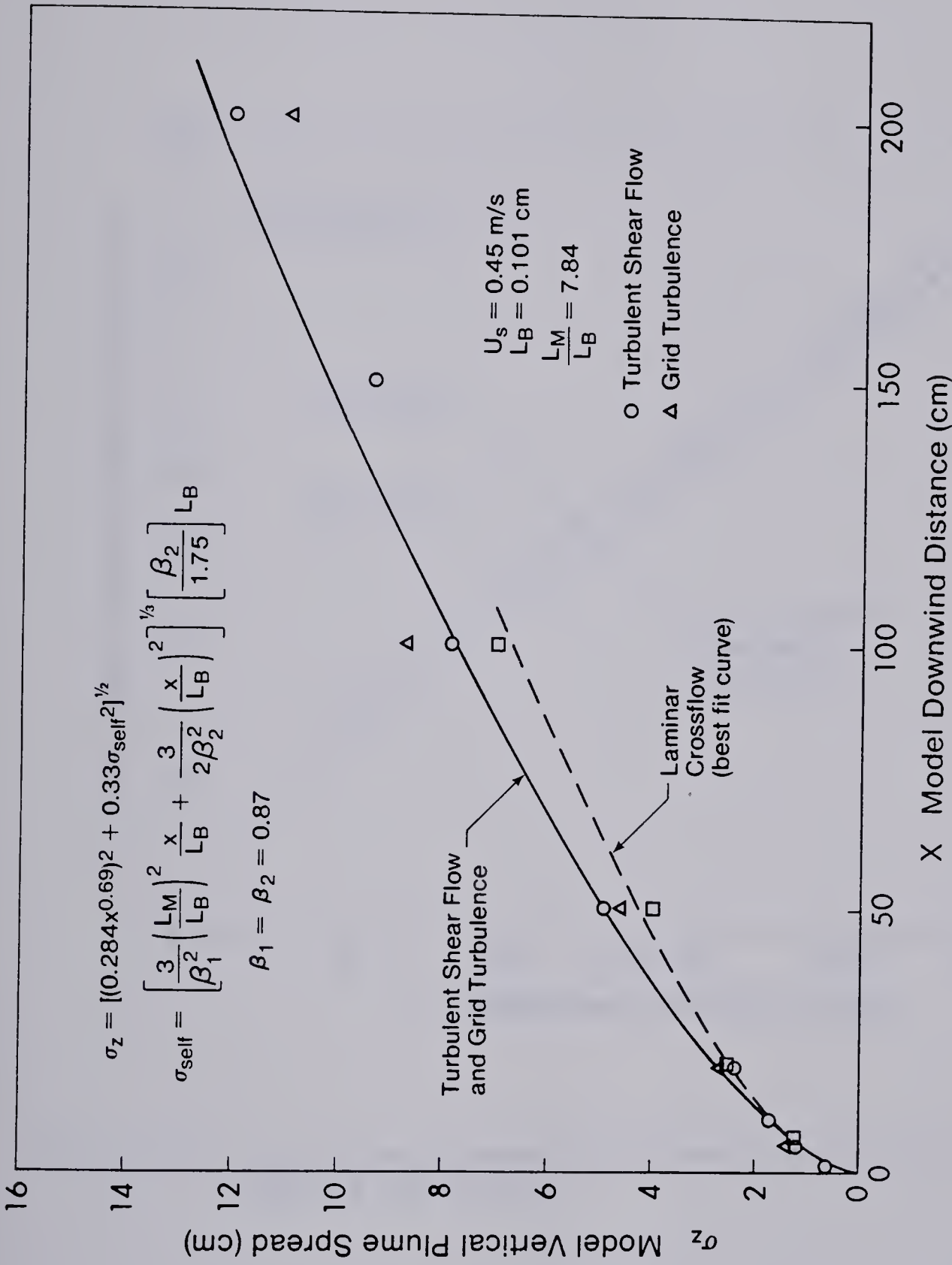


Fig. 5-8 Comparison of Vertical Spread for Different Approach Flows

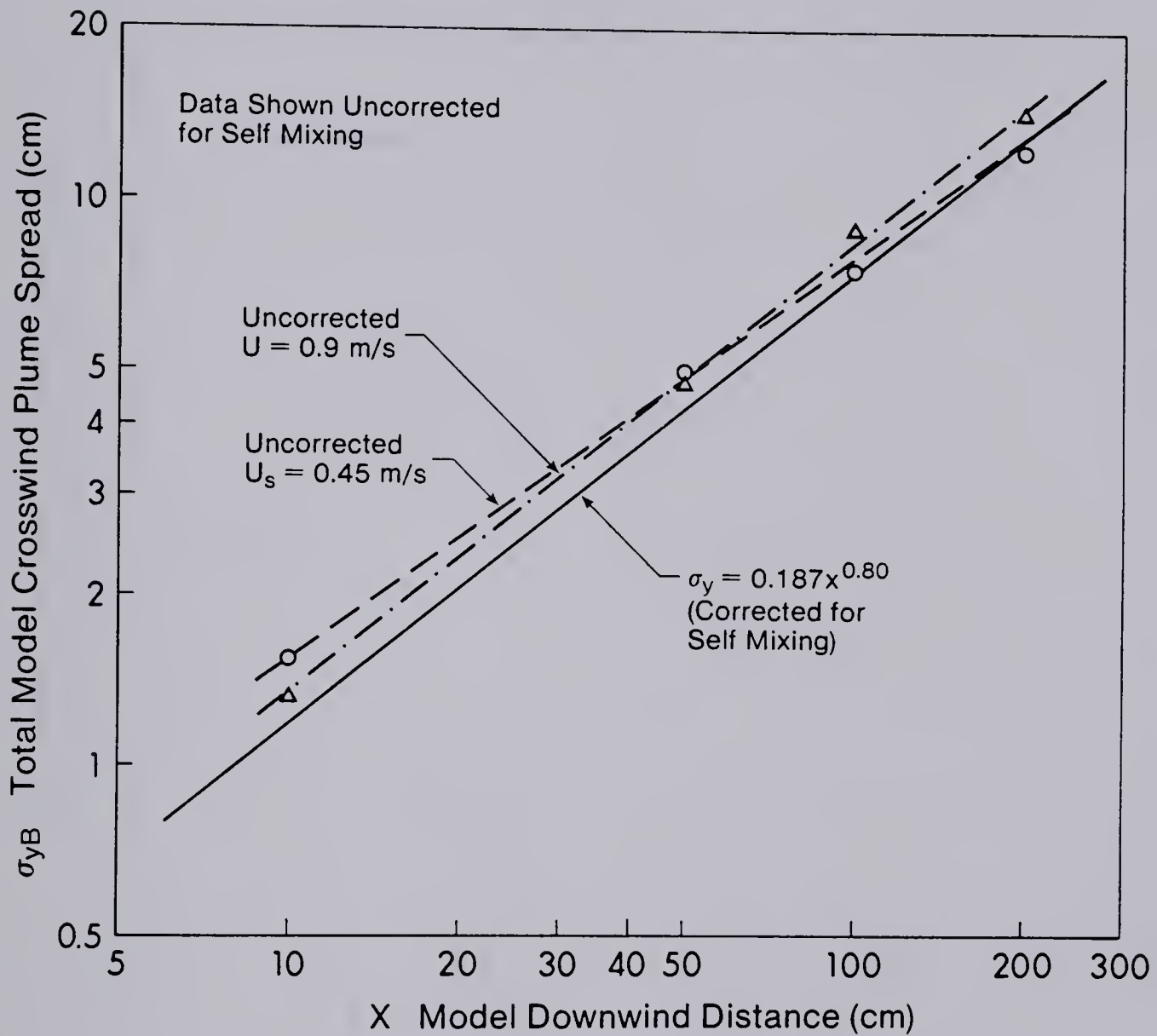


Fig. 5-9 Correcting Crosswind Plume Spread for Buoyancy Induced Spreading

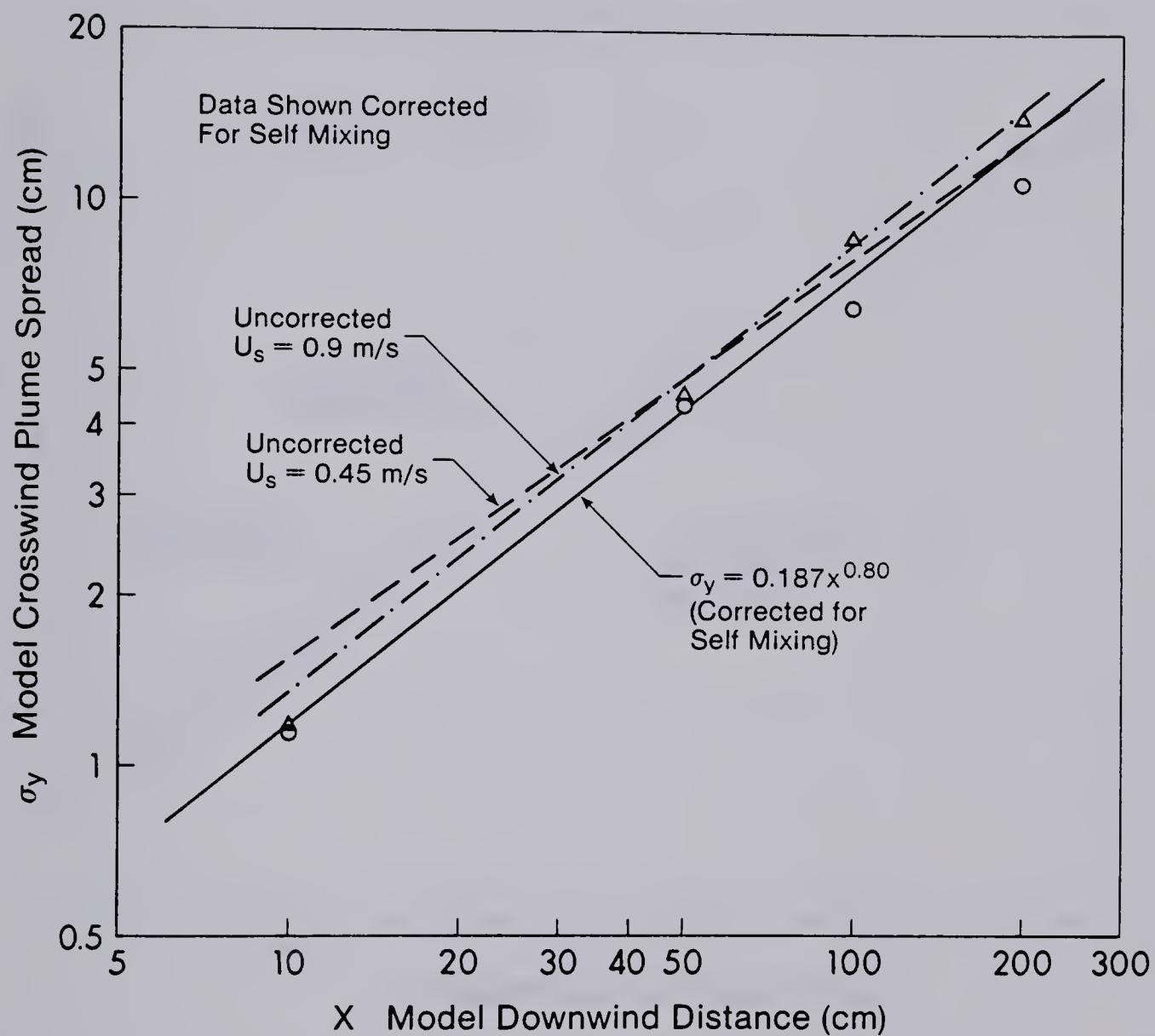


Fig. 5-10 Correcting Crosswind Plume Spread for Buoyancy Induced Spreading

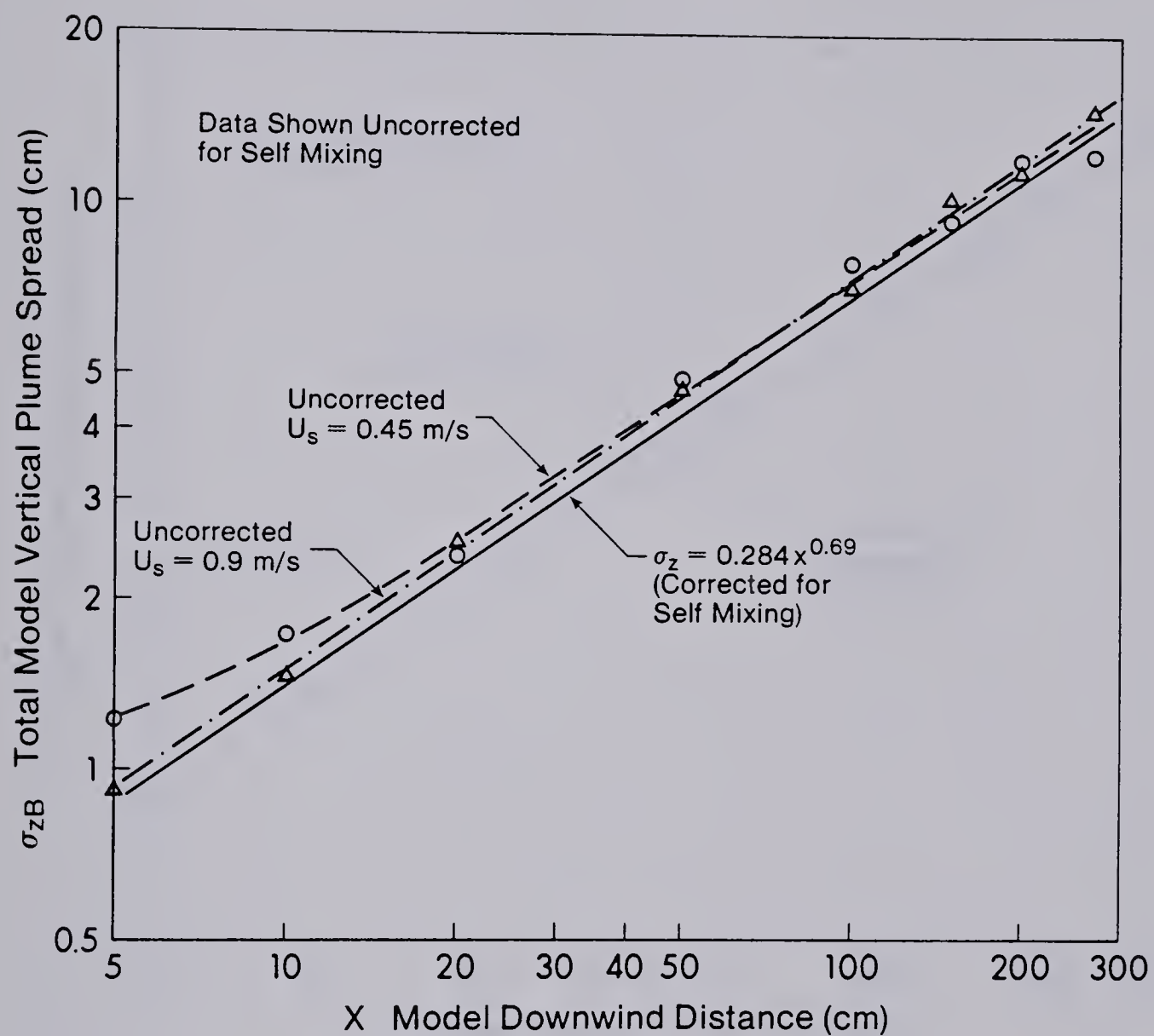


Fig. 5-11 Correcting Vertical Plume Spread for Buoyancy Induced Spreading

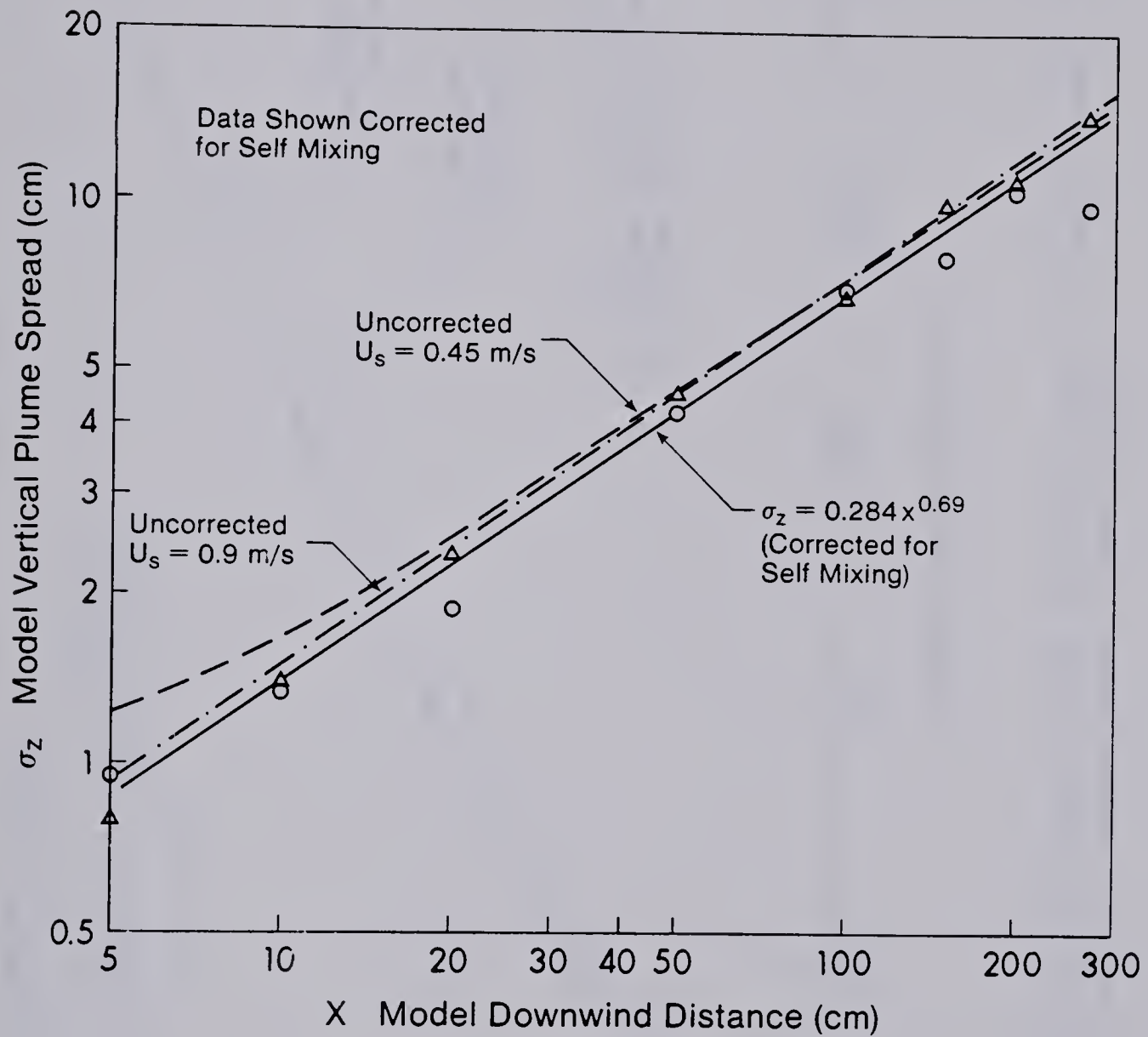


Fig. 5-12 Correcting Vertical Plume Spread for Buoyancy Induced Spreading

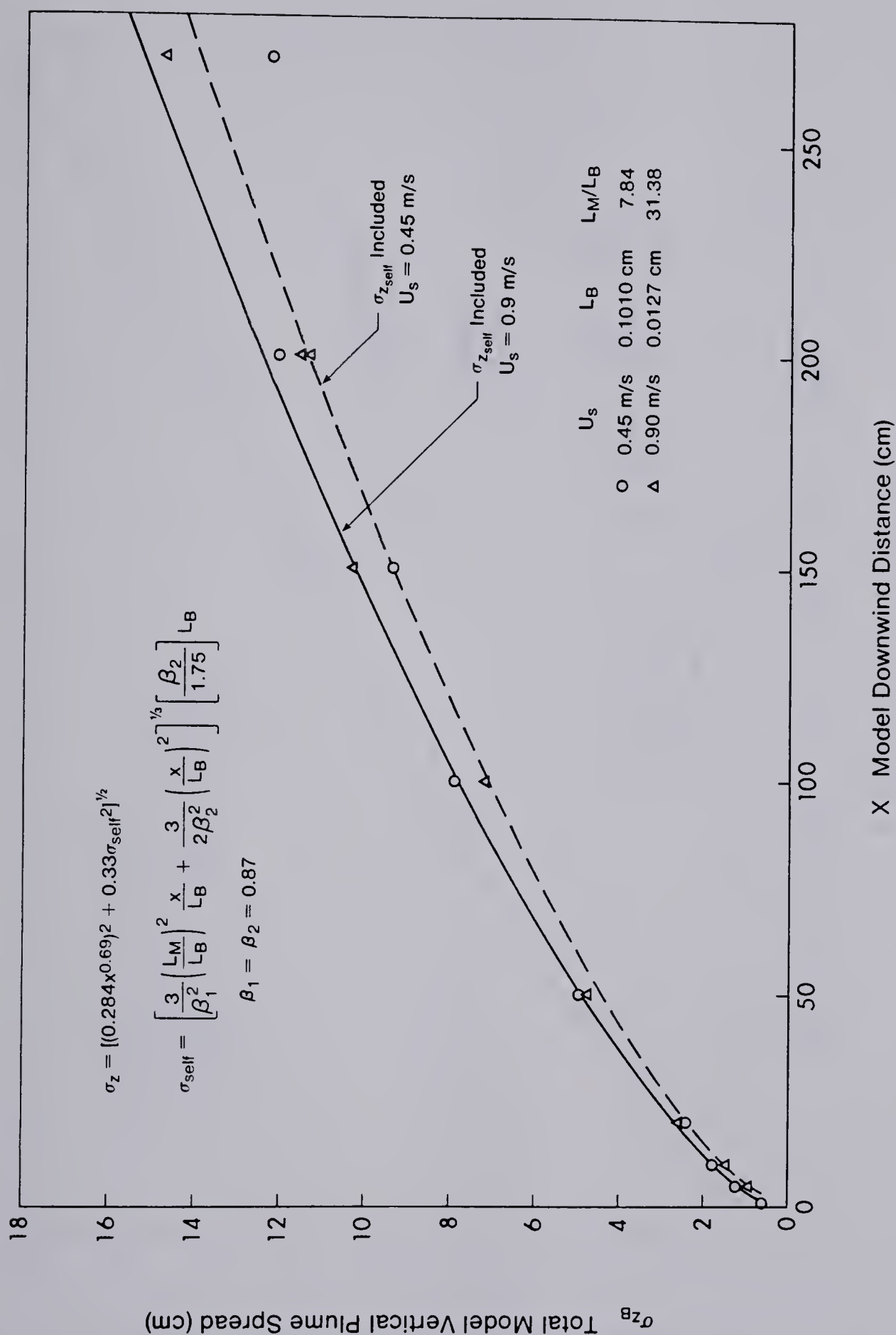


Fig. 5-13 Computed Vertical Plume Spreads From a Single Power Law Relation for Nonbuoyant Plume Spread

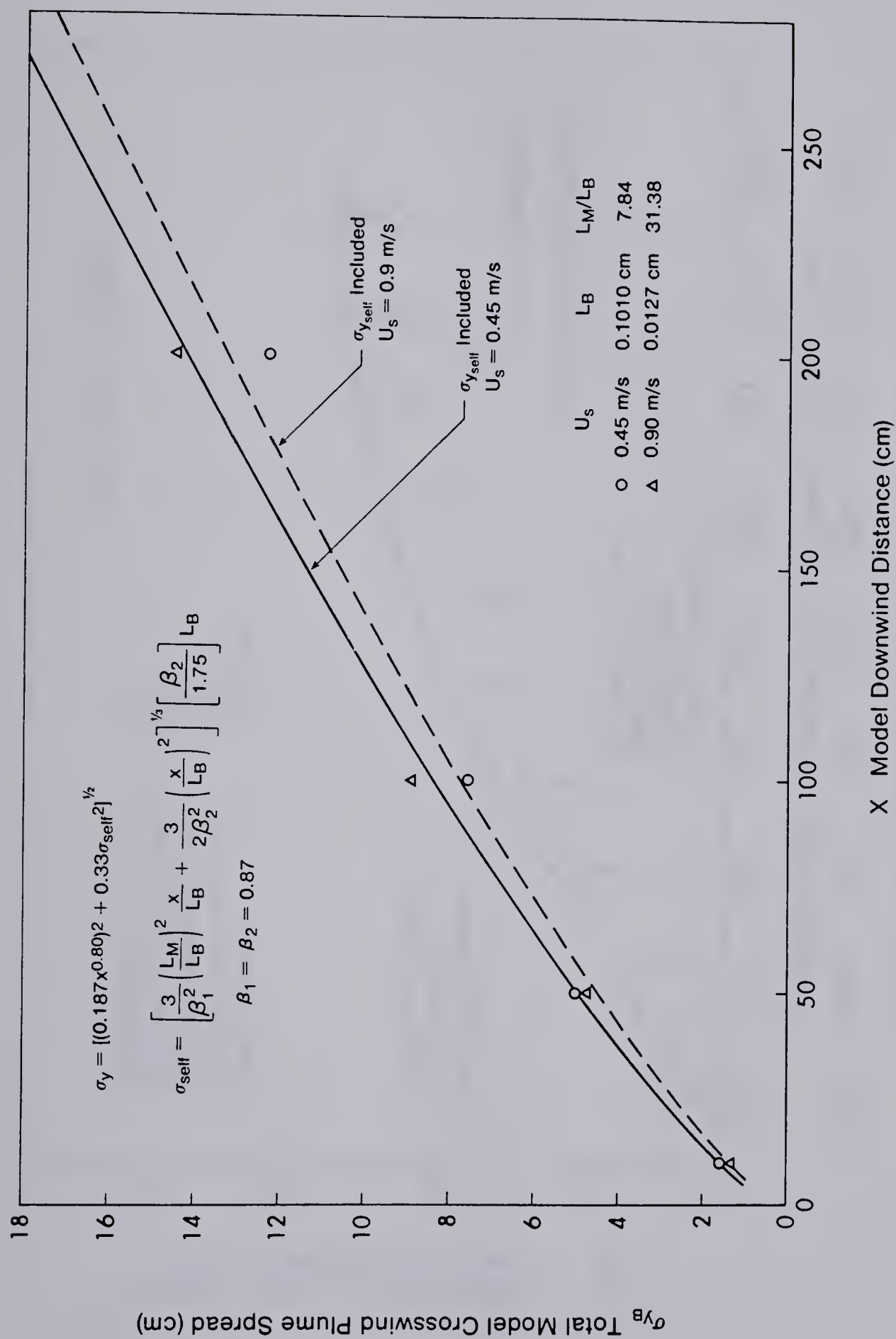


Fig. 5-14 Computed Crosswind Plume Spreads From a Single Power Law Relation for Nonbuoyant Plume Spread

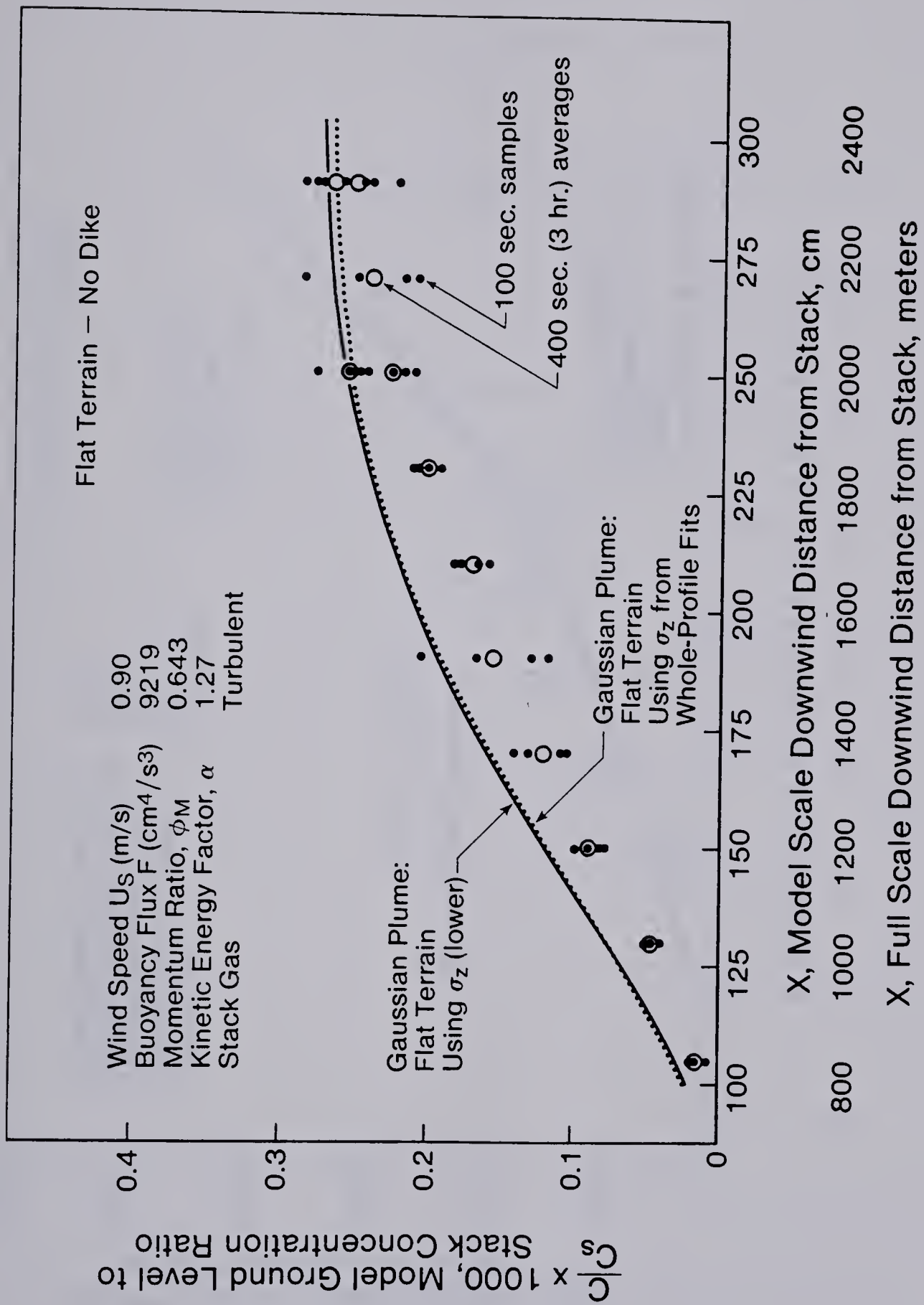


Fig. 5-15 Prediction of Ground Level Concentrations for $U_s = 0.9 \text{ M/S}$

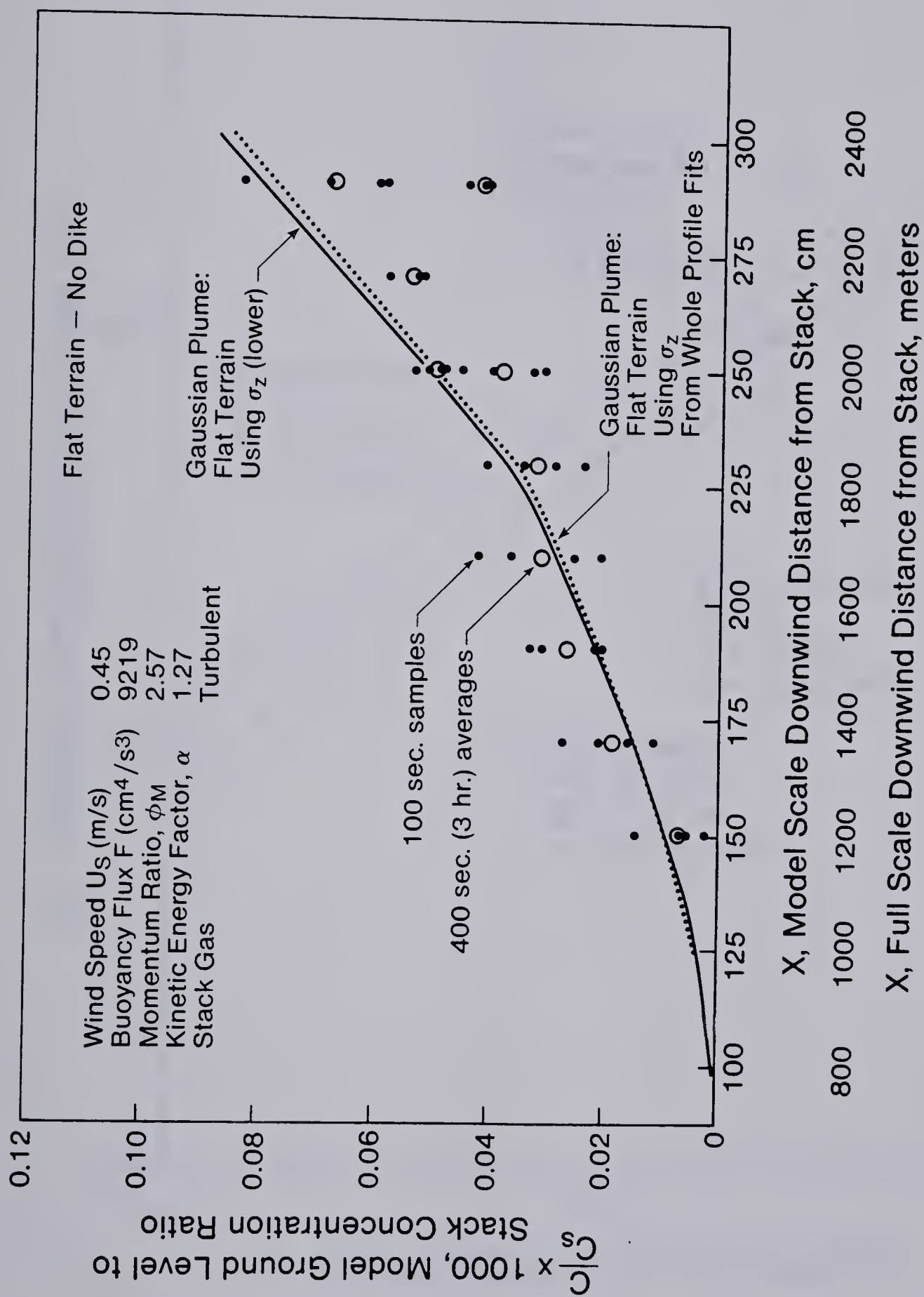


Fig. 5-16 Prediction of Ground Level Concentrations for $U_s = 0.45$ M/S

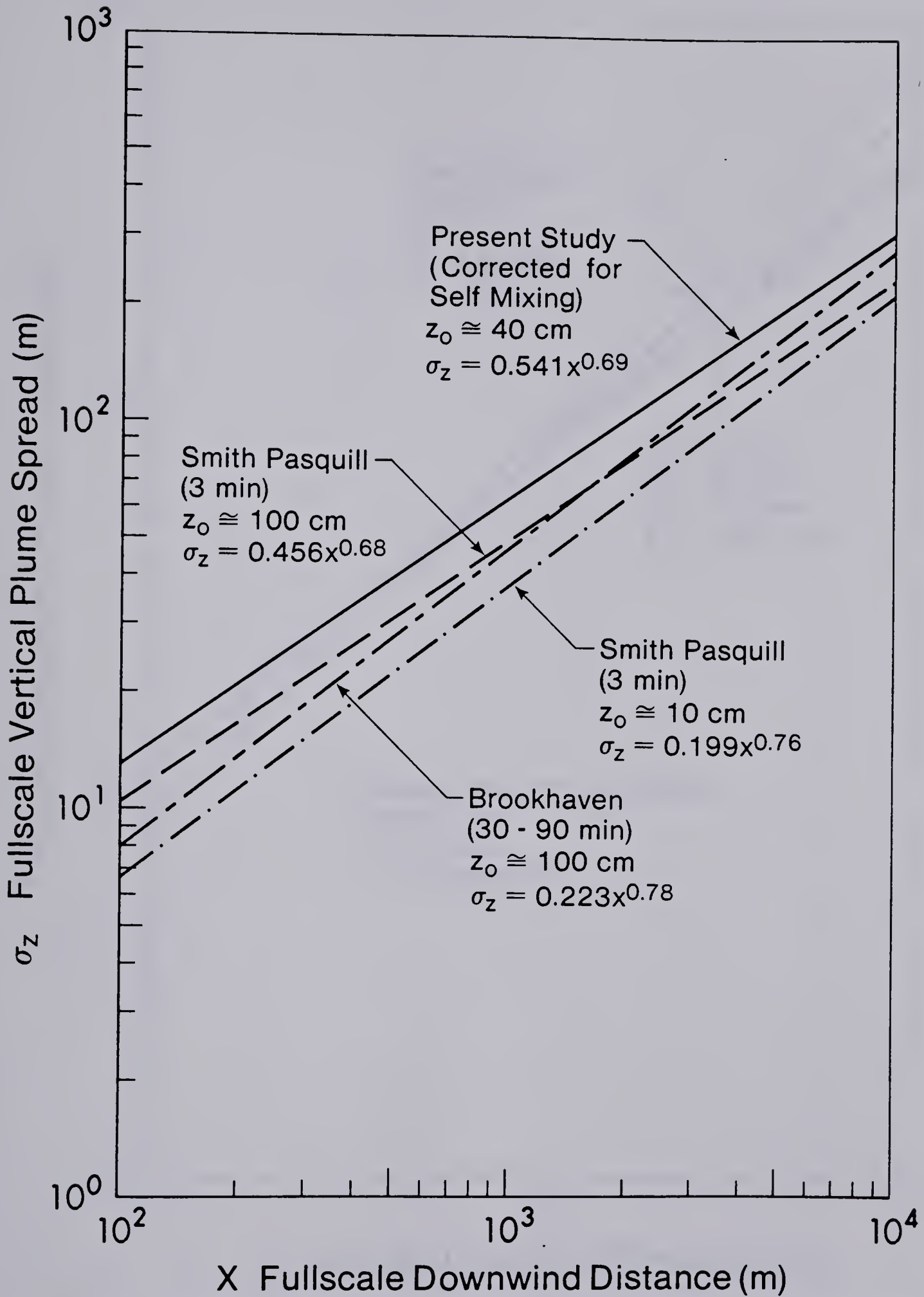


Fig. 5-17 Comparison of Vertical Plume Spread From Model and Fullscale Studies

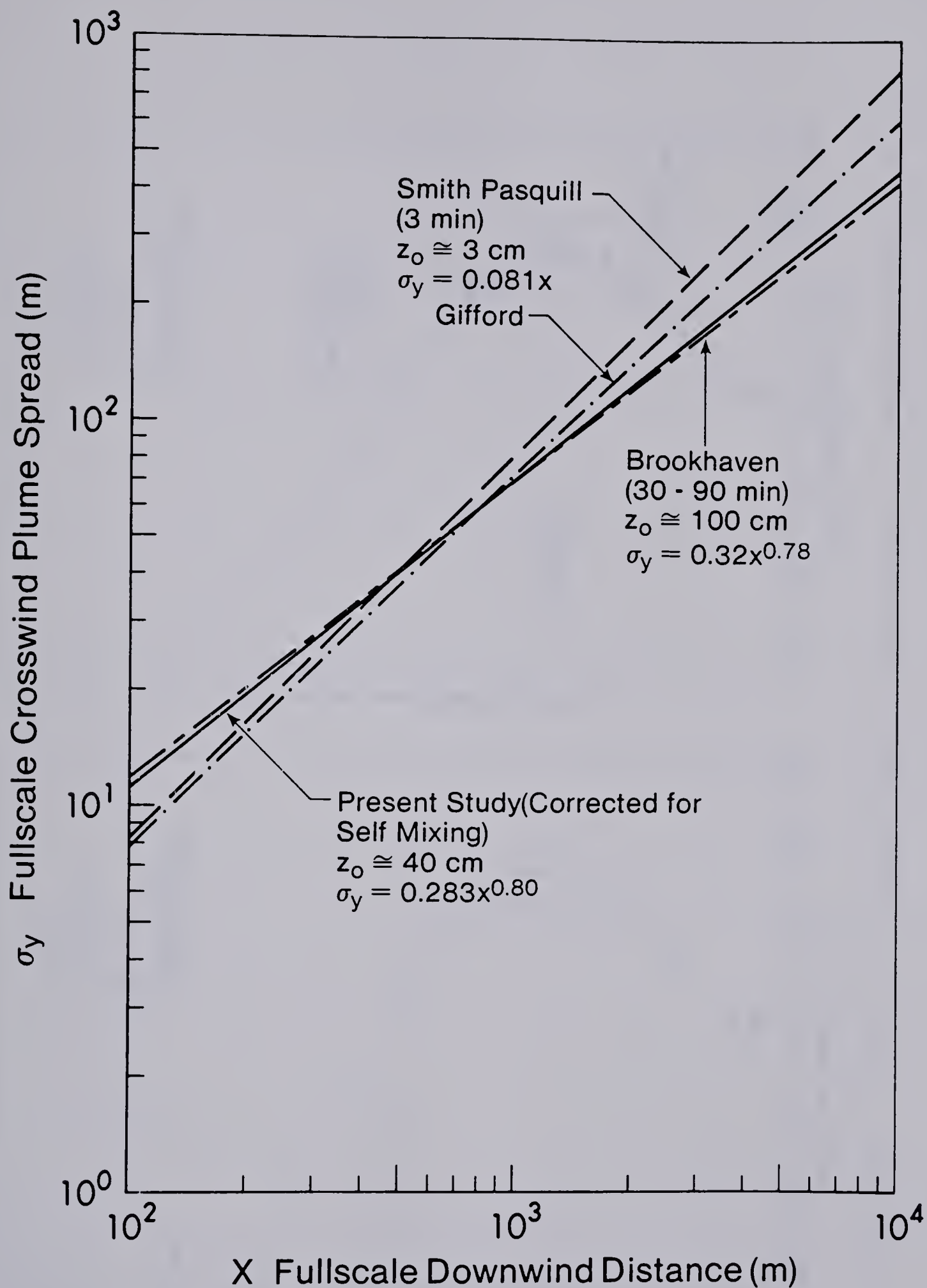


Fig. 5-18 Comparison of Crosswind Plume Spread From Model and Fullscale Studies

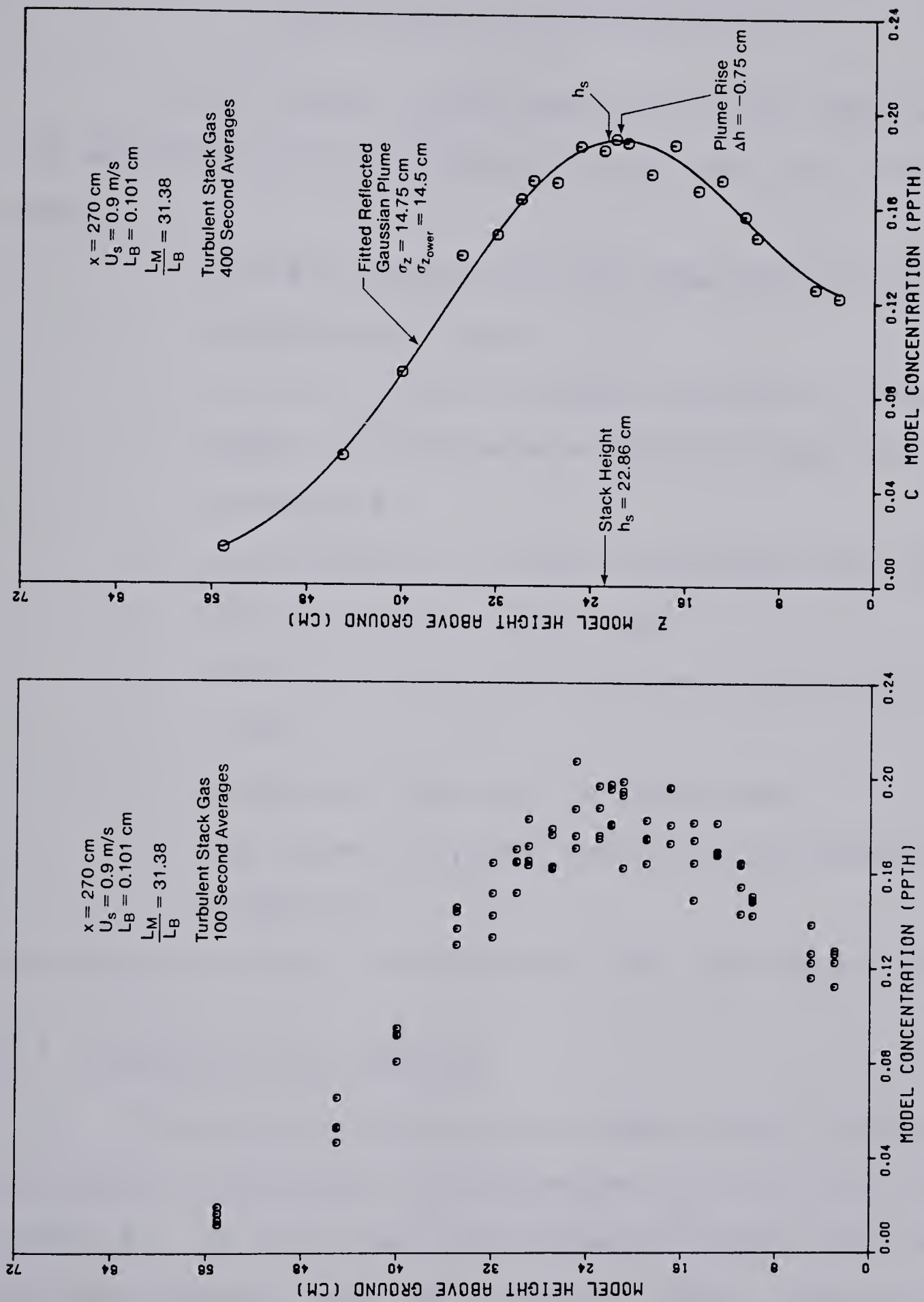


Fig. 5-19 Effect of Sample Time on Measurement of Concentration Profiles

CHAPTER VI

CONCLUSIONS AND RECOMMENDATIONS

In the present study, experiments were conducted in the wind tunnel to investigate the following six problem areas.

1. Scaling criteria for the momentum and buoyancy effects in a plume.
2. Effects of varying stack gas density between model and fullscale to achieve higher wind tunnel velocities.
3. Contribution of stack gas momentum and buoyant forces to total plume rise.
4. Termination of plume rise in a wind tunnel boundary layer.
5. Effect of wind shear on plume rise.
6. The growth of plume spread due to buoyancy induced turbulence.

The result of these investigations are summarized below:

6.1 Modeling Plume Buoyancy

The buoyancy effects in a plume can be characterized by either the buoyancy flux parameter ϕ_B or the bulk Richardson number R_i . In this study, the buoyancy flux was used as a modeling parameter and the resulting buoyancy length L_B was

successfully used to correlate plume rise and dispersion data with different expressions. From this it may be concluded that the "flux" modeling of a plume is a valid way to simulate full scale systems.

6.2 Modeling Plume Momentum

The importance of velocity profile shape, as expressed by α , in correcting the momentum flux has been demonstrated. The change in the total average momentum flux as determined by the shape of the stack gas velocity profile, can substantially alter plume rise if α is not used to correct for this effect.

α did not account for all the effects of velocity profiles across the stack exit. The velocity profile shape also affected diffusion near the source. For example, the low momentum fluid in a laminar stack gas was sucked down by the low pressure region in the stack wake. The added entrainment due to the stack wake skews concentration profiles so that the plume center of gravity is lower.

Larger values of α in a model than those in full scale result in an increase in freestream velocity with respect to the stack efflux velocity. This and the interaction of velocity profile shape with stack wake can alter the character of a plume even though ϕ_M is modelled.

6.3 Effect of Stack Gas Density

By lowering the stack gas density in the model, higher freestream velocities can be used in the wind tunnel. The present study showed that the use of lower stack gas density is a valid procedure if the momentum flux and buoyancy flux are used as modeling parameters. Altering the stack gas density did not result in any significant changes in plume rise or dispersion for constant values of ϕ_M and ϕ_B .

6.4 Plume Rise

Plume rise data obtained from the experiments in the wind tunnel showed that:

1. Total plume rise is a combination of rise due to initial upward momentum of the stack gas and rise due to the action of buoyant forces. The contribution of momentum rise Δh_m and buoyant rise Δh_B to the total plume rise Δh is given by

$$\Delta h = (\Delta h_m^3 + \Delta h_B^3)^{1/3} \quad (4-8)$$

Both Δh_m and Δh_B depend on source conditions and an entrainment constant.

2. The entrainment constant for momentum rise can be related to source conditions by

$$\beta_1 = 0.33 \left(\frac{\rho_s}{\rho_a} \right)^{1/2} + \frac{1}{\sqrt{\phi_M}} \quad (4-18)$$

The relation was first suggested by Briggs (1975) and modified by Wilson (unpublished). Equation (4-18) was verified by experimental data in the present study. The use of (4-18) makes the momentum rise Δh_M entirely dependent on source conditions.

3. Turbulent eddies can break up a plume to the extent that atmospheric turbulence dominates plume motion and causes termination of plume rise. Plume rise terminates at a downwind distance of $2200 L_B$ for the shear flow tested.
4. The presence of velocity shear in the flow lowered plume rise about 20% compared to a uniform flow. The shear correction of Djurfors and Netterville (1978) was found to slightly overcorrect the plume rise data in a uniform flow. However, the final rise of the plume in shear flow was accurately predicted by their correction.
5. For a turbulent stack gas, turbulence in the approach flow had no significant effect on plume trajectories. This was indicated by plume rise data taken in a laminar crossflow as compared to that in grid wake turbulence.
6. A dependence of the entrainment constant β_2 on source conditions is suggested by plume rise data

for uniform crossflows. A strong dependence on whether the stack gas was laminar or turbulent is indicated. Thus, initial source conditions strongly affect plume rise and should be given more attention when modeling buoyant plumes.

6.5 Plume Dispersion

Turbulent diffusion of a stack plume showed that:

1. The commonly used Gaussian diffusion model correctly characterizes plume dispersion. The model was shown to accurately fit experimental concentration profiles. Using the model to predict both centerline and ground level concentrations showed good agreement with experimental measurements.
2. The comparison of different dispersion models as given by (5-19) and (5-20) indicates that the Gaussian model is a viable choice for modeling atmospheric diffusion.
3. The Gaussian model is derived with the assumption that freestream velocity is uniform with height. Application of the Gaussian model in a shear flow requires the choice of a plume convection speed. Centerline concentration data showed good agreement with values computed from the Gaussian model when the measured velocity at stack height was used

in the calculations.

4. The value of plume spread due to buoyancy σ_{self}^2 could be measured by releasing a plume in laminar crossflow. Using a plume radius ξ normalized with plume spread gave $\xi = 1.75$. The dispersion data in a laminar crossflow could then be predicted by the expression

$$\sigma_{\text{self}}^2 = \left[\frac{3}{\beta_1} L_M^2 x + \frac{3}{2\beta_2} L_B x^2 \right]^{1/3} \left[\frac{\beta_2}{1.75} \right] \quad (5-31)$$

5. The interaction of buoyancy induced turbulence and atmospheric turbulence is nonlinear. The total plume spread variance σ_b^2 was found to relate to the spread due to atmospheric turbulence σ_{nb}^2 and the spread due to plume buoyancy σ_{self}^2 by the relation

$$\sigma_b^2 = \sigma_{\text{nb}}^2 + 0.33 (\sigma_{\text{self}})^2 \quad (5-32)$$

6. The sample time in wind tunnel experiments cannot be directly related to that in the fullscale. However, averaging times sufficient for the plume to be close to statistically stationary in the wind

tunnel likely correspond to a sample time of 60-90 minutes in the fullscale. Periods longer than 90 minutes in the atmosphere are likely to show diurnal variation.

7. The use of plugs with small holes to produce a turbulent stack gas resulted in large values of 0.20 for the turbulence intensity of the stack gas. However, this had no discernable effect on plume spread.

6.6 Recommendations

The present study showed a wind tunnel simulation could be used to successfully model plume rise and dispersion. The following recommendations are given for further modeling studies.

1. The effects of stack gas exit velocity profile and stack wake should be carefully considered as plumes were found to be very sensitive to source conditions.
2. The model stack gas density can be varied to achieve higher windspeeds in the wind tunnel if ϕ_M and ϕ_B are used as scaling parameters. However, stack gas density should be modelled when possible.
3. To investigate plume behaviour, a plume trajectory should be taken in a uniform velocity crossflow so

that the effect of velocity shear does not enter into the results.

The present study showed a wind tunnel simulation could be used to successfully model plume rise and dispersion.

REFERENCES

REFERENCES

- Asme Task Group (1973), Recommended Guide for the Prediction of the Dispersion on Airborne Effluents, 2nd ed., American Soc. Mech. Eng., New York, New York, U.S.A.
- Baines, W. D. and Peterson, E. G. (1951), "An Investigation of Flow Through Screens", Trans. American Soc. Mech. Eng. 73, pp. 467-480.
- Briggs, G. A. (1969), Plume Rise, U.S. Atomic Energy Commission.
- Briggs, G. A. (1975), "Plume Rise Predictions", Air Resources Atmospheric Turbulence and Diffusion Laboratory, Oak Ridge, Tennessee, U.S.A., ATDL Contribution File No. 75/15.
- Cermak, J. E. (1975), "Applications of Fluid Mechanics to Wind Engineering--A Freeman Scholar Lecture", Jour. Fluids Eng. 97, pp. 9-38.
- Counihan, J. (1975), "An Improved Method of Simulating an Atmospheric Boundary Layer in the Wind Tunnel", Atmospheric Environment 3, pp. 197-214.
- Djurfors, S. and Netterville, D. (1978), "Buoyant Plume Rise in Nonuniform Wind Conditions", Jour. Air Poll. Control Assn. 28, pp. 780-784.
- Fan, L. (1967), "Turbulent Buoyant Jets into Stratified or Flowing Ambient Fluids", Cal. Inst. of Tech., Report KH-R-15.
- Frenkiel, F. N. (1953), "Turbulent Diffusion: Mean Concentration Distribution in a Flow Field of Homogeneous Turbulence", Advances in Applied Mechanics 3, pp. 61-107.
- Gifford, F. (1960), "Peak to Mean Concentration Ratios According to Fluctuating Plume Dispersion Model", Int. Jour. Air Poll. 3, pp. 253-260.
- Hanna, S. R., Briggs, G.A., Deardorff, J., Egan, B.A., Gifford, F.A. and Pasquill, F. (1977), "AMS Workshop on Stability Classification Schemes and Sigma Curves - Summary of Recommendations", Bulletin American Met. Soc. 58, pp. 1305-1309.

- Hewett, T. A., Fay, J.A. and Hoult, D.P. (1971), "Laboratory Experiments of Smokestack Plumes in a Stable Atmosphere", *Atmospheric Environment* 5, pp. 767-789.
- Hinds, W. T. (1969), "Peak to Mean Concentration Ratios from Ground Level Sources in Building Wakes", *Atmospheric Environment* 3, pp. 145-156.
- Hino, M. (1968), "Maximum Ground Level Concentration and Sampling Time", *Atmospheric Environment* 2, pp. 149-165.
- Hinze, J. O. (1975), *Turbulence*, 2nd ed., McGraw-Hill.
- Högström, U. (1963), "An Experimental Study on Atmospheric Diffusion", *TELLUS XVI* 2, pp. 205-251.
- Hoult, D. P., O'Dea, S.R., Touchton, G.L. and Ketterer, R. J. (1977), "Turbulence Plume in a Turbulent Cross Flow: Comparison of Wind Tunnel Tests with Field Observations", *Jour. Air Poll. Control Assn.* 27, pp. 56-60.
- Isyumov, N., Jandali, T. and Davenport, A.G. (1976), "Model Studies and the Prediction of Full Scale Levels on Stack Gas Concentration", *Jour. Air Poll. Control Assn.* 26, pp. 956-964.
- Isyumov, N. and Tanaka, H. (1979), "Wind Tunnel Modeling of Stack Gas Dispersion--Difficulties and Approximations", *Proc. 5th Int. Conf. on Wind Eng., Colorado State University, Colorado, U.S.A.*, pp. 1-26.
- Ludwig, G.R. and Skinner, G.T. (1976), "Wind Tunnel Modeling Study of the Dispersion of Sulphur Dioxide in Southern Allegheny County, Pennsylvania", U.S. Environmental Protection Agency, Report EPA 903/9-75-019.
- Melbourne, W.H. (1968), "Wind Tunnel Modeling of Buoyant Chimney Plumes", *Proc. 3rd Australian Conf. on Hydraulics and Fluid Mechanics, Sydney*, pp. 81-85.
- Melbourne, W.H. and Gartshore, I.S. (1975), "A Wind Tunnel Model Study of Air Conditioning Contamination by Intake of Flue Gas", *Proc. 6th Int. Congress on Instrumentation in Aerospace Simulation Facilities*, pp. 92-96.

- Morton, B.R., Taylor, G.I. and Turner, J.S. (1956), "Turbulent Gravitational Convection from Maintained and Instantaneous Sources", Proc. Roy. Soc. 234, pp. 1-23.
- Neiman, O.E. (1979), M. Sc. Thesis, Dept. of Mech. Eng., University of Alberta, Canada.
- Pasquill, F. (1974), Atmospheric Diffusion, Halsted Press.
- Pasquill, F. (1976), "Atmospheric Dispersion Parameters in Gaussian Plume Modeling, Part II: Possible Requirements for Change in the Turner Workbook Values", Environmental Sciences Research Laboratory, Research Triangle Park, North Carolina, U.S.A., Report EPA-600/4-76-030b.
- Ricou, F.P. and Spalding, D.B. (1961), "Measurements of Entrainment by Axisymmetrical Turbulent Jets", Jour. Fluid Mechanics 11, pp. 21-32.
- Singer, I.A., Imai, K. and Del Campo, R.G. (1963), "Peak to Mean Pollutant Concentration Ratios for Various Terrain and Vegetation Cover", Jour. Air Poll. Control Ass. 13, pp. 40-42.
- Singer, I.A. and Smith M.E. (1966), "Atmospheric Dispersion at Brookhaven National Laboratory", Int. Jour. Air Poll. 10, pp. 125-135.
- Slade, D. H. (1968), Meteorology and Atomic Energy, U.S. Atomic Energy Commission.
- Stern, A.C. (1976), Air Pollution, Academic Press.
- Turner, D.B. (1969), "Workbook of Atmospheric Dispersion Estimates", U.S. Dept. of Health, Education and Welfare, Report 999-AP-26.
- Wilson, D.J. (1977), "Effect of Vent Stack Height and Exit Velocity on Exhaust Gas Dilution", ASHRAE Trans. 83, Part 1, pp. 157-166.

B30257